CALIBRATION OF SEISMIC AND WELL DATA

Towards Improved Quantitative Seismic Reservoir Characterisation of the Triassic to Middle-Jurassic Gullfaks Reservoir Units of the northern North Sea

Isaac Bisaso

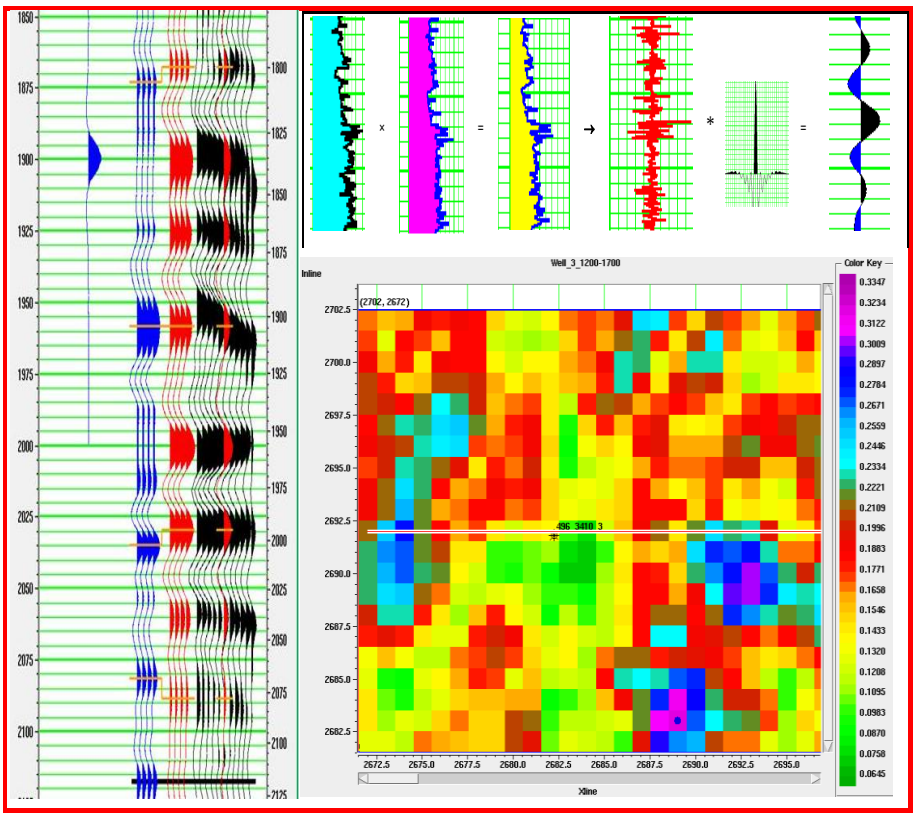

Master of Science Thesis

Discipline: **Petroleum Geophysics**

Department of Earth Science

University of Bergen

December, 2011

Project Supervisors: Prof. Tor Arne Johansen (UiB)

Eng. Dr. Bent Ole Ruud (UiB)

[†] E-mail: isaacbisaso@yahoo.com.au

Abstract

Characterization and evaluation of (oil and gas) reservoirs is typically achieved using a combination of seismic and well data. It is therefore critical that the two data types are well calibrated to correct and account for the fact that seismic data are measured at a scale of tens of meters while well data at a scale of tens of centimeters. In addition, seismic data can be poorly processed; some well logs can be damaged, affected by mud filtrate invasion or completely missing. This research addresses the methods of (1) editing, conditioning and petrophysical analysis of well logs and (2) joint calibration of seismic and well data to improve correlation and consistency between the two data types. A case study using a data set from the Gullfaks filed is presented; this field is in tail production and therefore improved seismic reservoir characterization to prolong its production life is quite essential. With the help of Geoview, Elog and AVO modules of Hampson-Russell software and Geovation/Geocluster software; post-stack processing, petrophysical modeling and analysis, and joint-calibration of the data were carried out. The results show that locally calibrated rock physics models (of for instance Gardner's and Castagna's equations) produce more accurate synthetic well logs (of missing or damaged curves) than those produced using 'Global' relations. Fluid replacement modeling was carried out to factor in the presence of hydrocarbons in the reservoir zones; the results show more accurate prediction of well logs in the reservoir zones. The quality of well logs was greatly enhanced, in preparation for the joint calibration process. Multi-well wavelet extraction and analysis was done to extract a single wavelet; the wavelet so extracted produced synthetic data that correlates well at all well locations. In some of the wells the correlation coefficient was over 0.50. In one of the wells the correlation coefficient rose from -0.40 (for an individually extracted wavelet) to 0.30 (using a multi-well extracted wavelet). The study demonstrates that it is possible to obtain a high correlation between seismic and well data, if the data are well processed and conditioned. Multi-well wavelet extraction produces a wavelet that is applicable at all well locations.

Keywords: Rock physics, Fluid Substitution, AVO, Seismic and well logs, Wavelet extraction, petrophysical modelling, joint calibration

Table of Contents

List of tables

Acknowledgments

I am highly indebted to Prof. Tor Arne Johansen and Eng. Dr. Bent Ole Ruud under whose supervision and guidance this research was undertaken. The duo is credited for their selfless support throughout my period of study at the Earth Science Institute in Bergen. Prof. Johansen, accepted me at a time when he knew nothing of my abilities and inabilities; why did you have to take such a gamble? Eng. Bent spent a lot of time teaching me how to use Software packages and offered helpful suggestions and guidance on the results presented herein.

I thank Dr. John Mary Kiberu (Makerere University) for the helpful guidance on the layout of the report and for reading through and making constructive comments on the presentation style.

I am very grateful to my colleagues: Kenneth Bredesen and Cathrine Eide ("Princess Kate") for the love, care and support that kept me reading and writing. The duo read through and made useful comments unto this thesis.

I thank my family and friends who have had to bear with my long period of absence, amidst all the misfortunes that befell the family.

Statoil and CGGVeritas are acknowledged for providing the data set and software tools, respectively.

My entire Masters education, this research inclusive, would not have been undertaken without the generous financial support from the government of the Royal Kingdom of Norway; may God unreservedly bless the Norwegian people.

Dedication:

1. In Loving Memory of my beloved Grandmother and Grandfather who rested while I was in a land so far away in pursuit of knowledge‡. Rest in Peace.
2. Mum and Dad – above all beings on earth, you are treasured

‡ "Wisdom is supreme; therefore get wisdom. Though it cost all you have, get understanding." – Proverbs 4: 7 (NIV)

List of Acronyms

AVA: Amplitude Variation with Azimuth

AVI: Amplitude Variation with Incidence angle

AVO: Amplitude Variation with Offset

EOR: Enhanced Oil Recovery

GC: Gas Chromatography

GOR: Gas Oil Ratio

IOR: Improved Oil Recovery

MS: Mass Spectrometry

NGL = Natural Gas Liquids

NORSAR: Norwegian Seismic Array

NPD: Norwegian Petroleum Directorate

OWC: Oil Water Contact

scm = standard cubic meters

TOC: Total Organic Carbon

TWT: Two Way Time

UiB: Universitetet i Bergen (= University of Bergen)

VSP: Vertical Seismic Profiling

RSI: Rock Solid Images

1.0 Introduction

A reservoir geophysicist enjoys significant advantages over an exploration geophysicist, who (with limited or no access to well data) cannot always tie the seismic data and its character (attributes) to properties of the formation as evidenced from the well data. Simply put, while the former works with un-calibrated seismic data the latter works with calibrated seismic data. And the increasing use of 3D seismic data for quantitative reservoir characterization arouses the crucial importance of a reliable well to seismic calibration, (Nathalie and Pierre, 2000). Unfortunately, there has not been a case (so far) where seismic data and well data perfectly and out rightly correlate without some 'intelligent' processing and 'shifting' schemes, as for instance, those presented by Roy and Tlanyue (1998).

Well data (of all types) are measured to the order of tens of centimeters while seismic data samples lithologies at a scale of the order of tens of meters. This calls for advanced mathematical processing of well data to upscale it so that it may be compared with seismic data. Well data are not always recorded all the way up the borehole, and it can be poorly recorded, corrupted or damaged. The data can be greatly erroneous in damaged well bore sections and highly porous zones (due to mud filtrate invasion). These are a few among the many issues that have been examined in this study; to develop a framework which can help reservoir geophysicists (geologists and engineers) to take full advantage of the availability of both well and seismic data.

Seismic data is in itself based on assumption of noise free zero-offset traces (convolution model), yet it is constructed from non-zero offset traces that have to be rid of multiples and migration artifacts and other forms of noise. This falls in the domain of seismic data processing, which by all measures, is too broad a topic to be addressed alongside the present research. Because of the breadth of the topic of seismic data processing, this research uses a presumably well processed seismic data set. However, limited post stack processing was carried out to condition the data for this research (e.g. 'windowing' (reducing the volume of) the seismic data to cut out unwanted parts.

Regarding the actual integration of well and seismic data, a number of approaches are studied, for instance: using VSP (Vertical Seismic Profiling) data and seismic forward modeling (computing synthetic data from well logs). A more 'hybrid' tool published by Linari et al (2004) is to 'invert' the seismic data for velocity and directly compare the inversion result to sonic data from wells. All these methods are considered in this research.

The single most important link between seismic and well data within the context of forward seismic modeling (a key topic in this research) is wavelet extraction. A detailed multi-well wavelet extraction scheme has been developed to increase the likelihood of achieving a high correlation and consistency between seismic and well data.

1.1 Scope and objectives this research

In a broad sense, the objective of this research is to develop a framework under which geologists, geophysicists and engineers can improve the integration of seismic data and well data (like never before). This involves intentionally 'deleting' some of the details in well logs (called upscaling), simulating high quality synthetic seismic data from the well logs and integrating them with real seismic data. Special attention is paid on ensuring that the well logs are as close to the 'ground' truth as possible. Much emphasis is given to wavelet extraction a key link in seismic to well calibration. The work flow involves the following steps:

- Edit, condition and upscale well logs, synthesize missing or damaged logs. Editing and conditioning to remove spikes, the effects of mud-filtrate invasion and formation damage. Upscale the well logs to remove details which are much loved by geologists but are a nuisance to calibration and integration of seismic and well data. Synthesis of missing and damaged logs by petrophysical modelling to make a complete suite of logs necessary for subsequent reservoir studies.
- Assess the suitability of traditional methods as well as recently developed methods of seismic to well data calibration. One of the key methods examined is the Forward seismic modelling method, regarding which a detailed multi-well wavelet extraction technique is developed.
- Investigate how well calibrated seismic and well data improves seismic reservoir characterisation

A brief description of the methodology involved in implementing the steps above is discussed in the next section. The detailed methodology is presented in proceeding chapters.

1.2 Database and methodology: Project requirements and software tools

This research was conceived on the basis of an existing oil reservoir or at least one that is in advanced stages of development. The Gullfaks field which is located in the northern North Sea (fig. 1.1), a famous and mature oil province, provides a rich data set of well and seismic data for a study of this kind. The field has been produced since 1986 from three platforms. A detailed description of the study area is given in chapter 2.

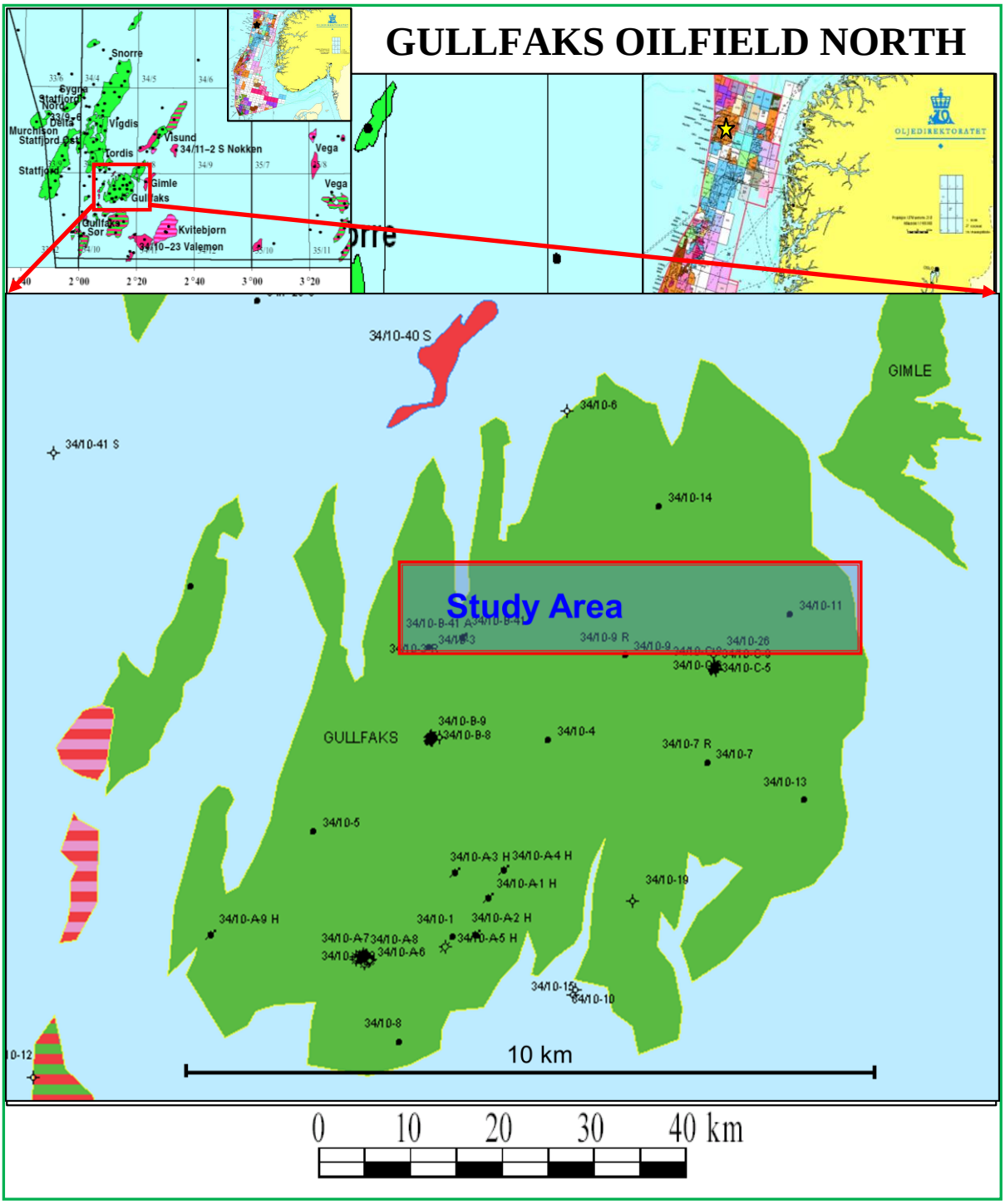

Figure 1.1: Location of Gullfaks field in the northern North Sea, modified from Norwegian Petroleum Directorate, NPD (2010)

Statoil (the operator of Gullfaks field) generously provided the following well and seismic data set for this project:

1. **Seismic dataset**

   3D seismic data (size: 3.875 km x 8km = 31km^2): sorted into: full offset stack; near (5-15 degrees), mid (15-25 degrees) and far (25-35 degrees) partial angle stacks.

Five vintages (1985, 1996, 1999, 2003 and 2005) were provided. The vintages acquired after 1985 have shadow zones around the oil platforms and other infrastructure in the Gullfaks area (fig. 1.2). In this study we used the base line data (1985) to avoid the shadow zone.Also all the wells used in this study were drilled prior to the onset of production; as such there was no need to incorporate production history.

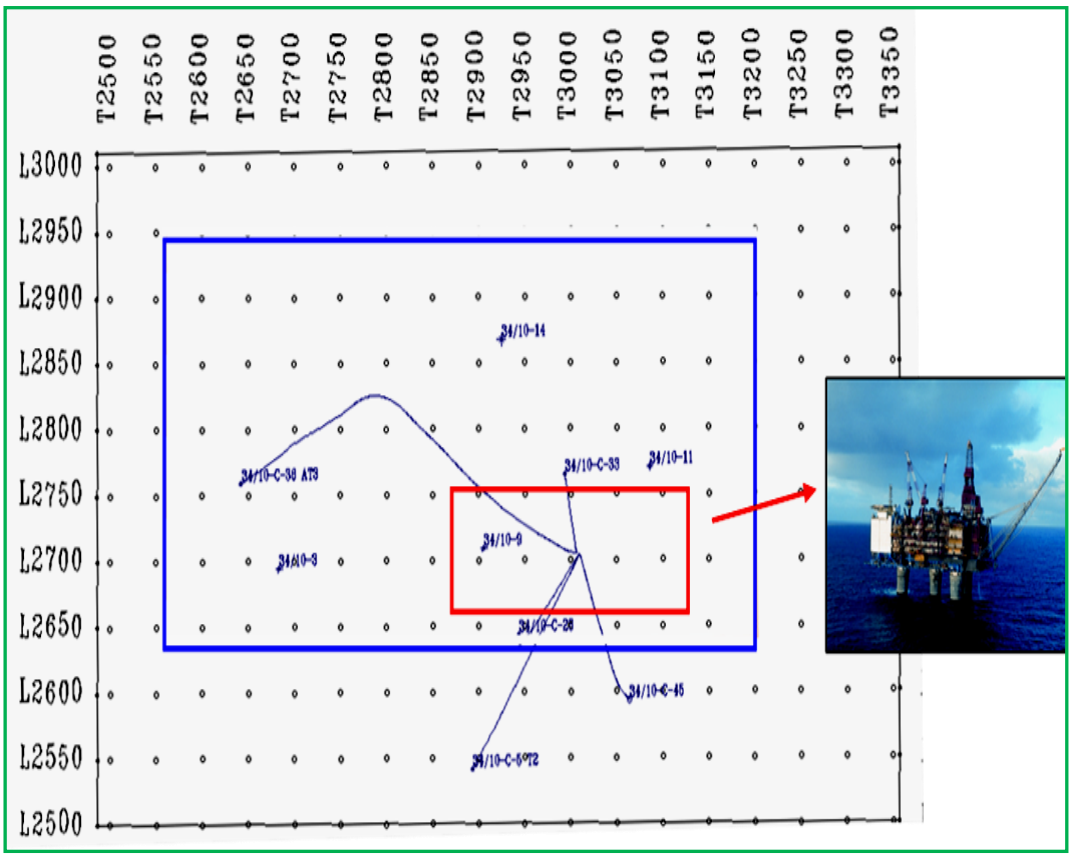

Figure 1.2: Location of oil wells within the 3D seismic cube used in this research, the red rectangle encloses the 'shadow' zone where the production platform is located. Modified from data provided by Statoil

2. Seven (7) Interpreted Seismic horizons

The following interpreted horizons were provided in depth and time domains:

- BCU (Base Cretaceous Unconformity)
- Top Tarbet
- Top Ness
- Top Ness 2A
- Top Broom
- Top Cook
- Top Stratfjord

A detailed description of these stratigraphic units/surfaces is given in Chapter 2. In this research, we did not concentrate on a particular reservoir; these tops were mainly

used in understanding the stratigraphy of the area and in identifying the area extent of reservoir units in between the wells studied.

3. **Well data**

   There are nine wells in the area; two of which are outside the fully migrated seismic cube. Of the remaining seven wells, one is within the 'shadow' zone (see figure 1.2), three are highly deviated. This leaves only three 'usable' wells, that is, within the scope of this study.

   The well data that for the three wells are summarized in table 1 below:

Table 1: Original well log data for the three wells used in this project. In the text the wells are referred to by their 'short name'.

Official Well name	**Short name**	**Depth range (of logged section)**	**Original log curves provided**
34/10-4	*Well 4*	**180-2799**	• Gamma ray: 1532-2465 m • Caliper: 1532-2465 m • Deep Resistivity: 1532-2465 m • Neutron porosity: 1532-2465 m • Bulk density: 1532-2465 m • Compressional velocity: 1758-2465 m • **No shear velocity**
34/10-11	*Well 11*	**1798-2155**	• Gamma ray: 1798-2154 m • Caliper: 1798-2155 m • Deep Resistivity: 1800 -2155 m • Neutron porosity: 1799-2154 m • Bulk density: 1709-2155 m • Compressional velocity: 1800-2155 m • **No shear velocity**
34/10-14	*Well 14*	**1719-2647**	• Gamma ray: 1719-2647 m • Caliper: 1800-2647 m • Deep Resistivity: 1900 -2100 m • Neutron porosity: 1749-2647 m • Bulk density: 1748-2651 m • Compressional velocity: 1721-2647 m • **No shear velocity**

- In addition to the original curves shown in the table above, we also received a suite of well logs that were edited, processed or synthesized by Rock Solid Images (RSI) using their commercial Geophysical Well Log Analysis™ tool. Some of the RSI curves were used to benchmark our own results.

- As can be noted from table one above, one of the inherent problems of most well data is incompleteness: some logs exist only in the logged sections while others are completely missing. The solution is to turn to petrophysical modelling and synthesis using empirical models as addressed in chapter 3 of the thesis. In the same chapter we discuss other processing flows necessary to condition well data in preparation for integration with seismic (and other data types).

Data analysis and interpretation were done using Hampson-Russell software packages from CGGVeritas. Well data treatment and analysis were done using Geoview and Elog modules. Elog module was particularly used for editing, conditioning and petrophysical modelling (Fluid replacement modelling and synthesis of missing logs). For the joint calibration of seismic and well data (wavelet extraction, synthetic modelling and multiwall analysis), we used Elog and AVO modules.

Basic post-stack seismic processing (for instance windowing the seismic data) was carried out using Geovation/Geocluster processing suite from CGGVeritas. Xjob, Geopad and Team view modules were used for 'job building', database management and visualisation, respectively.

A detailed description of methods and specific processing schemes is given in the relevant chapters; this was done to keep the results and discussion closer to the methods so that the material flows well.

1.3 Chapter description

Chapter 2 contains a description of the geography and geological background (regional structural and stratigraphic setting) of the Gullfaks field and the surrounding areas. The chapter also gives an overview of the petroleum system, production history and prognosis of the field based on published data.

Chapter 3 is dedicated to editing, calibration and petrophysical analysis of well data. Issues such as synthesis of missing logs, repair of damaged logs are all addressed in this chapter. A special section within chapter three is dedicated to fluid substitution modelling as applied to correcting for mud filtrate invasion and incorporating production history (in case of 4D seismic data).

The 'core' part of the research, that is, the integration of seismic and well data in the context of joint calibration is given in Chapter 4. Special sections on wavelet extraction and multi-well analysis of wavelets are included in this chapter.

Chapter 5 provides a summary of the entire work; the major conclusions and contributions thereof. Limitations and recommendations for future work are also given in the same chapter.

1.4 Literature review

There are a substantial number of articles, papers, masters and PhD theses that have been published covering some of the themes under this research. Unique to the presentation style of this work, the author chose to review the previous work at the beginning of the relevant sections/chapters throughout the thesis. This should help the reader to compare the results of previous workers to those of the current researcher.

2.0 The Gullfaks field

2.1 Geography

The Gullfaks oil field lies approximately 175 km northwest of Bergen. It is situated in the shallowest structural element of the Tampen spur area, in the central part of the East Shetland Basin, on the western flank (side) of the Viking Graben (Fossen et al, 2000). It lies in the Norwegian sector of the northern North Sea, in block 34/10 (Fig. 2.1) where it occupies the eastern half of a 10-25 km wide, NNE-SSW-trending fault block system (Fossen 1998, 1996). The water depth in the area is 130 – 220 metres.

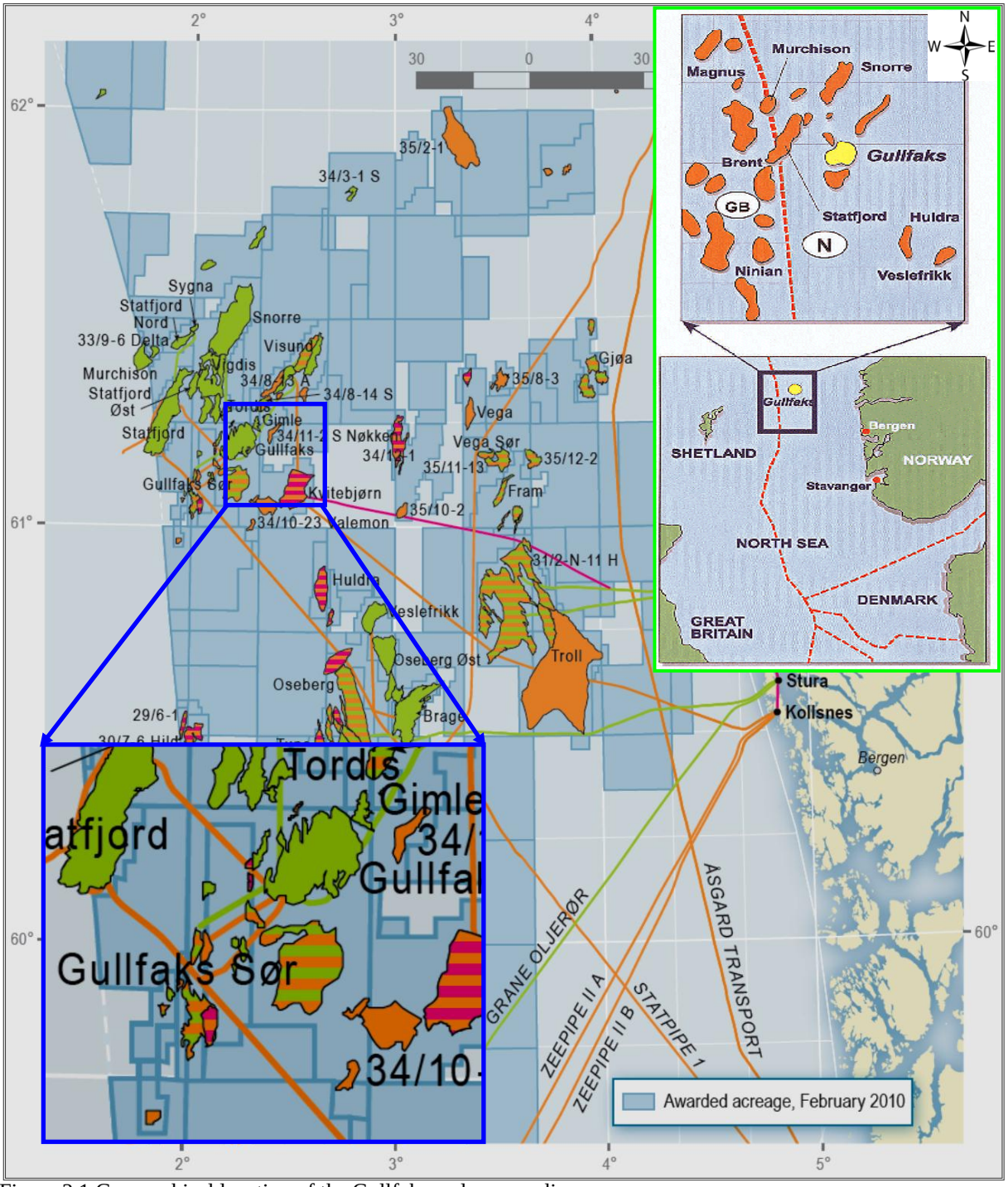

Figure 2.1 Geographical location of the Gullfaks and surrounding areas.
Modified from Hesjedal, A. (nd) and Norwegian Petroleum Directorate, NPD (2010)

The field was discovered in 1978 by exploration well 34/10-1 (spudded 20 June 1978). The exploration well was based on interpretation of an earlier 2D seismic data set that delineated a pre-cretaceous structural high in the north-eastern part of block 34/10. By the end of the initial exploration period (with at least 10 discovery wells), it was clear that the field covers the entire eastern half of the 10-25 km wide Gullfaks fault block with an area extent of up to 55 km^2. This made it clear that at least three platforms were needed to fully exploit the reserves (fig. 2.2). The field has three integrated processing, drilling and accommodation facilities with concrete bases and steel topsides (Gullfaks A, B and C). Gullfaks A (on stream since 22nd December, 1986) and C (on stream since 4th November, 1989) are fully independent processing platforms, while Gullfaks B (on stream since 29th February, 1988) has only first-stage oil separation (Petterson, et al. 1990). Gullfaks A and C also receive and process oil and gas from the neighbouring Gullfaks Sør, Gimle and other satellites (Statoil, 2011).

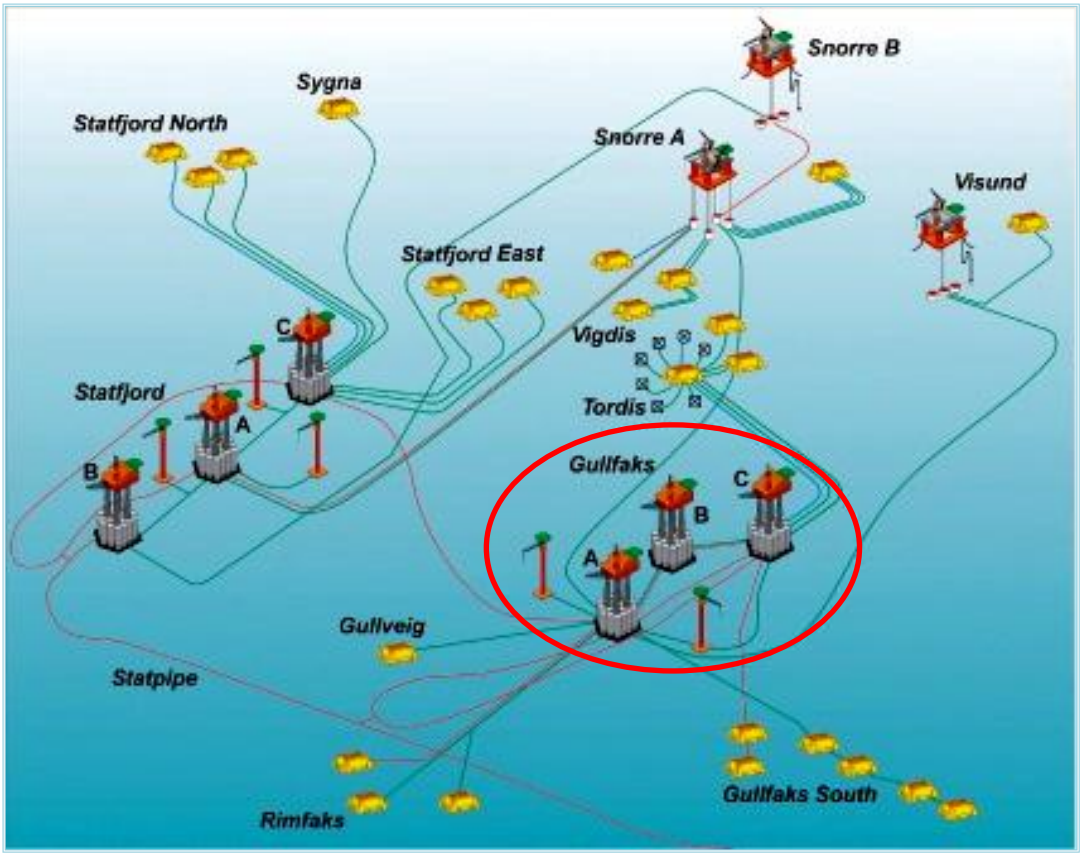

Figure 2.2 Facilities in the Tampen spur area, encircled in red is the study area.
Modified from NPD (2010)

2.2 Structural style and basin architecture

Extension tectonics as a precursor to the formation of the North Sea oil province can be traced to as far back as Devonian times. Its formation has also been linked to the Caledonian

orogeny (Fossen 1992). When the European, Greenland, and North American plates begun to separate, a triple-rift junction developed somewhere to the northeast of Scotland; two of its arms opened up forming the Norwegian Sea and the Atlantic Ocean. The southeastern branch of the triple-R junction subsided but failed to open, providing the present day North Sea oil province (Selley, 1998). In this respect therefore, the North Sea is an Aulacogen (failed rift) basin. Subsequently, it is believed to have experienced at least two main rifting episodes:

- First is the older Permo-Triassic rifting episode which is prominent on regional seismic data. It Shows up as the larger N-S to NNE-SSW faults, reflecting the overall E-W extension across the rift. This rifting created the Viking Graben and a series of westerly dipping fault blocks (which is characteristic of the present day Gullfaks field) and half Grabens in the eastern East Shetland Basin.
- The second major rifting episode occurred during Middle Jurassic to early Cretaceous times. This suite of younger roughly E-W trending faults are very visible in local seismic vintages and it is where majority of the hydrocarbon bearing formations within the northern North Sea are located. Of course, this gives an idea about the timing of hydrocarbon migration.

Most of the faults terminate against a regional base cretaceous unconformity which separates the faulted and rotated Triassic and Lower-Middle Jurassic sediments from mainly unfaulted and flat-lying Cretaceous and younger deposits. In fact it acts as the seal for the Gullfaks reservoirs. This unconformity represents a time gap of up to 100 Ma on structurally high areas like the Gullfaks Field (Fossen, 1996). The post-Jurassic history of the North Sea is characterized by basin subsidence and continuous sedimentation.

The Gullfaks Field is the most complex structure so far developed in Norwegian waters. This complexity is such that the Gullfaks reservoirs are located in rotated fault blocks in the west and in a structural horst in the east, with a highly faulted E-W transitional zone in-between (fig. 2.3):

1. A western domino system comprising of a series of typical domino-style rotated fault blocks. In this compartment, the normal faults strike N-S dipping to the east at rather low angle of 30-40^{o} while the formations are west dipping (10-15^{o}). This is a peculiar combination of dips because with a fault dip of 30-40^{o} one would expect the bedding dip in the order of 20-30^{0}. Previous workers (for instance Petterson et al, 1990) believe this may be attributed to: (1) ‘domino-type’ deformation of several fault

blocks combined with rotational deformation of the blocks and (2) an internal shearing within the separate blocks.

2. An eastern horst structure, where the Stratfjord formation is uplifted approximately 300m compared to the central area (Petterson et al, 1990). This elevation of the sub-horizontal layers and the steepness of faults exposed and led to erosion of a great part of the upper Formations (Brent and cook reservoirs) as seen in figure 2.4.
3. Between the western and eastern regions is a transitional accommodation zone which could by itself be regarded as a Graben feature. These E-W faults separate the two domains of contrasting dips.

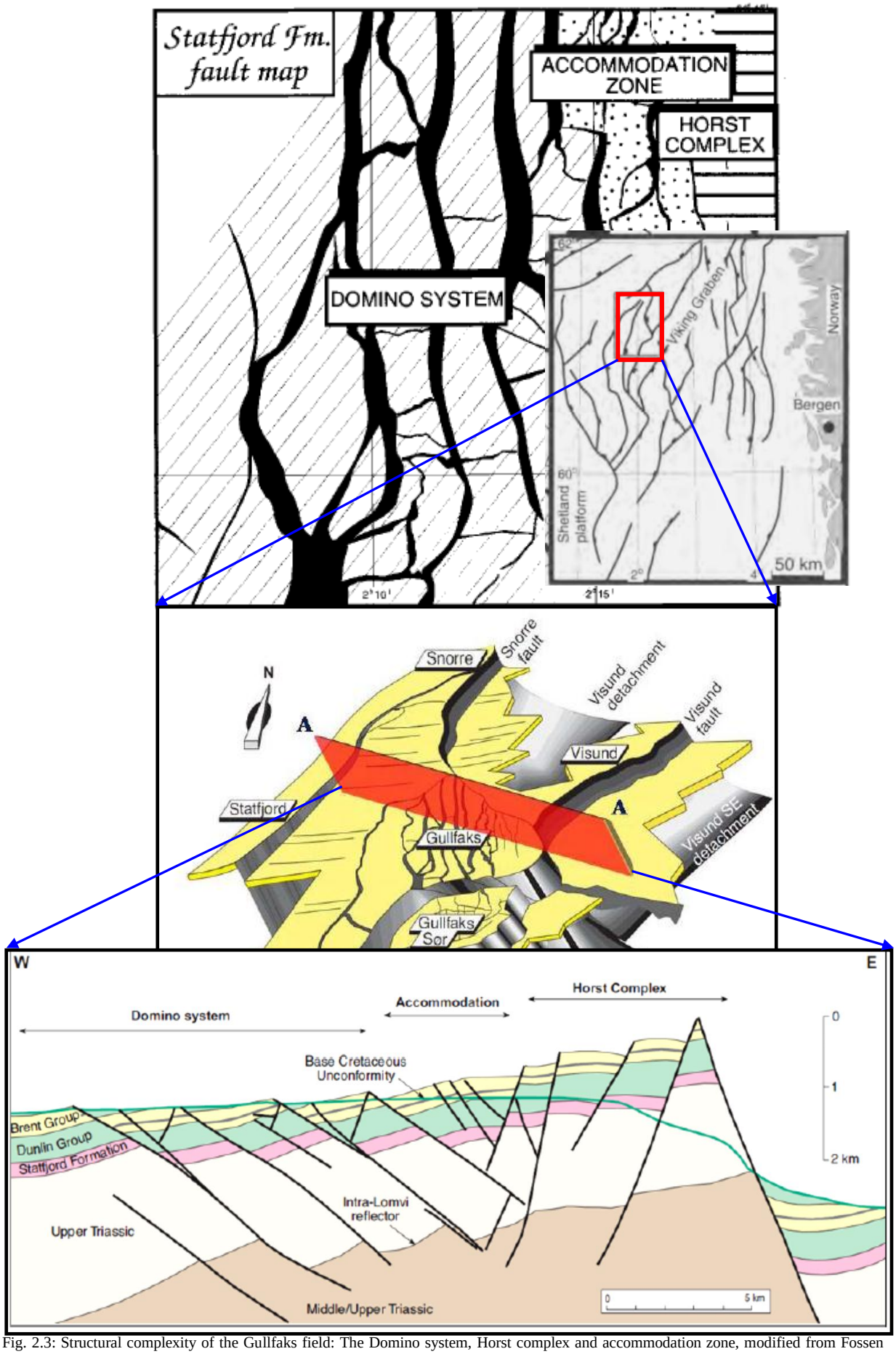

Fig. 2.3: Structural complexity of the Gullfaks field: The Domino system, Horst complex and accommodation zone, modified from Fossen and Hesthammer, 1998 and Evans et al (2003)

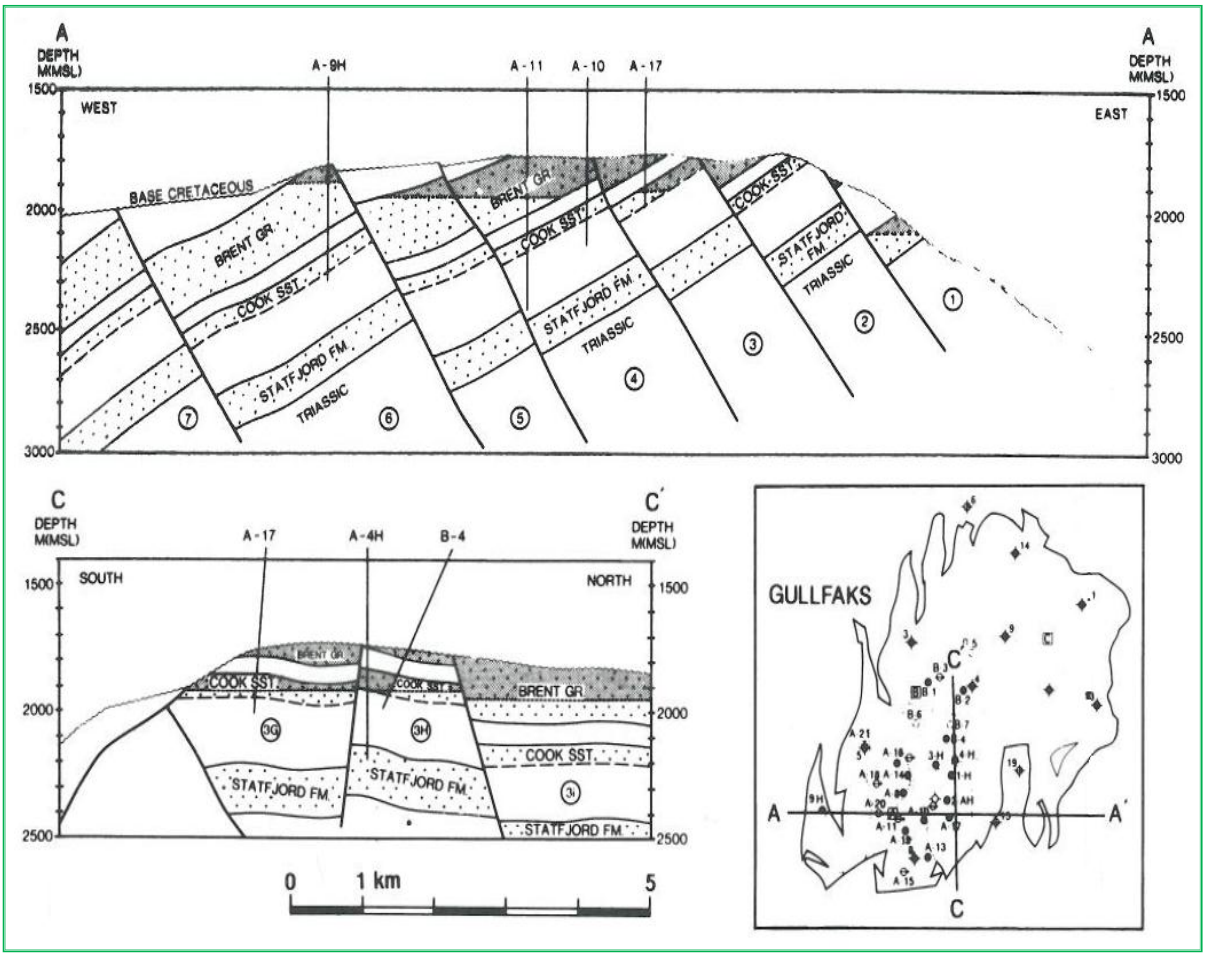

Fig. 2.4: Sections through the Gullfaks field showing erosion of Brent and cook Formations in the horst complex. Modified after Petterson, 1990

2.3 Stratigraphy and depositional environment

The oldest reservoir formations penetrated by the deepest well (34/10-13, 3350m deep) in the Gullfaks area are the medium grained alluvial fan and lacustrine clastics of the Triassic Hegre Group (Lunde and Lomvi Formations). They were un-conformably deposited on Caledonian basement. The Lunde Formation attracts less attention because its reservoir quality is generally poor; Lomvi Formation has no reservoir potential. Most of the oil in the Gullfaks field is primarily recovered from three early to middle Jurassic age sandstone reservoir units (fig. 2.5, also see figures 2.3 and 2.4):

- The Statfjord Formation.
- The Cook Formation of the Dunlin group.
- The Brent Group.

Growth faulting occurred during deposition of these reservoir rocks along some fault trends, probably or at least partly due to differential compaction of Triassic rocks (Goff, 1983)

2.3.1 Stratfjord Formation

Alluvial sandstones of the Rhaetian-Sinemurian Stratford Formation overlie the Hegre group. This Formation represents an environment that changed its character from a well drained semi-arid setting with episodic sheet flood deposition to a more humid alluvial plain setting. The Stratfjord Formation is subdivided into the Raude, Eiriksson and Nansen members (fig. 2.5). A detailed description of these smaller subdivisions has been well outlined by a number of previous workers see for instance Petterson et al. 1990. The reservoir quality within the Stratford Formation ranges from very good to poor potential.

2.3.2 (The Intra Dunlin) Cook Formation

The Cook formation is the most attractive unit in the Dunlin Group. The others are: (1) Amundsen (Sinemurian-Toarcian marine clay- and siltstones), (2) Drake (Marine shale with varying amounts of silt) and (3) Burton Formations.

The Cook Formation is further subdivided into Cook-1 (a marine silty claystone with zero reservoir potential), Cook-2 (consisting of bioturbated muddy sandstones with poor to moderate reservoir potential) and Cook-3 (consisting of interbedded sand and shale with good reservoir potential) units.

2.3.3 Brent Group

The Middle Jurassic (Bajocian-Early Bathonian) deposits of the Brent Group form the uppermost part of the Gullfaks reservoir. The deposits consist of a sequence of sandstones, siltstones, shales and coals. The Brent group was deposited in a deltaic environment. The Brent group is subdivided into five major stratigraphic units: Broom, Rannoch, Etive, Ness and Tarbert Formations (figure 2.6, also see figure 2.5).

In terms of in-place volumes, the Brent group is the most important of all the reservoir units.

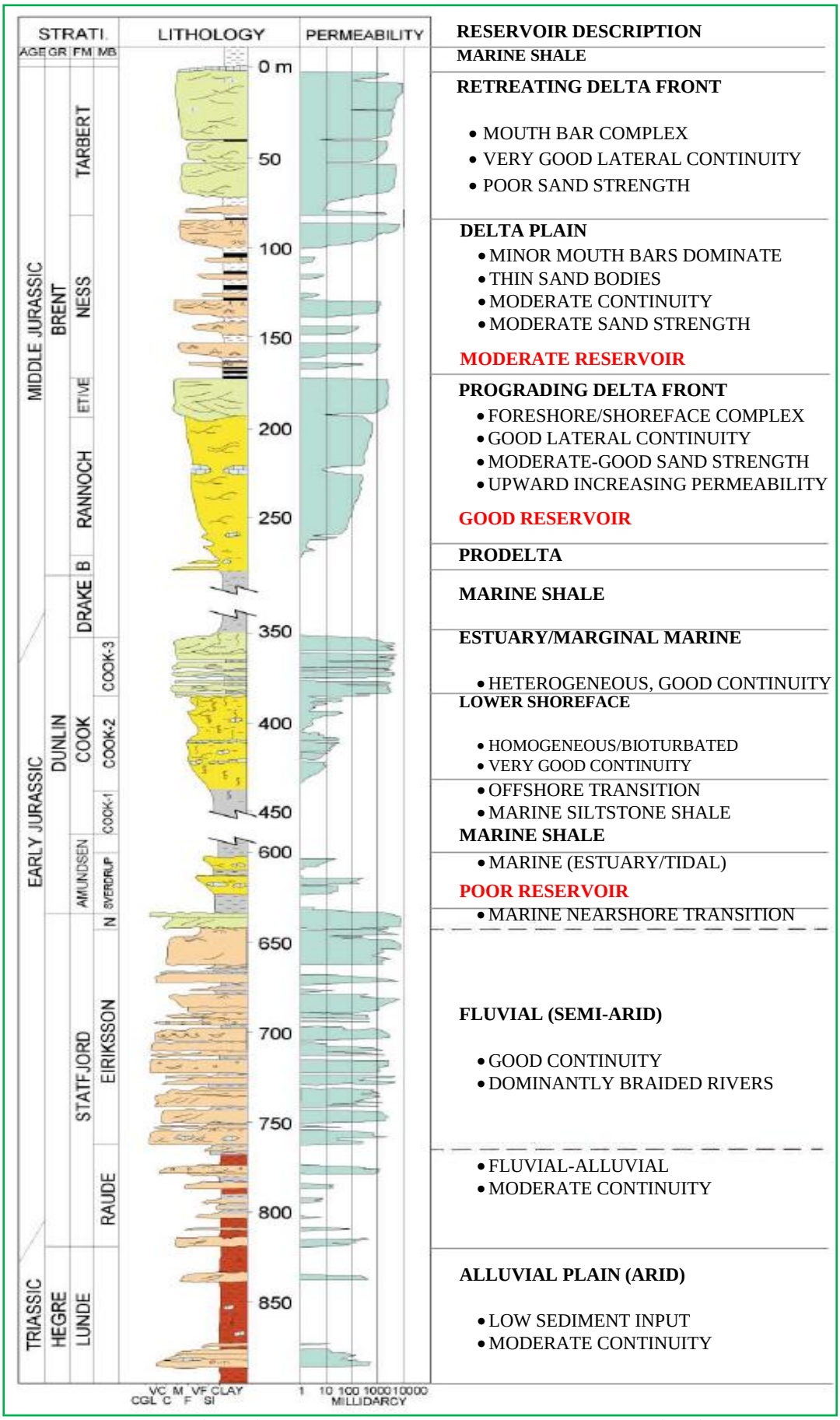

Figure 2.5: A Composite log for Gullfaks reservoirs showing variations in reservoir quality. Modified after Hesjedal, A. (nd) and Fossen et al (2000)

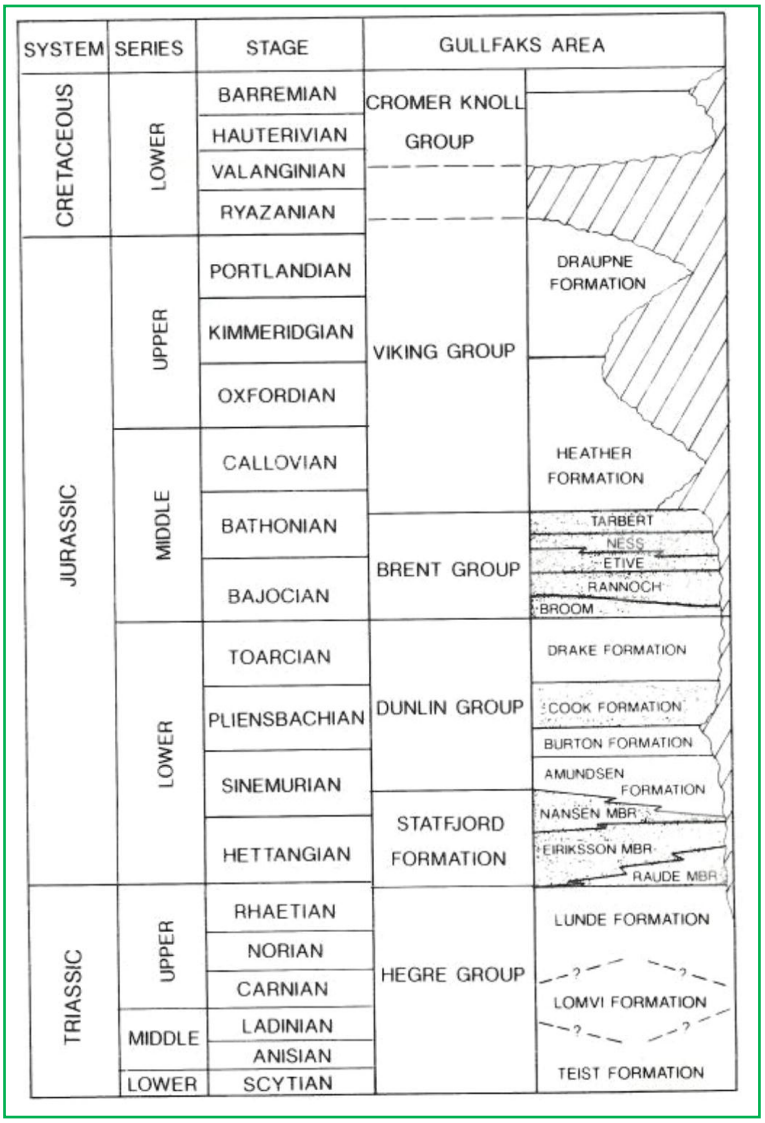

Fig. 2.6: Lithostratigraphic nomenclature of the Gullfaks field.
(Adapted from Petterson et al, 1990)

2.4 Petroleum System

2.4.1 The source and "devil's" kitchen(s)

Oil in the Viking Graben (and Shetland basin) is mainly 'sourced' form the upper Jurassic Draupne Formation (Kimmeridge Clay) (fig. 2.6). This Formation is often eroded on structural highs in the Gullfaks area but reaches a thickness in the order of 200-400m in the Viking Graben (Petterson et al, 1990) and up to 500m thick in the East Shetland basin (Goff, 1983). Supplementary source rocks albeit of less importance are assumed to be the shales of the Heather Formation as well as the marine shales of the Toarcian Drake Formation. Other potential source rocks are the shales and coals within the Ness Formation within the Brent group (Petterson et al, 1990)

There are three important "kitchens" serving the Tampen spur area (fig. 2.7): Oseberg kitchen to the south, the Troll kitchen in the east and the Møre kitchens to the north of Snorre (Petterson et al, 1990).

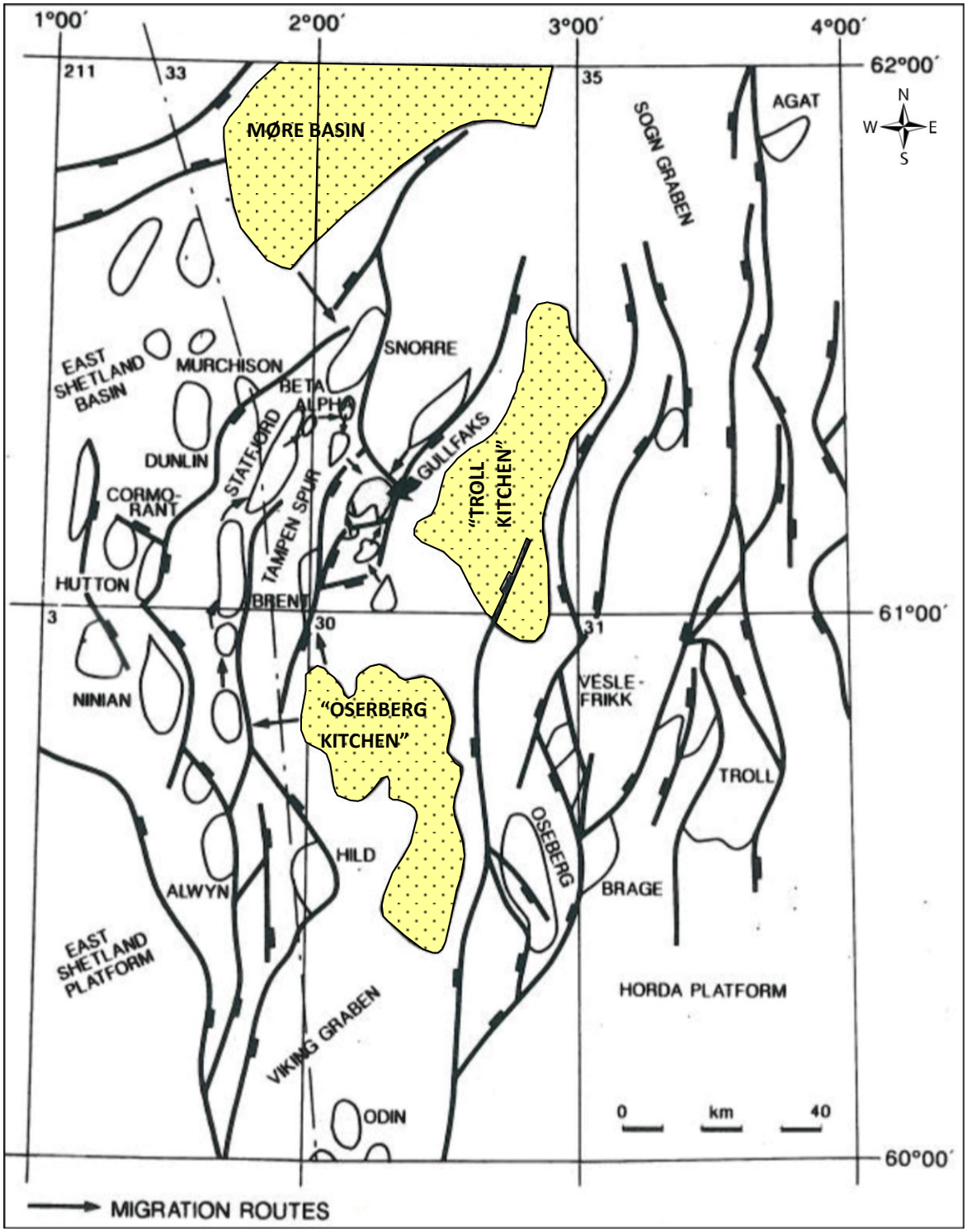

Fig. 2.7: The Kitchen and Migration pathways in the Tampen Spur area. *(Modified from Petterson et al, 1990)*

2.4.2 Reservoir and Cap rocks

The reservoir sands range in age from Triassic (Lunde Formation) to Middle Jurassic Brent Group units, the reservoir quality ranges from poor to very good (fig. 2.5). The sands were deposited in various environments like: Fluvial-alluvial and Marine environments. A more comprehensive description of the reservoir quality was outlined in section 2.3

The reservoir rocks in the Gullfaks area are capped by cretaceous shales and siltstones (Fossen, et al 2001). Most faults (but not all) terminate against a major unconformity, which seals off the reservoirs at approximately 1700m MSL in the crested area (Petterson, et al 1990).

Leakage: hydrocarbon leakage through the cap rock has been reported by a number of previous workers (see for instance Petterson et al 1990 and Larter & Horstad, 1992). It is reported that the leakage is because the integrity of the cap rock is compromised by some fault planes that can be seen crossing the top cretaceous horizon in a few places in the Gullfaks area. This leakage of hydrocarbons from Jurassic reservoirs is supported by the occurrence of minor amounts of hydrocarbons in Paleocene (Tertiary) sands (Petterson et al 1990 and Larter & Horstad, 1992); these gas chimneys above the main reservoirs turn seismic reflectors chaotic in places where they occur due to the geophysical phenomena of "velocity push-down".

2.4.3 Migration: valid pathway(s) and timing

Migration is believed to have commenced in Paleocene to Eocene times, fortunately the Gullfaks structure had already been sealed off by the Cretaceous shales and marls. Several workers (e.g. Goff, 1983 and Larter & Horstad, 1992) believe that primary migration was by oil phase expulsion through fractures created by abnormal pressures resulting from generation. Two other factors that may be important in primary migration are *creation of porosity* by conversion of kerogen to oil, and the reduction in oil/water interfacial tension with increasing temperature (Goff, 1983). Regarding secondary migration, short distance or direct migration from the nearest 'kitchen' in Troll (Viking Graben) might have been impeded by the major east bounding fault. However, (short distance) migration from spilling structures in the neighboring fields may have contributed to the oil in the Gullfaks. For instance, Petterson et al (1990) observed that the OWC for Brent Group reservoir in one of the Gullfaks blocks (6 A) is 56m shallower than in the main Brent reservoir, this coupled with an associated anomalously higher GOR was attributed to oil that migrated up-north from *Gullfaks Sør* field. Otherwise, only long distance migration from the other 'cooking areas' is

geologically plausible. Fig. 2.7 shows the possible migration routes into the Gullfaks field. Eastward, tertiary migration beyond the Gullfaks structure, being the shallowest part of the Tampen Spur area, through pre-Cretaceous strata is impossible (Petterson et al., 1990).

2.5 Reservoir Geochemistry

As pointed out in section 2.4.1, the richest source rocks in the study area are the oil prone Kimmeridge Clay (the Draupne formation to be specific to the Gullfaks). Thus description of source rock geochemistry will be restricted to the Kimmerigde Clay Formation. Goff, 1983 presented a more comprehensive source rock geochemical description for the entire northern North Sea. The immature organic matter of the Kimmeridge Clay (Draupne Formation) consists pre-dominantly of Type II kerogen. Its main macerals are inertinite and vitrinite. The Kimmeridge Clay is rated as an excellent oil source rock, capable of generating gas at high maturity levels. Its total organic carbon is of the order of 5-10%. This unusually high, Total Organic Carbon, TOC (and sapropel) content(s) as observed in the East Shetland Basin may be partly attributed to deposition in restricted fault bounded half grabens.

Goff, 1983, used Vitrinite reflectance versus burial history to estimate the uniform present day maturity gradient; the reported oil window (0.5-1.3% R_0) extends from 2550-4500m, while the wet gas zone (1.3-2% R_0) from 4500-5400 m (figure 2.8). At the present day the Kimmeridge Clay is mature over most of the East Shetland Basin and has reached peak generation throughout the axial region of the basin. The maturity level of the Kimmeridge Clay is close to the oil floor (1.3% Ro).

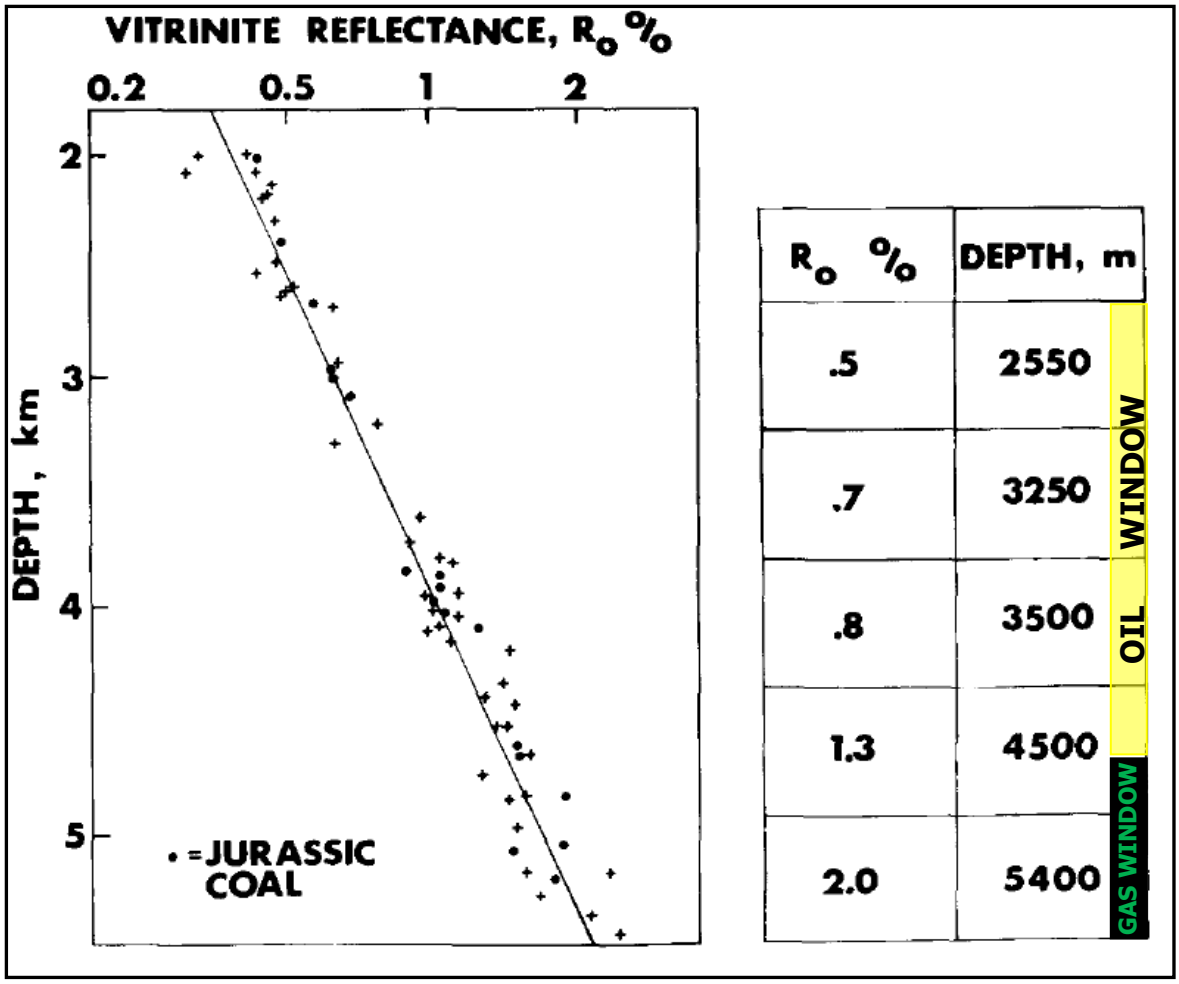

Figure 2.8: Vitrinite reflectance versus depth for Jurassic to early Cretaceous coals and mudstones in the northern North Sea. Modified after Goff 1983

Goff 1983, correlated Hydrocarbon/TOC ratio data for the Kimmeridge Clay with the vitrinite reflectance gradient to determine the vitrinite reflectance level corresponding to peak hydrocarbon generation; this was reported as 0.7% R_0 at 3250 m (Fig. 2.9). The associated oil expulsion efficiency from this source rock is over 20-30%.

Organic matter (spore) colouration and source rock electrical resistivity can also be used to estimate source rock maturity. From 2600 to 3200 m, plant material in the Kimmeridge Clay is light to medium brown, this according to organic matter (spore) colouration as a maturity indicator, means that it is moderately mature; between 3200 and 3650 m it is dark brown indicating that it has achieved peak generation (Books and Thusu, 1977). Goff, 1983 reported that, the electrical resistivity (of the Kimmeridge clay) increases from 2-3 ohm metres at 2500-2600 m to a maximum of 10-25 ohm metres at 3500-3600 m. These data indicate that peak generation has occurred between 3200 and 3500 m at a reflectance level of 0.7–0.8% R_0; which is consistent with other rock evaluation methods.

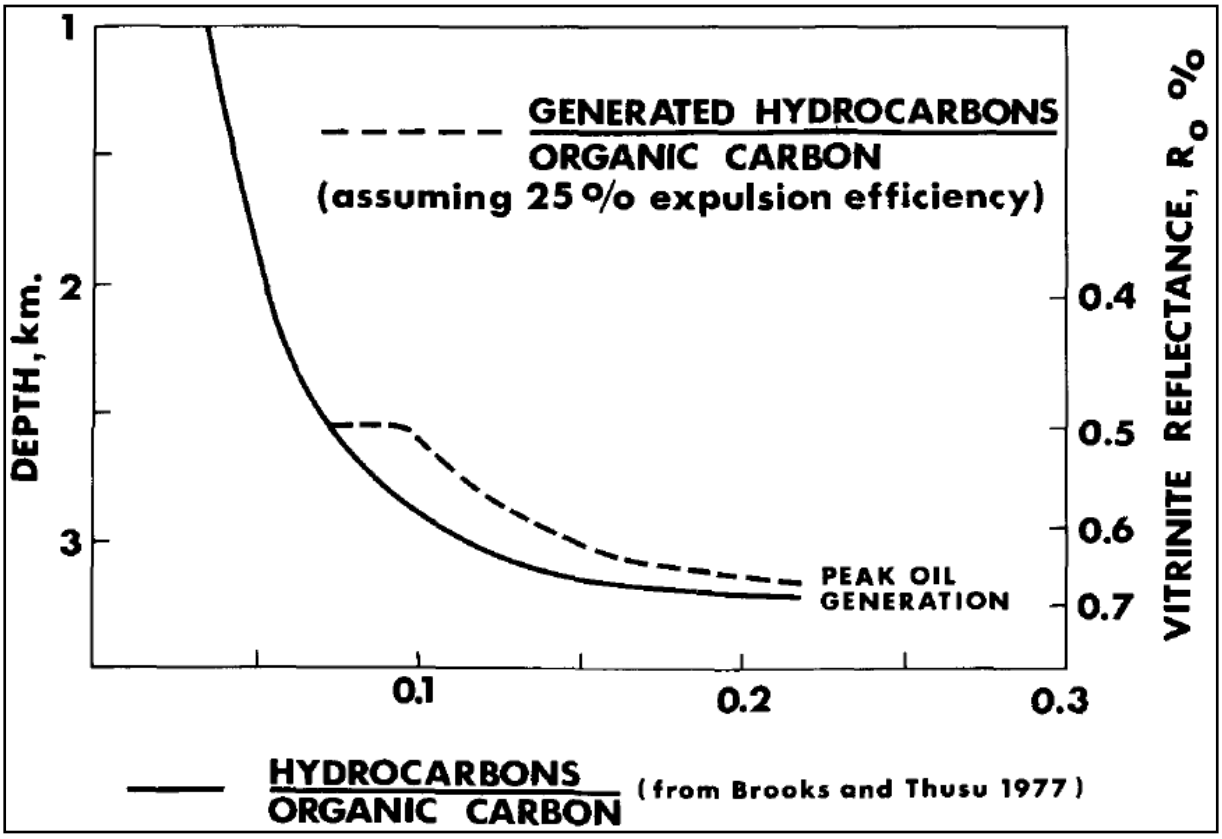

Figure 2.9: Hydrocarbon/organic carbon ratio versus depth and vitrinite reflectance for the 'Jurassic source rocks' Adapted from Goff 1983

Goff (1983) determined the timing of oil generation from the Kimmeridge Clay from its maturation history using the correlations of vitrinite reflectance with 'Time Integrated Temperature'[†] also knows as the maturity index. The areal extent of maturity was then deduced from isopach and structural contour maps of the study area. The study demonstrated that, oil generation from the Kimmeridge Clay began 70-80Ma ago in the Viking Graben; 65 Ma ago the Kimmeridge Clay was generating oil throughout the Viking Graben and in the deepest troughs of the East Shetland Basin. Peak oil generation was reached 55-65 Ma ago in the Viking Graben; 40 Ma ago peak generation had occurred in the deepest troughs of the East Shetland Basin, and throughout the Viking Graben. 20-40 Ma ago the Kimmeridge Clay entered the wet gas zone in the deepest synclines. Generation of gas by cracking of oil in the Kimmeridge Clay of the Viking Graben occurred during the last 50Ma. Gas generation from Brent Formation coals began 100 Ma ago in the Viking Graben; peak dry gas generation occurred during the last 40 Ma.

[†] Time Integrated Index as a maturation parameter is akin to Lopatin's Time Temperature Index, Goff (1983) discussed its mathematical basis

Compositional heterogeneities and oil degradation:

In the Gullfaks field, large-scale compositional heterogeneities in petroleum accumulations are well known. These chemical heterogeneities in the petroleum column have been interpreted geochemically by Larter & Horstad, (1992) among others. It seems from these studies that these chemical heterogeneities are beyond the usual aerobic (and anaerobic, if any) biodegradation and water washing effects, occurring after the oil has got entrapped. Instead these variations in petroleum column composition may be interpreted as being due to source facies and/or maturity variations in the petroleum charges feeding the oil accumulation. Larter & Horstad, (1992) mapped the petroleum column using a combination of thin layer chromatography-flame ionization detector system (TLC-FID) and Rock-Eval screening of reservoir cores to provide gross compositional information (i.e. concentrations of total petroleum, saturated hydrocarbons; saturated/aromatic hydrocarbon ratios etc.); this was in addition to G.C. analysis of whole oil samples with internal standard quantisation. These studies showed that, while at any location the vertical composition of petroleum is quite constant, systematic variations in the chemical composition of the petroleum within the Brent Group reservoir are recognized laterally across the field (fig. 2.10). Degradation is highest for oils in the western and least in the eastern part of the Brent Group reservoir; basically involving selective 'eating' of pristane and phytane. This anomaly led to the conclusion that: "the decrease in the absolute amount of n-alkanes across the field is due to biological degradation of petroleum" (Larter & Horstad, 1992). The second anomaly that was revealed by GC/MS analysis results (of Larter & Horstad, 1992 and also reported by Petterson et al. 1990) is that two different, distinguishable petroleum populations exist in the Gullfaks field: one early to mid-mature population present in the Brent Group in the western part of the field, and a slightly more mature population within the Cook, Statfjord and Lunde Formations in the eastern part of the field (figure. 2.10). Larter & Horstad (1992) deduced that the Brent Group reservoir was filled from a related but slightly different source to those filling the Cook/Statfjord Fm reservoirs. But Petterson et al (1990) attributed this anomaly to the fact that hydrocarbons in the Cook and Stratfjord Formations did not suffer from biodegradation as did those in the Brent Formation.

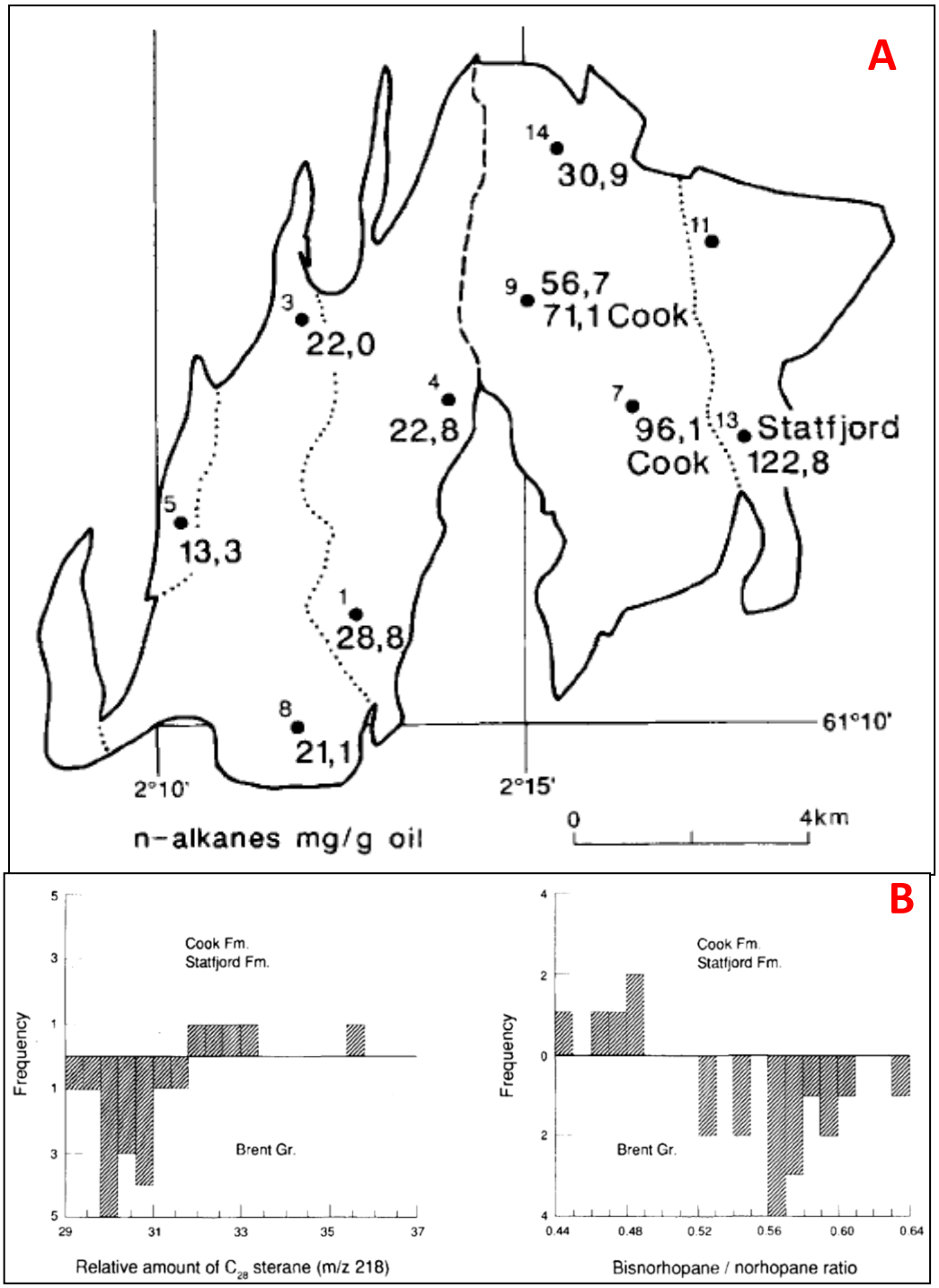

Fig. 2.10: Oil degradation in the Gullfaks area:
A) The absolute amount of n-alkanes increases eastwards due to more severe degradation in the western part of the Gullfaks field B) Statistical analysis of GC/MS data suggests that the Brent Group oils and the Cook/Statfjord Formations oils belong to two statistically different petroleum populations

2.6 Development and Production: History, Strategy and Prognosis

Gullfaks field was discovered in 1978 and has been producing since 1986 under production licence PL050, which was amended into licence PL050B (NPD, 2010) in 1995. The field is operated by Statoil (70%) in partnership with Petoro AS (30%). It was originally operated by Statoil in partnership with two other (now defunct) Norwegian oil companies: Norsk Hydro

and former Saga Petroleum; in what would turn out to be the first license ever run by a fully Norwegian joint venture corporation.

The original and remaining recoverable reserves (as of 31.12.2009, source: NPD, 2010) are:

Original:

361.5 million scm oil

22.7 billion scm gas

2.9 million tonnes NGL

NGL = Natural Gas Liquids
scm = standard cubic meters

Remaining as of 31.12.2009

16.8 million scm oil

0.1 million tonnes NGL

Production/Recovery Strategy:

The primary drive mechanism is massive water injection; the others being: gas injection or water/alternating gas injection (WAG). The drive mechanism varies between the drainage areas in the field, but water injection constitutes the main strategy.

Status and prognosis:

Production from Gullfaks reached its peak in 1994 setting a production record of 605,965 barrels for a single day on 7 October 1994 (fig. 2.11). Today it can be considered a 'dying' field, i.e. it is in tail production phase. The recovery factor on Gullfaks is an impressive 59 per cent. There are continuous efforts being made to increase recovery to at least 62 per cent (fig. 2.12), partly by locating and draining pockets of remaining oil in water-flooded areas, and partly through continued massive water injection. The other measures to improve recovery include horizontal and extended-reach wells, new completion and sand control technology, and water alternating gas (WAG) injection. Implementation of a chemical flooding pilot is under consideration (NPD, 2010 and Statoil, 2011). It is envisaged that if the recovery factor can be increased to around 70 percent then the Gullfaks can live on to up to 2030.

It should be noted that in the long run the single most important way of prolonging the production life cycle of a producing platform is not necessarily in squeezing out the already proven reserves (through IOR and EOR interventions), but through "infrastructure-led exploration which can yield highly commercial finds which can then be brought on stream quickly" (Tom Dreyer[f]). The most recent example to justify this fact is the August, 2011

[f] This is a slightly modified statement of Mr. Tom Dreyer, exploration head for the northern North Sea at Statoil. The original statement was retrieved on 24.10.2011 from http://www.worldoil.com

discovery of oil in the Gullfaks South area (Rimfaks valley). These if tied into the existing platforms at Gullfaks can help to keep the production rate above the economic cut off.

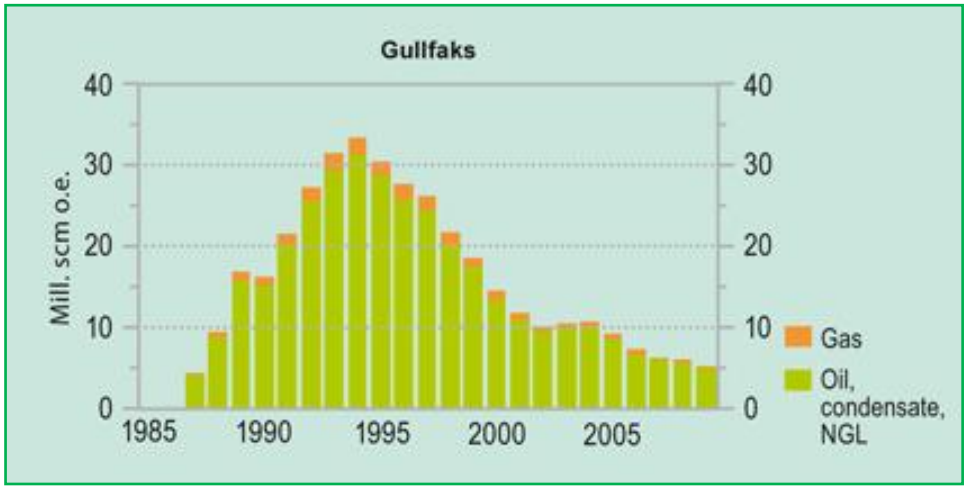

Fig. 2.11: Peak oil production of the Gullfaks field: Having peaked production in 1994 (in excess of 600 000 bbl/d), today the Gullfaks is clearly in tail production. Adapted from NDP (2010)

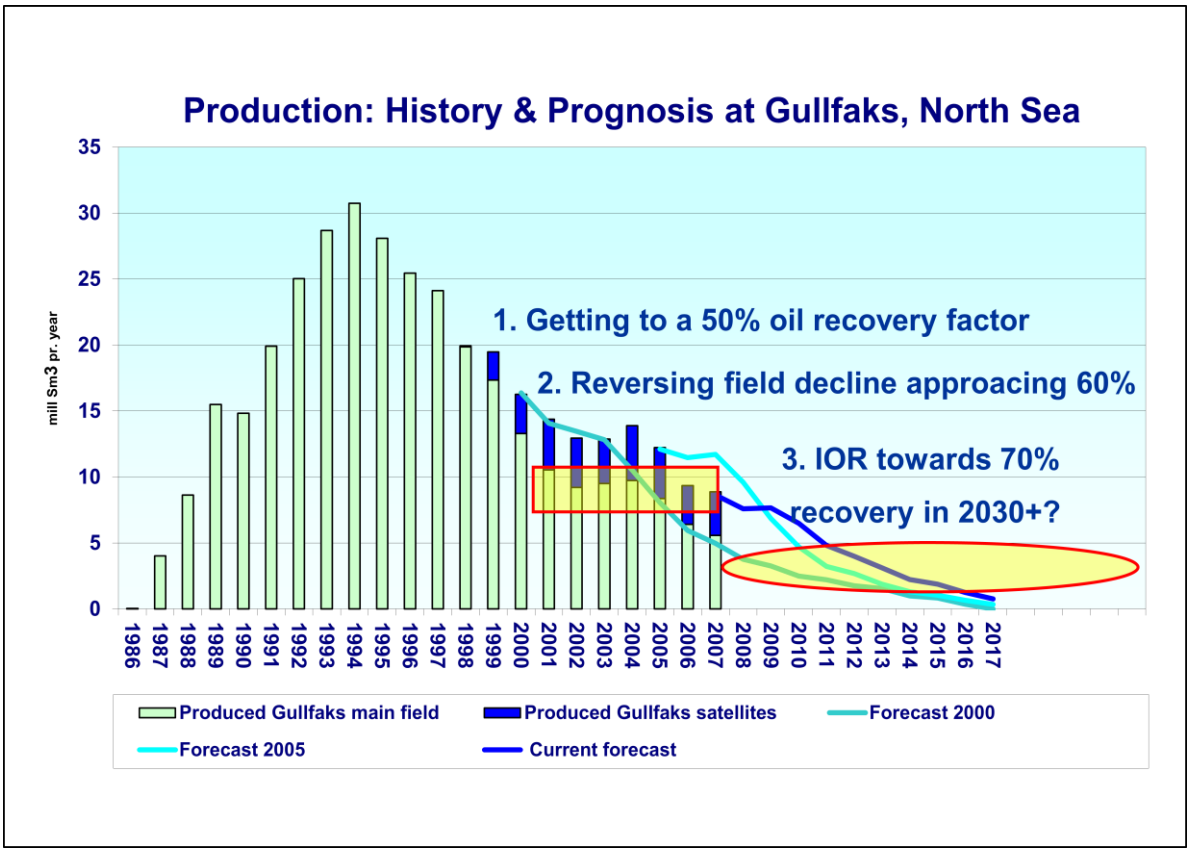

Fig. 2.12: Prognosis – the future of Gullfaks: it is envisaged that if the recovery factor is increased (to 70%); Gullfaks will live on up to year 2030. But the real future might be in aggressive infrastructure-led exploration to map out pockets of remaining hydrocarbons, like those that were recently (August, 2011) discovered in the Rimfaks valley in the neighbouring Gullfaks South field. Modified after, Eltvik (2011).

"... infrastructure-led exploration is important and yields highly commercial finds which can be brought on stream quickly," Tom Dreyer

3.0 Petrophysics: conditioning, editing and analysis of well logs

Reservoir characterization and evaluation are business critical functions in most oil companies; the increased demand of which is driven by economic realities: if reservoirs can be defined better using available technology, then the end results are higher drilling success and fewer development wells. Better reservoir definition and better reservoir management are the ultimate goals. It requires integration of all available subsurface data but the key data is normally seismic and well data (Vertical Seismic Profiling, VSP and 'check-shot' velocity data). Each of these data represents measurements, made using highly sophisticated equipments and highly developed software, but with a certain level of error. Although the technology involved is ever evolving and improving, the associated errors need to be properly dealt with, before the various data can be integrated for reservoir characterization. The manner in which these errors are handled affects the integration of the two data types and determines the quality of the final reservoir model (Jarvis, 2006). For instance, well logs are sometimes viewed by geophysicists as "hard data" and not subjected to the same level of scrutiny as the "soft" seismic data (see for instance: Nathalie and Pierre (2000), and Linari, 2004). This can be a mistake because well logs are susceptible to errors from a number of sources (Walls et. al. 2004). In this chapter, petrophysical control on well logs, methods and procedures of well log data conditioning are examined using a real well data set, the integration of the 'fine tuned' well data with seismic data is presented in the next chapter. Figure 3.1 shows a block diagram of an idealized reservoir characterization work flow.

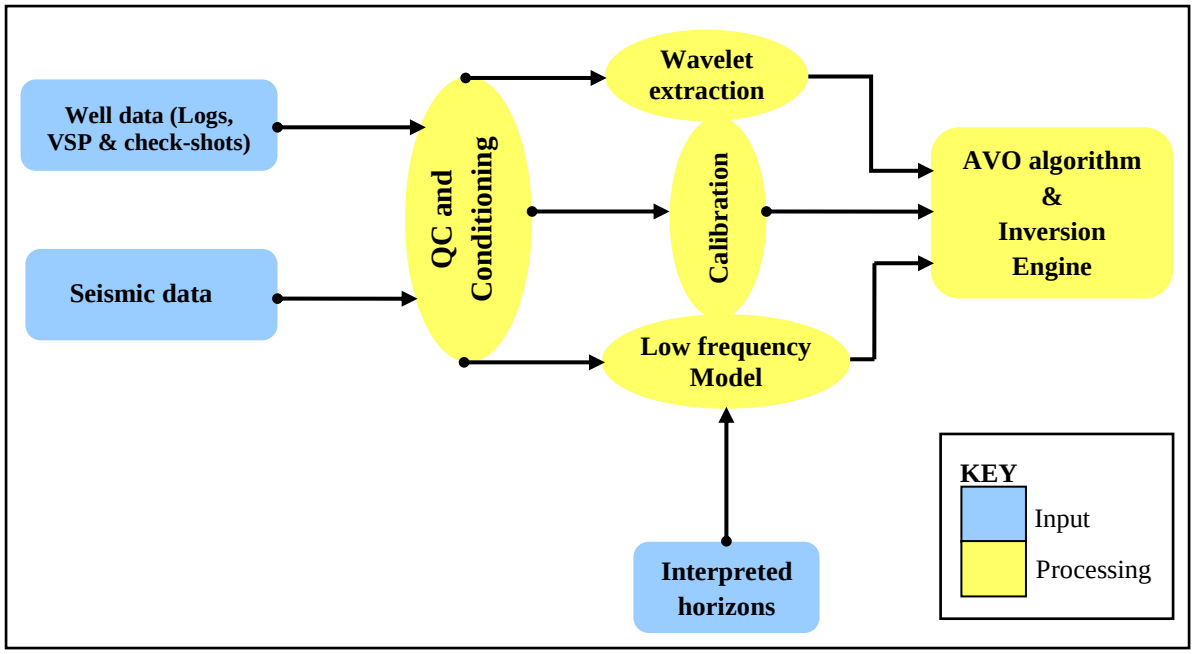

Fig. 3.1 A typical reservoir characterization workflow

3.1 Well log quality control, conditioning and editing

The continuous recording of a geophysical parameter along a borehole is called geophysical well logging; when the measured value is continuously plotted against depth, a geophysical well log is born.

Well logs are a result of physical measurement of the earth's properties taken within the confined space of a borehole (Jarvis, 2006). The probing instruments take the measurements from a very close range to the rocks under in situ (or nearly so) conditions; this is why the well log is the preferred benchmark ("hard data") in the calibration process. Unfortunately, these measurements are affected by borehole irregularities (rugosity), mud filtrate invasion, casing points and they very much depend on the elapse of time between drilling and logging of the hole among other factors. Therefore, the primary goal in processing well log data is to rid the data of measurement related errors and to obtain consistent and accurate logs from well-to-well. In addition, the logs represent data that is sampled at much higher frequencies (e.g. 20-40 kHz for a sonic log) than seismic data (5-50 Hz). This creates a lot of detailed information some of which is outside the seismic resolution; hence some type of dispersion correction (up-scaling) should be applied to account for the differences in frequencies between logging tools and surface seismic reflection before calibrating these data against each another. And quite often the time and/or tools for measuring some parameters are not available, in such cases there is need to synthesize such logs from other existing logs. The methodology and procedures of accounting for these problems and uncertainties follow.

3.1.1 Log editing and repair

For reasons mentioned above, well log data often requires some editing, normalization, and interpretation before they can be used in any reservoir characterisation study. The key steps involved in editing and repairing well logs are discussed hereunder.

a) Reconciling sonic logs with check-shot data

Check-shot (borehole velocity survey) data do not usually tie well with sonic data because of various reasons, for instance sonic data is highly contaminated by dispersion effects especially in damaged holes, it is also affected by mud-filtrate invasion effects in porous zones. And unlike sonic data, check-shot and surface seismic data probe the rock in its undisturbed state. Additionally, sonic velocities are usually higher than check-shot velocities because of dispersion effects (sonic logging uses higher frequency pulses which travel a lot faster). Much as check shot data can also suffer from "misfires, cycle-skips and poor processing flows" (Box and Loren, 2003), they are to be more trusted (than sonic data).

One of the first steps in calibrating well logs is to apply check-shot data. The goal of this step in the well log calibration process is to bring the timing of the sonic log into agreement with the "more accurate" seismic times from a checkshot survey. The theoretical background of check-shot surveys (acquisition and processing) is outside the scope of this study, it suffices therefore to simply present results of applying check-shot data on our sonic logs.

Results and discussion:

In figures 3.2, 3.3 and 3.4 are the results of applying check-shot data on P-wave logs of well 3, 11 and 14 respectively. The result for *well 3* is to be expected since the original sonic should be higher than the result after applying check-shot data. The check shot data for *well 11* is questionable; how can the sonic data be lower than the check-shot corrected data? The results for *well 14* show that there was little drift between the check-shot and sonic data for this particular well; this is why the resulting curve is just a little higher than the original curve.

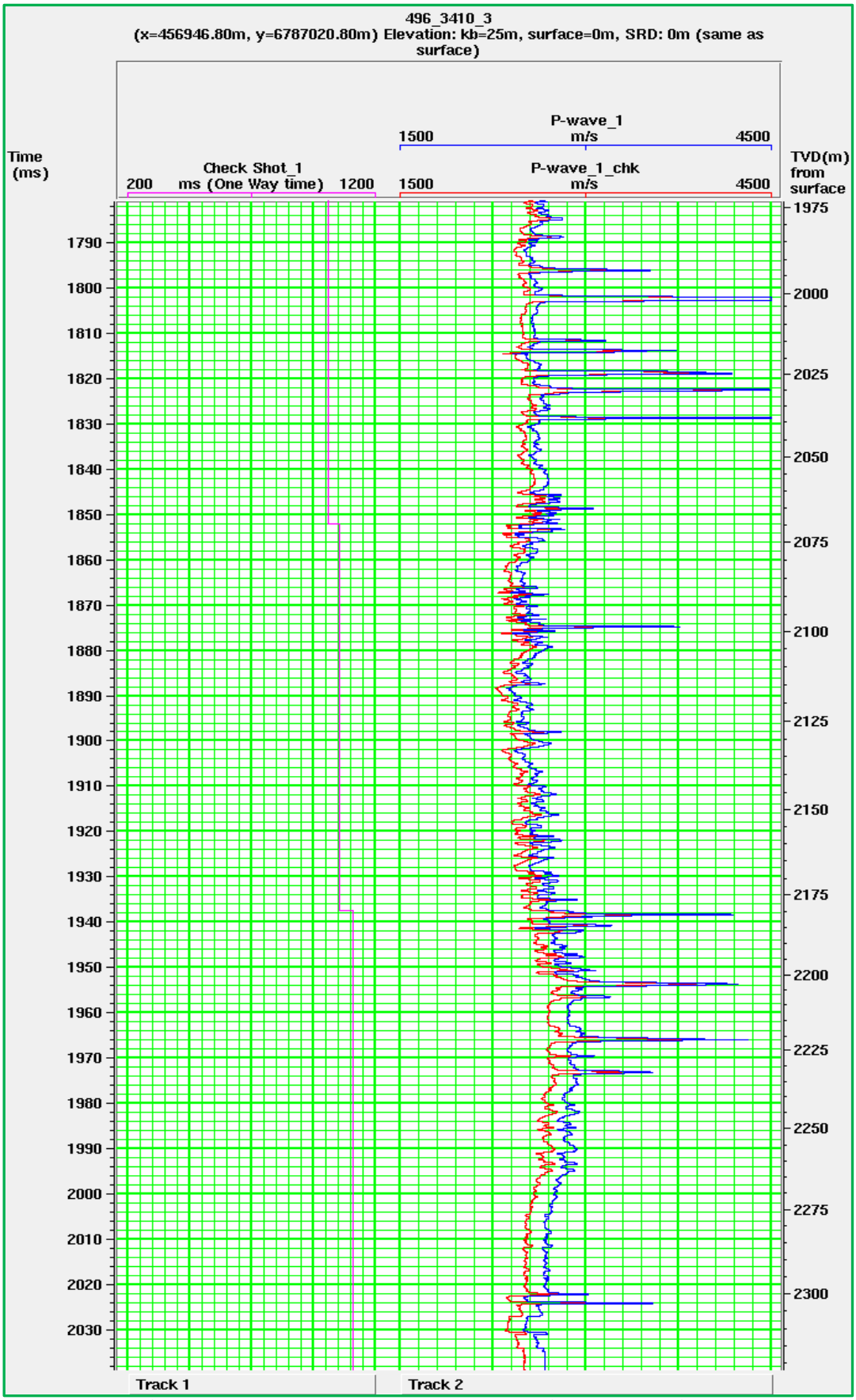

Figure 3.2: Results of applying check-shot velocities on P-wave velocity log for well 3. In the first track or panel is the checkshot log, in the second track, the blue curve is the resulting P-wave curve after applying check-shot data on the original (blue) P-wave log. The resulting sonic log has lower values since the check shot data is lower than sonic data as expected.

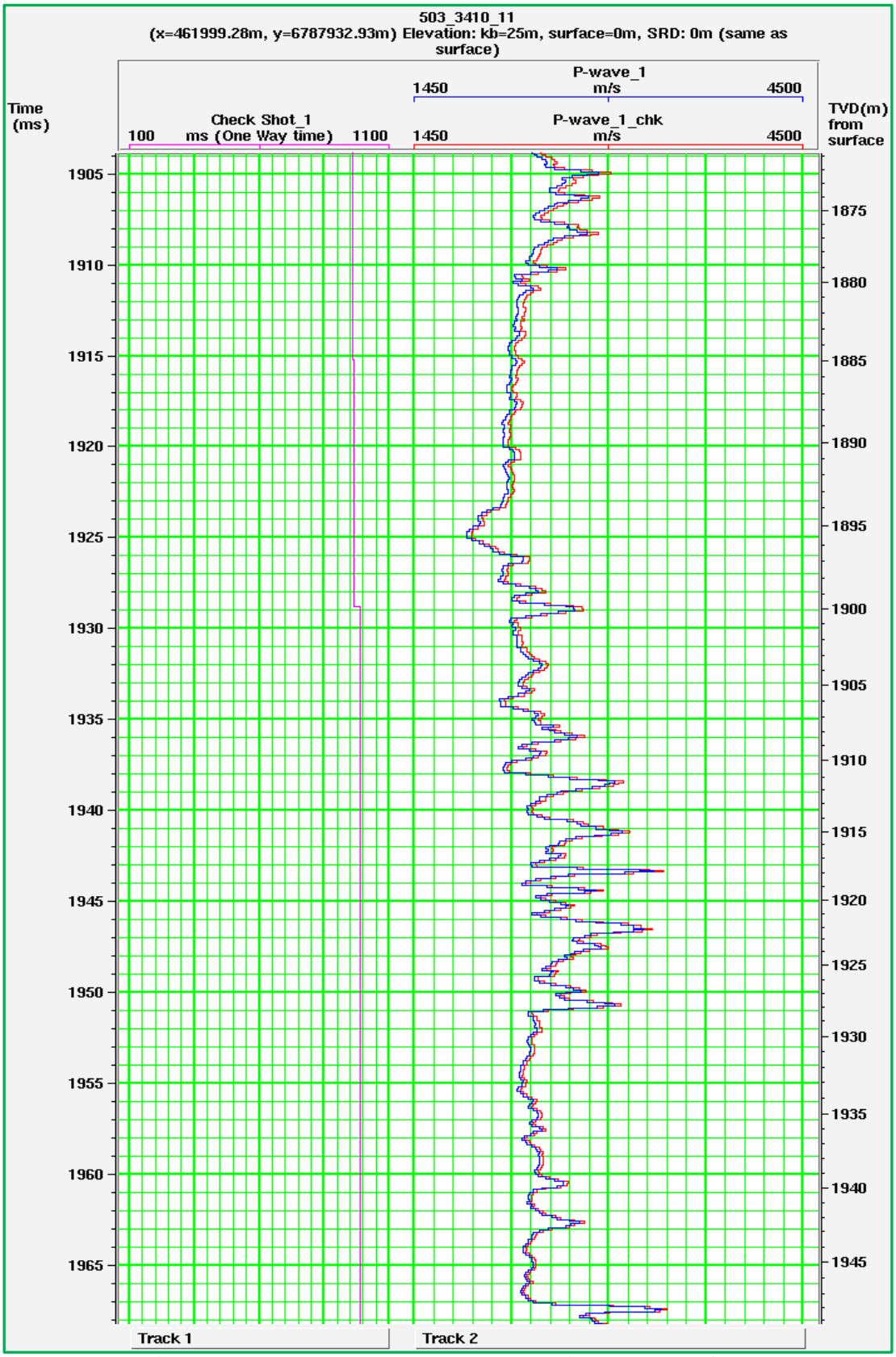

Figure 3.3: Results of applying check-shot velocities on P-wave velocity log for well 11. In the first track or panel is the checkshot log, in the second track, the blue curve is the resulting P-wave curve after applying check-shot data on the original (blue) P-wave log. The checkshot corrected data for this well is questionable because the resulting curve is higher than the original curve; how can the checkshot corrected data be higher than the sonic data?

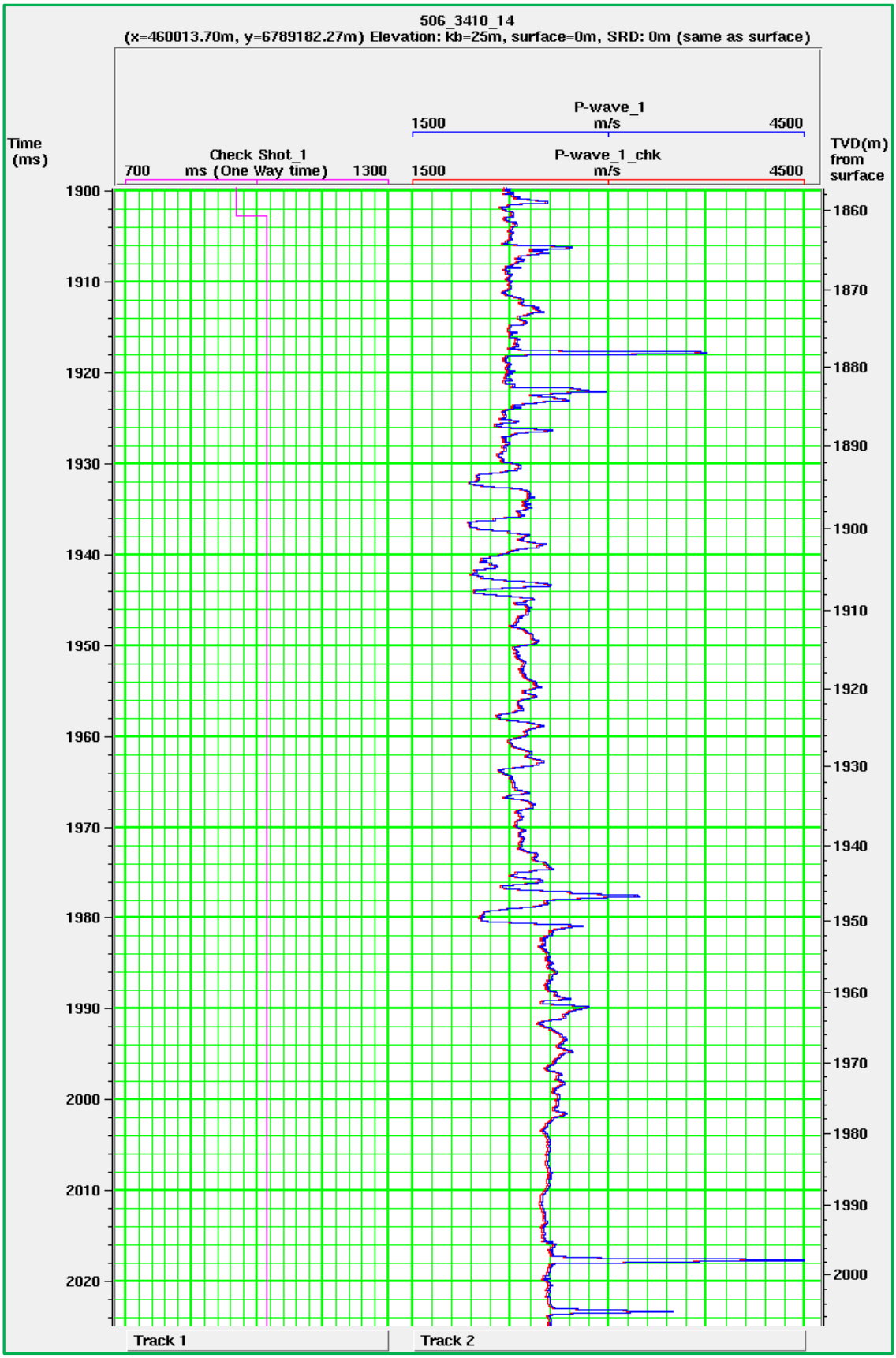

Figure 3.4: Results of applying check-shot velocities on P-wave velocity log for well 14. In the first track or panel is the checkshot log, in the second track, the blue curve is the resulting P-wave curve after applying check-shot data on the original (blue) P-wave log. In this case the difference between the original curve and the result is small, this means the drift between the sonic and checkshot was very small.

b) De-spiking:

Spikes in well log data can be caused by a number of factors, for instance:

- Ultra thin beds can cause constructive interference between the signals from the top and bottom boundaries of the thin bed (this is equivalent to what is known as "thin-bed tuning" in seismic theory).
- Fractured corridors: When an acoustic wave reaches a fluid filled fracture, part of it reflects back into the rock and part changes to a fluid wave in the fracture. When the fluid wave reaches the opposite fracture wall, there is further reflection loss and conversion back into compressional, shear and Stonely waves (Henderson, 2011). This can lead to spikes especially if the fractures are thinner (as is usually the case) than the log resolution
- Cycle-skips: this occurs due to failure of the instrumental transponder to detect signal levels that are above the preset threshold at the instance of the first cycle. This may also cause abnormally low readings against an otherwise high background.

Irrespective of their origin, spikes are often undesirable in data because they represent data that is either erroneous or that is outside the log (and seismic) resolution. There are a number of ways to remove spikes from the well logs. Those that are available in e-log^{TM} (the log editing module of Hampsom-Russell software) and also described by Handerson (2011) include the following:

1. **Manually editing** the section around the spiky section of the log. This method is excellent for removing obvious cycle-skips over short intervals but is tedious for long sections.
2. **Deleting sections** of bad data and replace with realistic values or interpolate between the top and bottom of the deleted interval. This may facilitate creation of synthetics, but valuable information may be lost.
3. Using **filters** to remove questionable data; examples of such filters include:
   - **3.1 Moving/running average filter**: This method smoothes out noise spikes but retains "relics" of bad data such as cycle skips and negative values. However the method degrades the vertical resolution of the log.
   - 3.2 The **median filter:** "this filter replaces the sample value at the center of the filter 'operator length' with the median of the sample values contained within the operator length" (Hampson-Russell, 2004). This method reduces curve variance in the filter window and eliminates unrealistic values. However, valid data is "clipped" from peaks and troughs in thinly bedded formations.

4. **Replacing bad sections** with rock physical estimates from other logs, for instance a poor sonic section can be deleted and replaced by one synthesized from resistivity (see section 3.1.3 for further discussion on log synthesis).
5. **Blocking:** Blocking a set of logs means replacing portions of them with one or more blocks, simplifying the logs and allowing them to be easily edited. This process can be used to remove anomalous spikes (Hampson-Russell, 2011). This is actually up-scaling (to which we return in section 3.1.2) in itself since the measured "instantaneous" value is replaced by a single value for the entire block size.

Results and discussion:

In figures 3.5, 3.6 and 3.7 results of de-spiking P-wave logs of wells 3, 11 and 14 are presented. The Check-shot data was first applied on each of the sonic logs before applying the "de-spiking" filter(s). The velocity logs were very spiky especially in the reservoir zones, this could be due to presence of thin cemented beds against a background of an otherwise clean sandstone reservoir zone, but it could also be due to processing artifacts or instrumental problems and mis-measurements during acquisition. Efforts were made to reduce, rather than eliminate the spikes, first using a *median* filter and then a *moving average* filter. The aim was to compare and discern the capabilities of the two techniques.

In some cases the *median* filter may be preferred while in other cases the *moving average* filter may be preferred because of the reasons that were earlier discussed. For instance, in well 3, there is a spike (encircled in red on figure 3.5) at 1796 seconds, the spike is nearly $4500ms^{-1}$. The spike was reduced to well below $3000ms^{-1}$ using the *median* filter, but it remained well above $3000ms^{-1}$ when filtered using the *moving average* filter. If it indeed is an unwanted spike, the *median* filter can be better but if it is real thin bed then the median filter would have cut it too short. Paradoxically, the *moving average* filter which maintains a higher value of the spike would still be worse if it were a real thin bed. This is because the *moving average* filter degrades the vertical resolution as can be seen in the result in figure 3.5 (see the spike encircled in red in the rightmost panel/track).

This demonstrates that it is very difficult to decide from the beginning which despiking method is more suitable for a particular formation. Therefore, the petrophysicist needs to seek additional guidance from other geological information or to compare the results with other borehole seismic (Vertical seismic profiling) data which are acquired at frequencies lower than sonic.

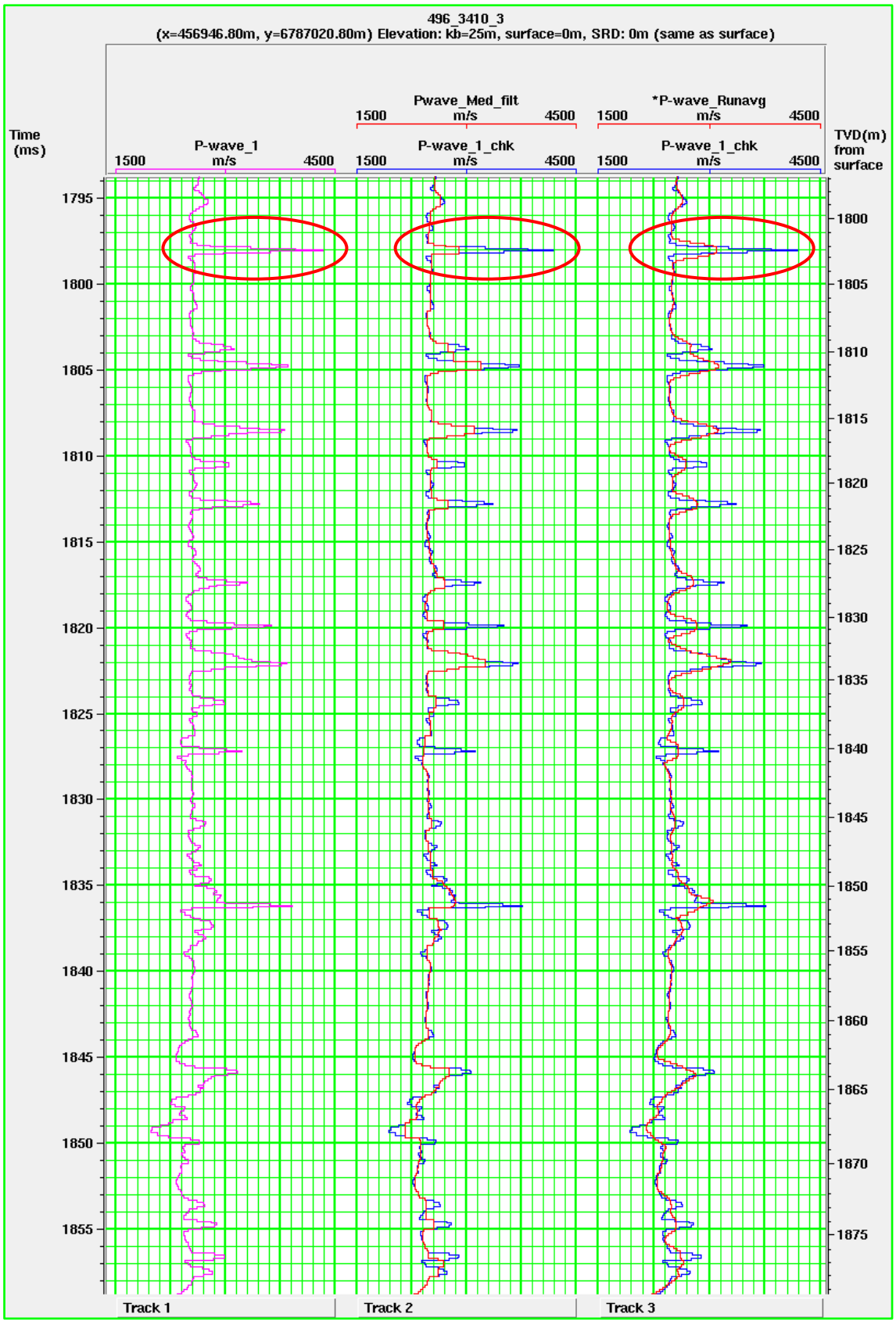

Figure 3.5: Results of de-spiking the P-wave log for Well 3, in the first panel (or track) is the original V_P log. In the second and third panels the red curve is the despiked log using a median filter and moving average filter, respectively; the blue curve is in both cases the V_P curve after applying checkshot data. The spike which is encircled in red is referred to in the text.

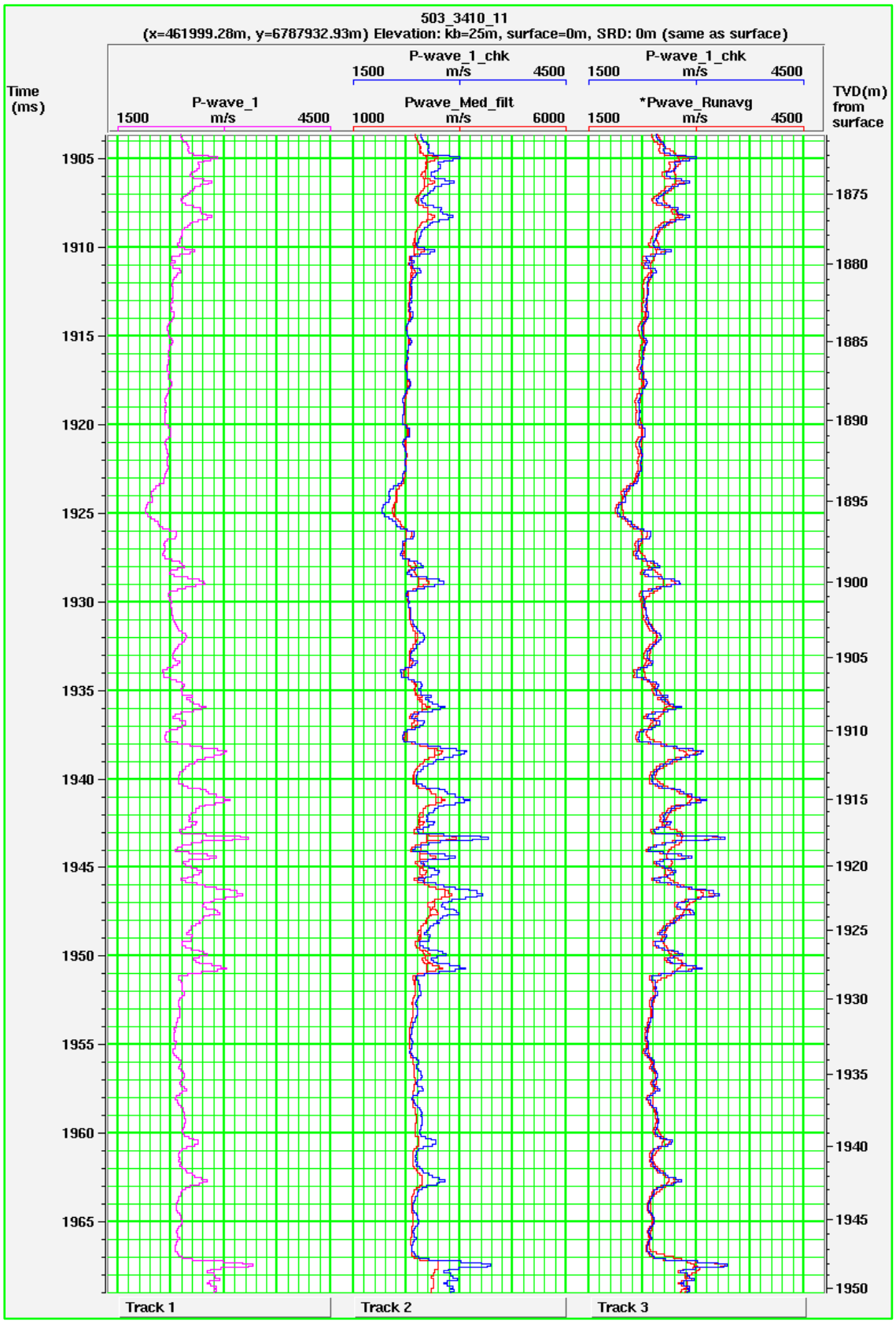

Figure 3.6: Results of de-spiking the P-wave log for Well 11, in the first panel (or track) is the original V_P log. In the second and third panels the red curve is the despiked log using a median filter and moving average filter, respectively; the blue curve is in both cases the V_P curve after applying checkshot data.

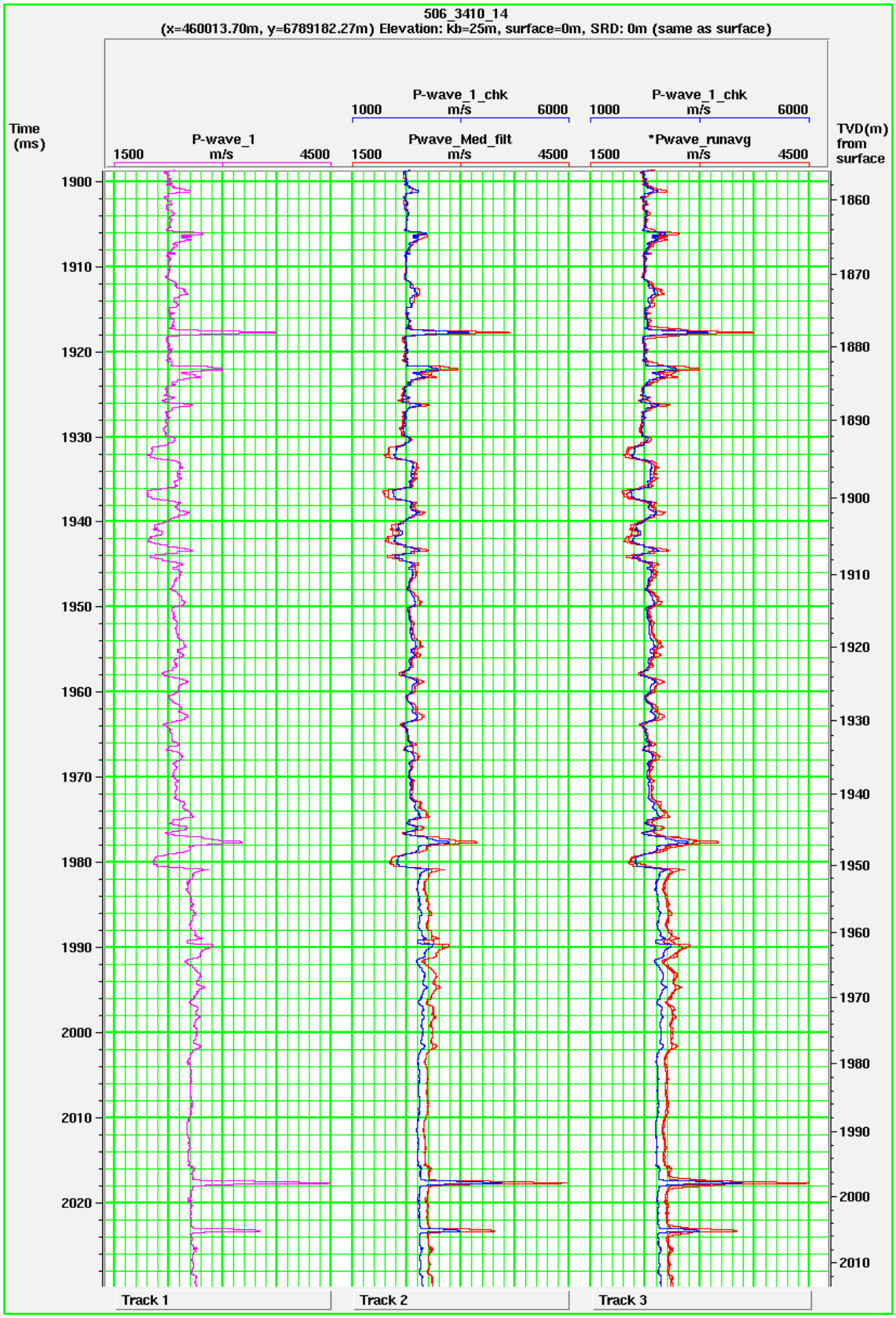

Figure 3.7: Results of de-spiking the P-wave log for well 14, in the first panel (or track) is the original V_P log. In the second and third panels the red curve is the despiked log using a median filter and moving average filter, respectively; the blue curve is in both cases the V_P curve after applying checkshot data.

3.1.2 Up-scaling well logs to seismic scale

The elastic properties of rocks are scale-dependent (figures 3.8 and 3.9) and in order to use the properties measured at one scale to solve problems at another scale, a scaling procedure is needed. For example, a prediction of properties from sonic (e.g. 2kHz) to seismic (e.g. 50–100Hz) frequency means a prediction of properties at a tens-of-meters scale from the properties measured at a tens-of-centimeters scale because well data is measured to the order of tens of centimeters while seismic data samples rock properties at a scale of the order of tens of meters. If the properties are predicted from a smaller to larger scale, this procedure is called upscaling, a prediction from a larger to smaller scale is called downscaling (Chesnokov et al., 2010). Upscaling is in this context thus defined: "the theoretical prediction of rock's elastic properties at lower frequency (seismic or cross-well data) using higher frequency logging data like sonic velocities (V_P, V_{S1} and V_{S2}), porosity and density (Bayuk et al., 2008). It is purely "a tens-of-centimeters to tens-of-meters problem" (Lindsay and Koughnet, 2001), as can be seen in figures 3.8 and 3.9.

Robust methods are required to predict the reservoir properties on a lower frequency or coarser scale to capture the influence of fine-scale structures that are seen at higher frequency sampling. Most of these methods are based on the effective medium theory; the effective medium theory allows one to find an effective stiffness tensor (which is in turn related to all known reservoir properties) relating, via Hooke's law, the strain and stress fields averaged over a representative volume (Tiwary et. al., 2009). This theory makes it possible to find the macroscopic (effective) physical properties (elastic and transport) of a heterogeneous, statistically isotropic medium, assuming that the wavelength is much greater than the size of heterogeneity (Chesnoskov et al., 2010). Heterogeneous is in this context referring to pores, cracks and voids (differentiable on the basis of their aspect ratio, "AR") and the preferential mineralogical and depositional orientation of the rock grains (anisotropy). These are the factors that count towards frequency dependence of elastic-wave velocities caused by scattering, intrinsic attenuation and internal dissipation (in form of heat), which is the reason why the resolution changes with frequency. There are a number of upscaling methods adapted to correct for one or more of these phenomena, three of which are considered in this research.

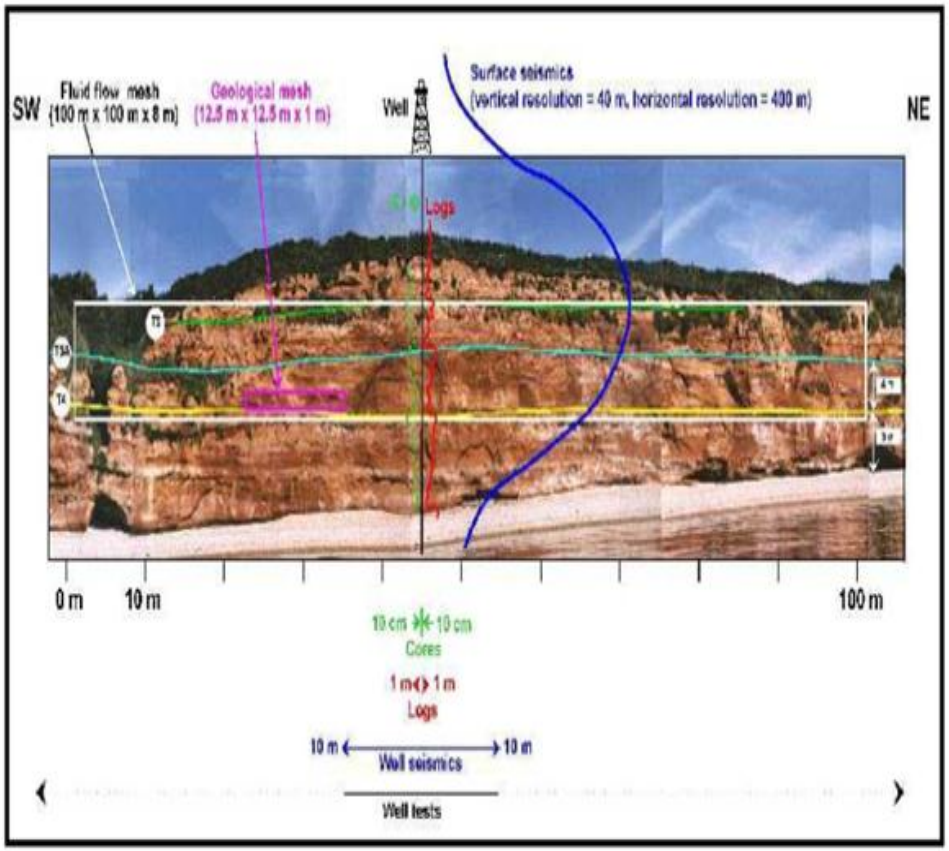

Fig. 3.8 The various subsurface data at different scales, adapted from Jakobsen, 2011

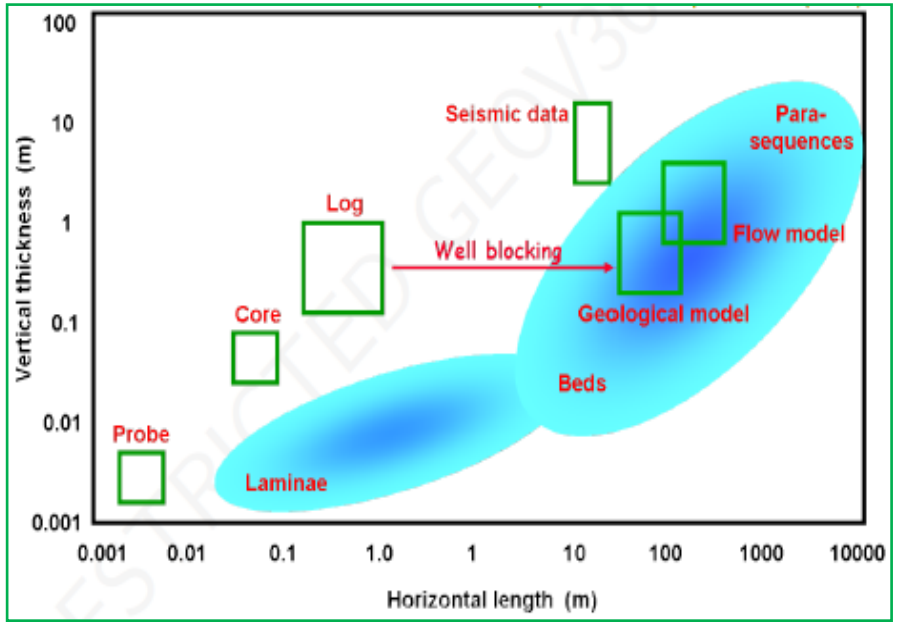

Fig. 3.9 Well blocking upscales the well logs, to match seismic data (and other higher scale data), adapted from Rivenæs, 2011

Figure 3.8 shows that well log data are to the order of tens of centimeters (1 meter), on the other hand seismic data is to the order of tens of meters (on a vertical scale). To integrate such data sets we need to either downscale the seismic data to the well log scale or to upscale the well logs to the seismic scale. In this research, we used the "blocking in conjunction with simple averaging" technique to upscale well log data to seismic scale so that the two data sets could be integrated.

First we note that there are two approaches to re-sampling of well data: Blocking and running window approach. The former involves subdividing the entire length of the log into sections called blocks, the measured samples within the block are "averaged" and the result is assigned to the given block. In the running window approach, the wavelength of the P-wave is calculated from V_P and density logs available at a given depth; a window whose size is equal to the wavelength is set up centered at that depth. The properties within the window are assumed to constitute a statistically homogeneous medium so that an "*average*" value is calculated and the result assigned to the centre of the window (figure 3.10). The advantage of using the running window approach is that no artificial blocks or layers are introduced (fig 3.11); but because of the sequential nature of the running window approach, the computational demands are more intensive and time consuming. In a personal communication with Nnamdi S. Nwaneri (Senior Petrophysicist at Statoil, August 28th, 2011), he pointed out that most commercial upscaling software packages use blocking as opposed to the running window approach to minimize computation times. The e-log module of Hampson-Russell software that was used in this research has both the running window (average) and blocking approach.

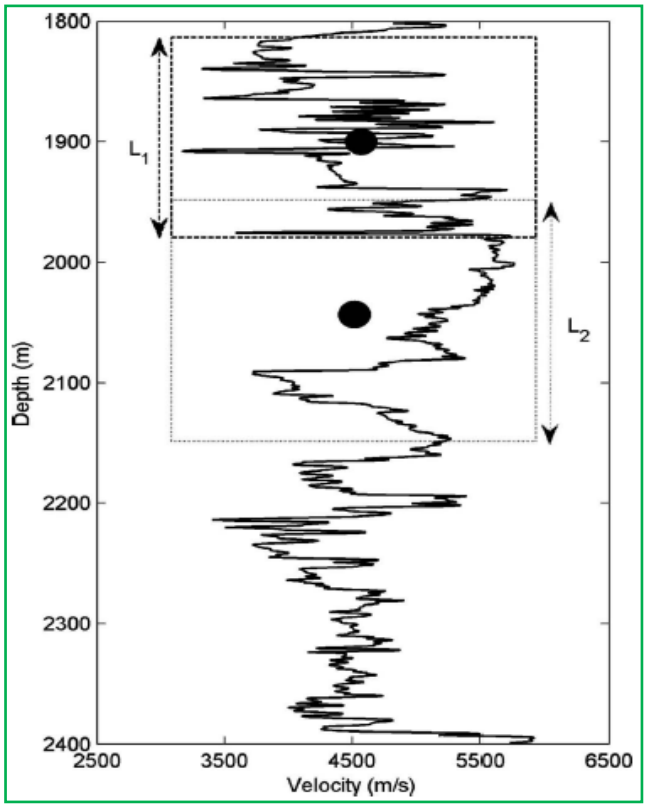

Figure 3.10: "Schematic of the running window concept. The averaged property inside the dashed window of length L_1 is shown by a dark solid circle. Then the window moves downward to the next location, represented by a dotted window where the length of the window is L_2 and the averaged property inside this window is shown by the next (lower) dark circle." – figure and caption adapted from Tiwary et al (2009)

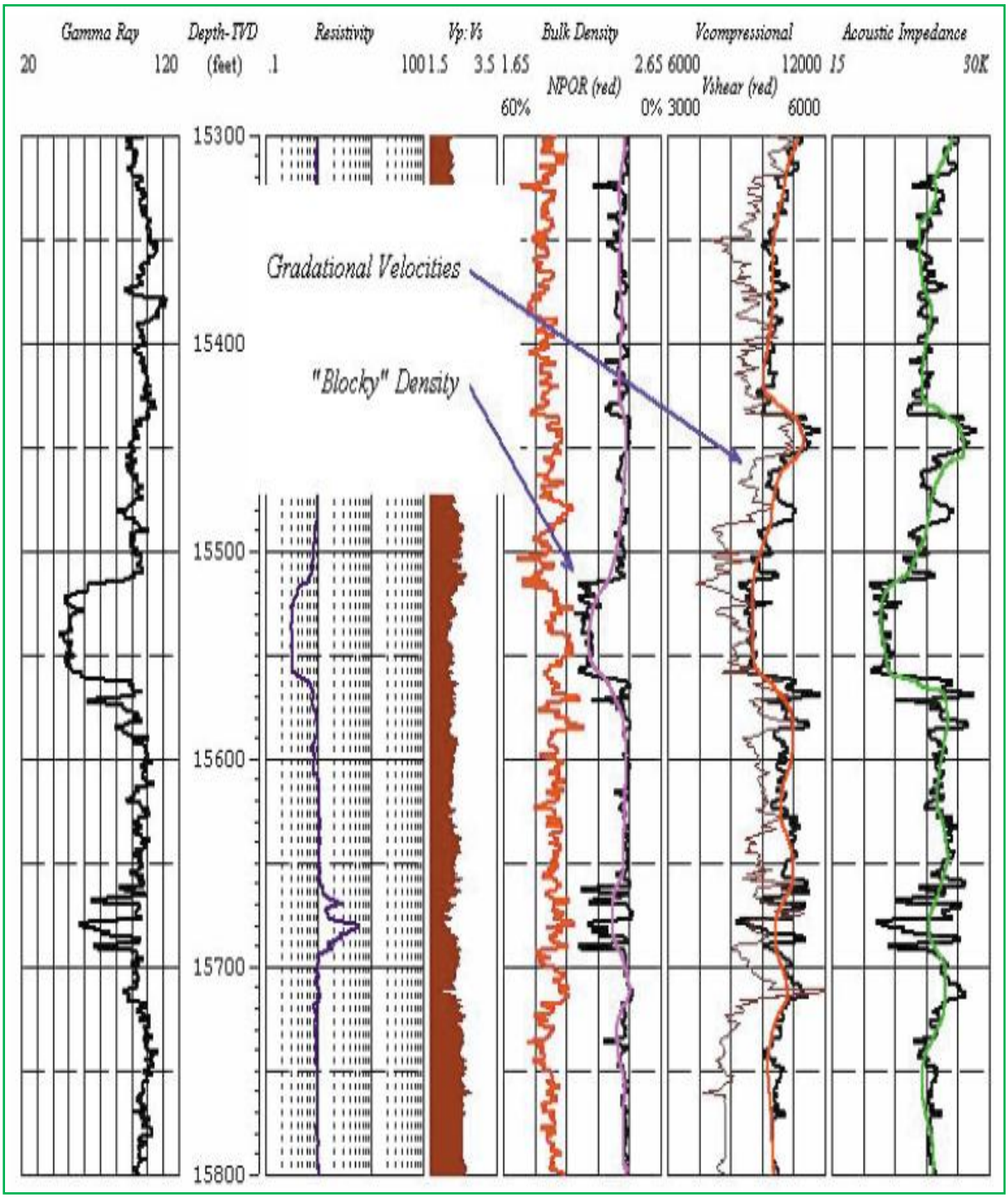

Figure 3.11: "The advantage of Sequential Backus Averaging is that no artificial "blocks" are introduced into the geology during the upscaling of the well-log data. In this example the density log is blocky, but the compressional- and shear-wave velocity logs have gradational tops and appear thicker. Blocking would distort the amplitudes. Furthermore, if blocking were based solely upon either the density or the sonic curves, the result would be wrong for the other curve" – figure and caption adapted from Lindsay et al 2001.

To "*average*" the physical properties is in this context the actual upscaling i.e. the computation of the effective (rock) property and re-assigning it to the appropriate block or center of the running window. Tiwary et al. (2009) compared the three most commonly used upscaling methods, that is:

(1) Simple averaging

(2) Backus averaging (this is good for anisotropic and thin-layered media)

(3) The pair correlation function (PCF) method of random media theory. This is recommended for strong multi-scale heterogeneities.

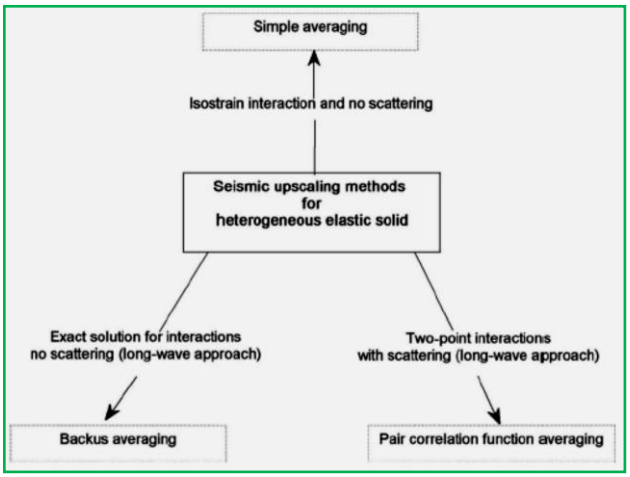

Figure 3.12: Physical basis behind simple, Backus and Pair correlation function averaging/upscaling methods. Adapted from Tiwary et al (2009).

Lindsay and Koughnet (2001) and Earthworks (2003) showcased examples using the Backus averaging technique. A more recent comparative study of all these three methods was conducted by Tiwary et al. (2009), (figure 3.12). The mathematical background behind these methods is hereby left out for simplicity; otherwise it has been outlined by among others: Bayuk et al. (2008), Chesnoskov et al. (2010), Tiwary et al. (2009) and Mavko et al. (2009). Hereunder is a three-step generalised upscaling algorithm, albeit, solely based on the simple averaging technique in order to keep the mathematics to a minimum:

Step 1: Extract the dynamic bulk and shear moduli from the original V_P, V_S and ρ :

$$K = \rho\left((V_P)^2 - \frac{4}{3}(V_S)^2 \right) \tag{3.1}$$

$$\mu = \rho(V_S)^2 \tag{3.2}$$

Step 2: Compute the upscaled density, ρ^*, bulk modulus, K^*, and shear modulus, μ^* to be assigned to every centre of the running window. The simple averaging technique uses

the Voigt isostrain model whereby at each point of the heterogeneous medium we neglect the deviation of actual strain field from the strain field averaged over a representative volume (Tiwary et al., 2009), so that we have:

$$K^* = \langle K \rangle \equiv \frac{1}{L}\sum_{i=1}^{N} L_i K_i \tag{3.3}$$

$$\mu^* = \langle \mu \rangle \equiv \frac{1}{L}\sum_{i=1}^{N} L_i \mu_i \tag{3.4}$$

$$\rho^* = \langle \rho \rangle \equiv \frac{1}{L}\sum_{i=1}^{N} L_i \rho_i \tag{3.5}$$

Where K_i, μ_i, and ρ_i are, respectively, the bulk and shear moduli and density of the i^{th} layer within the averaging window of thickness, L

Here, the angle brackets indicate volume averaging over a presumably statistically homogeneous layer within the medium. If the blocking approach is chosen, the effective property is assigned to the entire length of the block.

Step 3: Compute the upscaled velocity fields (V_P^* and V_S^*) from the relations below:

$$V_P^* = \sqrt{\left(K^* + \frac{4}{3}\mu^*\right)\Big/\rho^*} \tag{3.6}$$

$$V_S^* = \sqrt{\mu^*/\rho^*} \tag{3.7}$$

Note that the actual upscaling formulae will vary if another averaging method (e.g. Backus averaging or PCF) is chosen, but the entire upscaling recipe is quite standard.

In this research we employed the blocking approach on P-wave and density logs of the three wells (well 3, 11, and 14). The results and discussion(s) follow.

Results and discussion(s):

Figure 3.13, 3.14 and 3.15 show results of up-scaling the P-wave and density logs using the blocking technique.

- Blocking uses one log as the ‘base log’ upon which all the other logs are blocked; the disadvantage is that the other log will not be very accurate; this normally results in poor estimation of the other log by this method. This is one of the shortfalls of this method. In this case the P-log was the ‘base log’, consequently the density log was poorly estimated see for instance the section between 1770 and 1760 ms (Two way time, TWT) for *well 3* (figure 3.13) and between 2020 and 2125 ms (TWT) for *well 14* (figure 3.15). If the density log is instead used as the base curve the P-wave log would also be inaccurate. It is always better to choose the base log to be the one that shows most variation with depth so that this degrading effect is on the less varying log.

- The other shortfall of this method is that the results are blocky as can be seen on figures 3.13, 3.14 and 3.15). In this respect, the running window and Backus averaging techniques are superior, albeit, computationally demanding hence a little more time consuming
- It is also clear that the re-sampling interval (called block size in the software) is very important. The smaller the block size, the closer the result does approximate the real curve. This is why the red curves (5 m block size) are closer to the real curves than the blue curves (10 m block size).

Figure 3.16 shows cross plots of the original and upscaled P-wave velocity against true vertical depth and the original and upscaled density logs against true vertical depth for *well 3*. The following observations can be made:

- Depth trends are not clear in the cross plots of the original curves. After applying a 10 m long upscaler, the trends are very clear. Interestingly, a 5 m upscaler shows a trend that is much similar to that of the 10 m long upscaler. This means that a 5m upscaler would give a closer approximation without losing as much information as would be lost using a 10 m upscaler.
- Therefore, it is not easy to choose the appropriate upscaler length without losing too much data and without retaining unnecessary details.

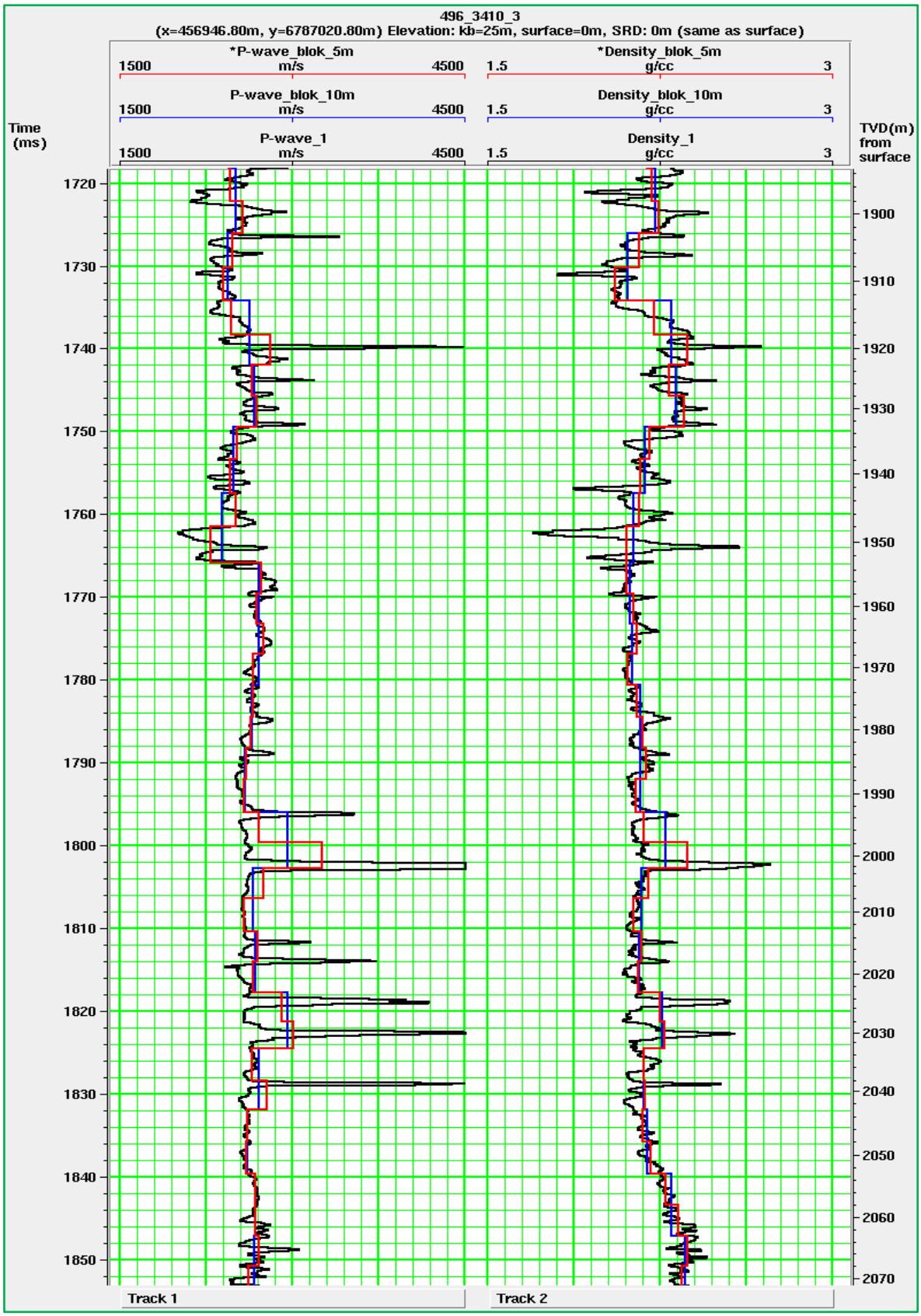

Figure 3.13: Results of blocking the P-wave and density log of well 3, track 1 shows the p-wave curves while track 2 shows density curves. The black curves are the original logs; the blue and red curves represent the logs that were blocked at 10 m and 5 m, respectively. As expected of the blocking method, the resulting logs are blocky. In this case, the base log is the p-wave curve, thus the density log is poorly redefined (see for instance between 1770 and 1760). The smaller the block size, the more accurate are the results. This is why the red curve is closer to the real curve than the blue curve.

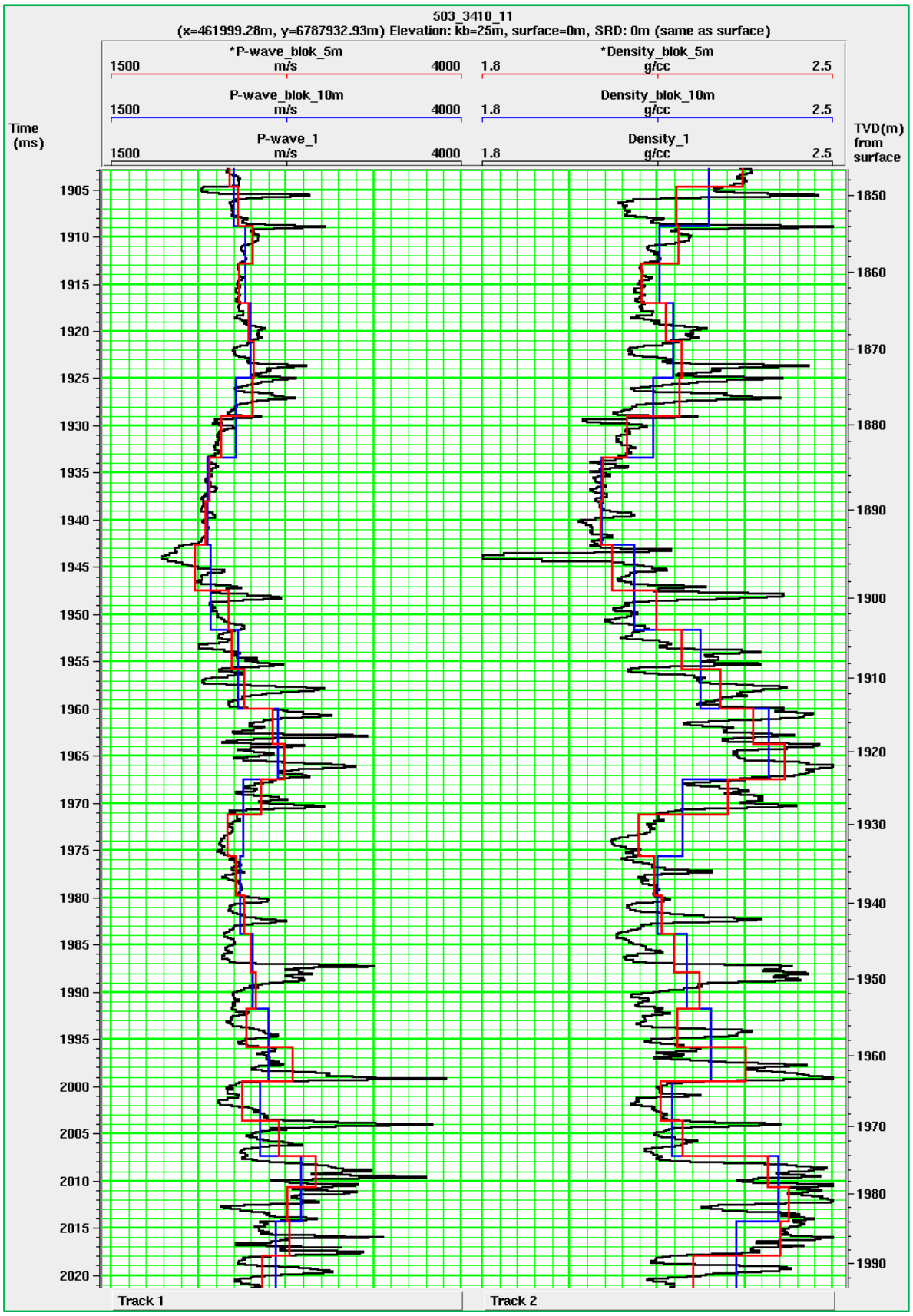

Figure 3.14: Results of blocking the P-wave and density log of well 11, track 1 shows the p-wave curves while track 2 shows density curves. The black curves are the original logs; the blue and red curves represent the logs that were blocked at 10 m and 5 m, respectively. The red curve which was resampled at 5 m is closer to the real curve than the blue curve which was resampled at 10 m.

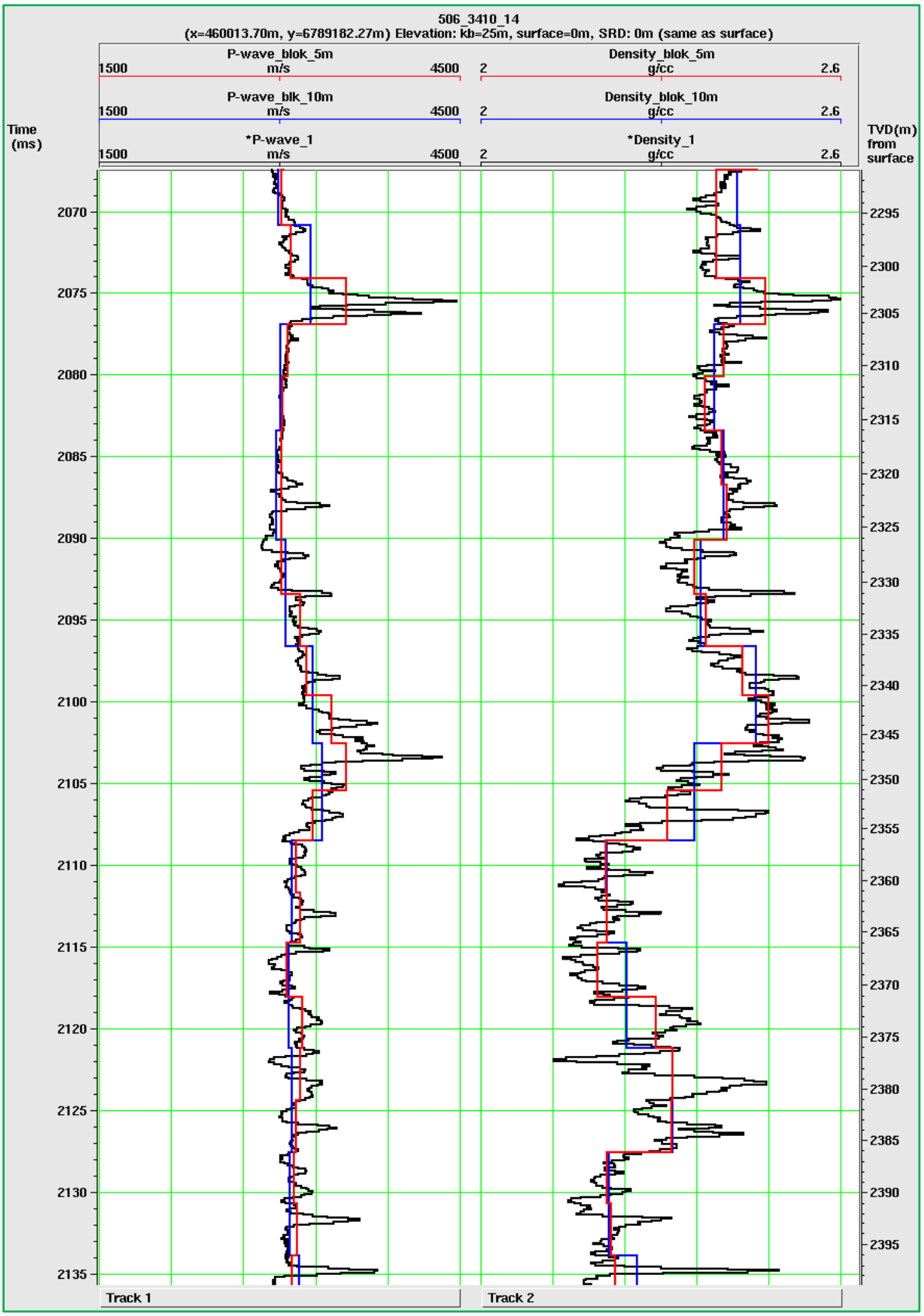

Figure 3.15: Results of blocking the P-wave and density log of well 14, track 1 shows the p-wave curves while track 2 shows density curves. The black curves are the original logs; the blue and red curves represent the logs that were blocked at 10 m and 5 m, respectively. As expected of the blocking technique, the resulting logs are blocky. In this case, the density log is poorly redefined (see for instance between 2120 and 2125 ms, TWT) because the base log was the P-wave

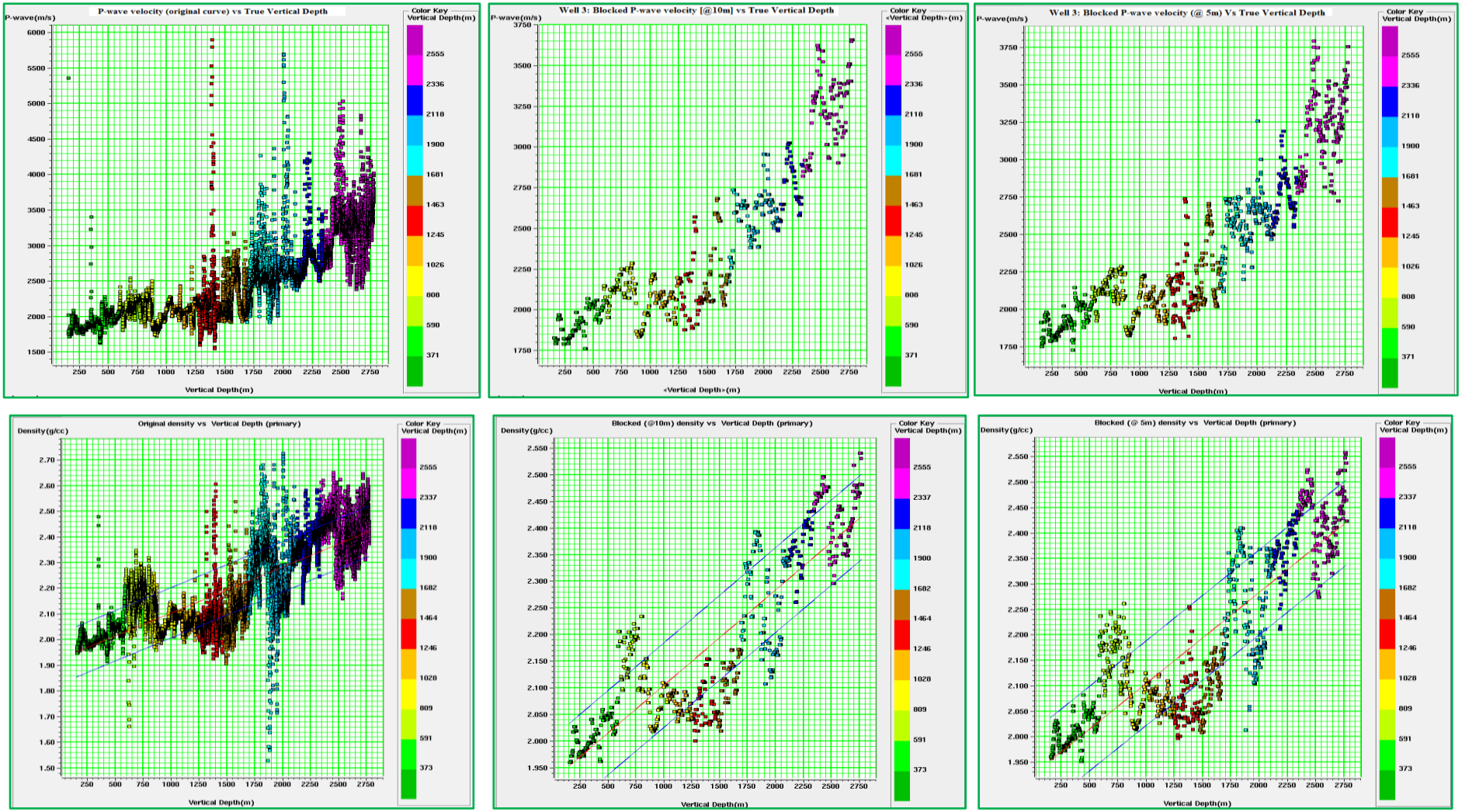

Figure 3.16: Cross plots of P-wave velocity against true vertical depth (in the upper row) and density against true vertical depth (in the lower row) for well 3. In the first (from left) column are the original curves, in the second and third columns are the curves upscaled at 10 m and 5 m respectively. Upscaling helps to more clearly and more accurately reveal the background trend. These results show that using a very long upscale could cast out a lot of data and yet a too short upscale may retain unnecessary details.

3.1.3 The missing logs: Petrophysical modeling

To accomplish a reservoir characterization project (inversion, rock physical and AVO modeling), at least seven input curves (logs) are required, these are:

- ⊗ P-wave sonic
- ⊗ Density
- ⊗ S-wave
- ⊗ Poisson ratio
- ⊗ Resistivity
- ⊗ Gamma Ray
- ⊗ SP (Self-potential)

Of the seven, Poisson ratio is customarily calculated from the P-wave and S-wave velocity; in other words it is not empirically determined. The other six should in principle be available as a complete suite of well log data; unfortunately this is not always the case (especially for old well data). This is because of one or more of the following:

- the immense cost of halting drilling limits the amount of time available for geophysical well logging, so that some tools may not be run over the entire borehole but only over the 'interesting' (reservoir) sections alone or not to be run altogether.
- Some logs may turn out to be too bad (noisy) to be of any value: this may for instance be due to instrumental problems.
- In case of very unstable formations, the drilling engineer has to immediately case (and cement) the hole whence dipmeter, resistivity image, nuclear magnetic resonance, and SP cannot be run. These are traditionally open-hole (i.e. uncased hole) logs.

So, what if some crucial logs are missing? In the words of Walls et al (2004): "missing log curves can often be computed with a reasonable degree of certainty. There are two major ways this is done. The first is through application of modern rock physics principles. For example, several deterministic methods exist for obtaining density from sonic logs or sonic logs from resistivity. The other approach is to use neural network technology. This is often required when no direct physical relationship is available." In this research empirically determined relationships were used to derive estimates of missing logs from those that were available. In particular, no S-wave velocity data was available for any of the wells used in this project; we will shortly demonstrate how to synthesize such missing logs.

The mathematics that goes into (some of) these petrophysical modeling algorithms and the results of applying the algorithms on our well logs follows:

a) Relationship Between P-wave Velocity and Density

There are two principle empirical equations for deriving P-wave velocity, V_P from density, ρ (or, in an inverse fashion, deriving density from P-wave velocity); they are named after the individuals who first published them:

Gardner's equation:

$$\rho = aV_p^b \tag{3.8}$$

where: a = 0.23

b = 0.25

Lindseth's equation:

$$V = a(\rho V) + b \tag{3.9}$$

where: a = 0.308

b = 3400 ft/s

Gardner's equation is the better known of the two equations, and it is applicable to a wide range of sedimentary rocks. Lindseth's, is a linear fit between velocity and acoustic impedance (ρV). It should be noted that the values of constants "*a*" and "*b*" stated above are "global" i.e. they are general values that were empirically derived by Gardiner and Lindseth after examining lots of data from various sedimentary basins. Luckily, it is possible to "localise" these relations to the area being studied by constraining/calibrating the constants to local conditions (see section 3.1.4 for further discussion); this produces more accurate logs than those obtained using these relations in their global form.

Results and discussion(s):

Figures 3.17, 3.18 and 3.19 show results of simulating a density log from a measured P-wave log for three wells (well 3, 11 and 14) using Gardner's relationship. The results show that the simulated curves are lower than the measured logs, but the general trend is similar on both curves. Where the input log is spiky or erroneous, the simulated data will be questionable (see for instance figure 3.19). If some curves are missing or damaged, this kind of modeling can provide a good starting point for further petrophysical studies and AVO modelling. If Gardner's relationship is 'localised', the accuracy of the simulated curves can improve. To this we return in section 3.14.

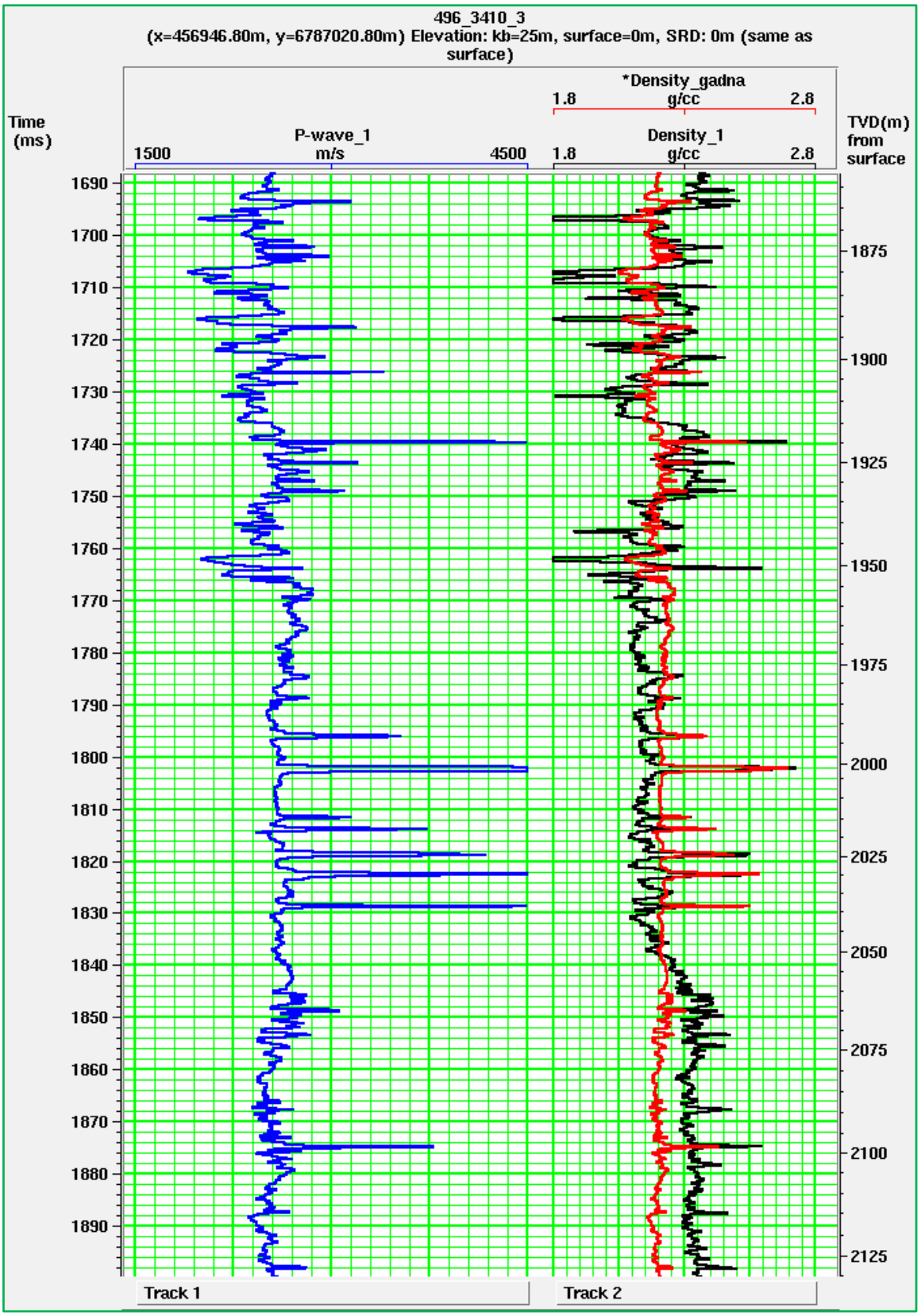

Figure 3.17: Well 3; a density log (red curve in track 2) synthesized from the P-wave log (blue curve in tack 1) using Gardner's equation. The black curve in track 2 is the measured density log. It can be seen that the simulated log is comparable to the actual log, although the density is underestimated in some sections of the log.

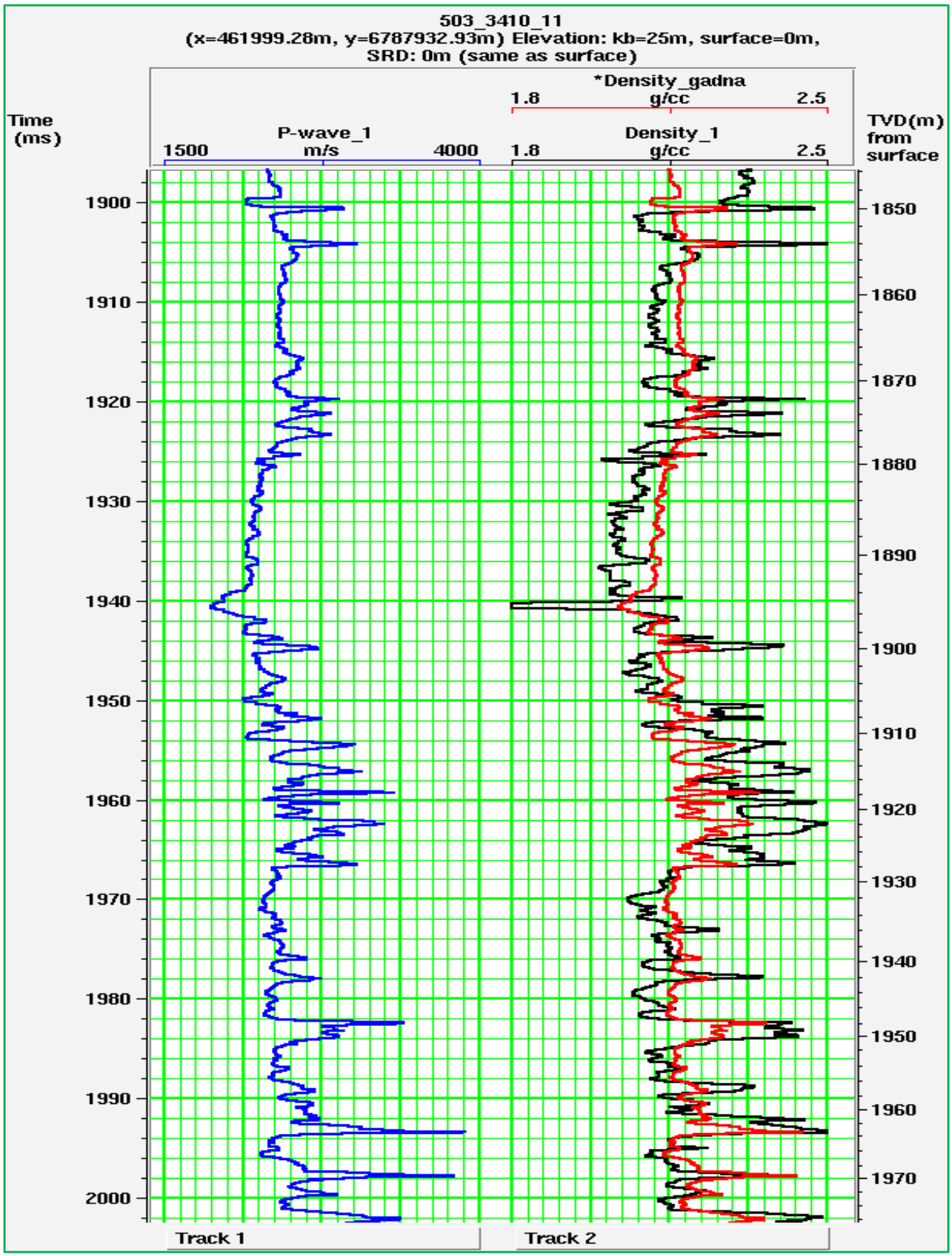

Figure 3.18: Well 11; a density log (red curve in track 2) synthesized from the P-wave log (blue curve in tack 1) using Gardner's equation. Again the simulated log (reed curve) is pretty close to the measured density curve; it can be a good starting point in case the real log is damaged or unavailable.

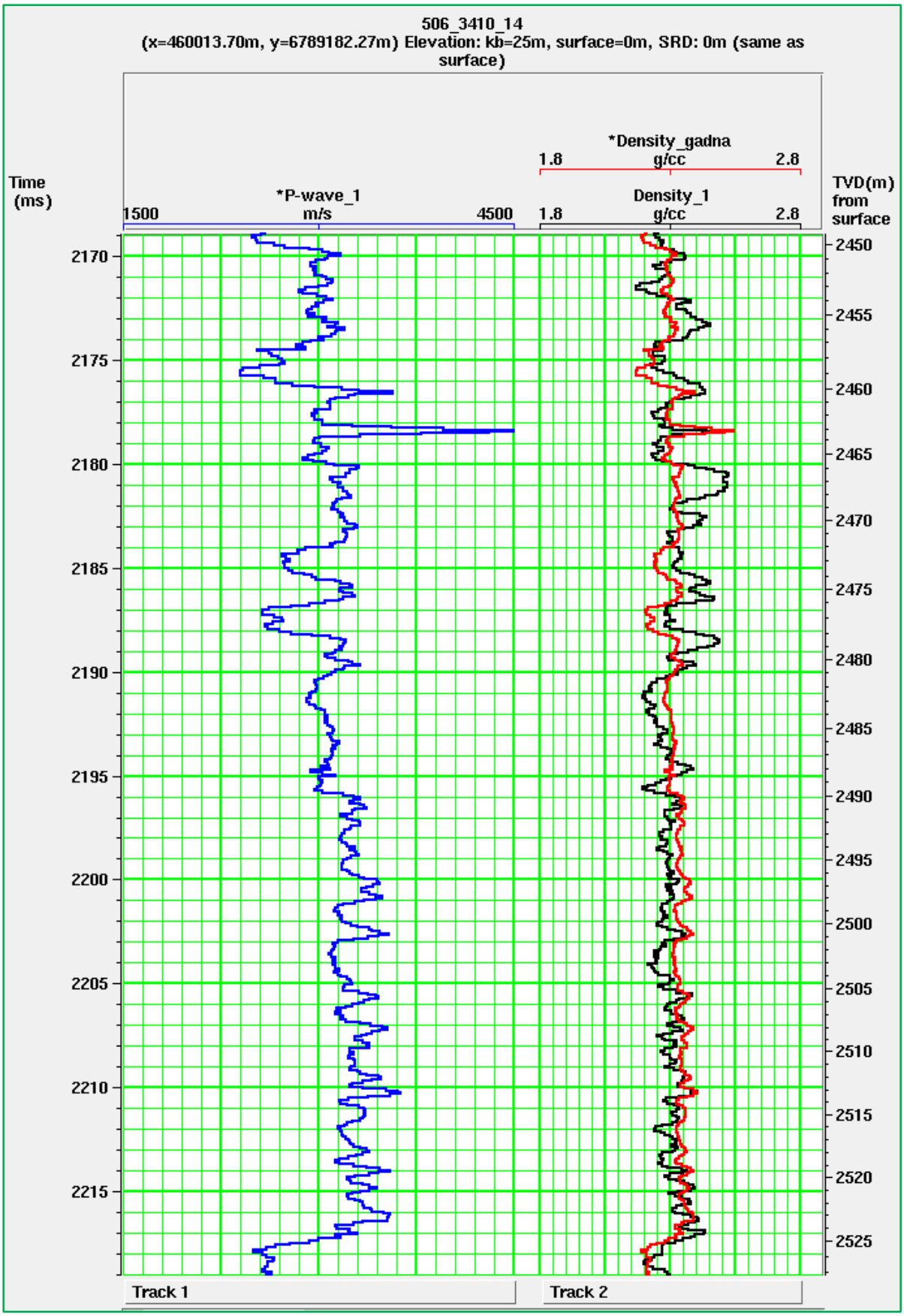

Figure 3.19: Well 14; a density log (red curve in track 2) synthesized from the P-wave log (blue curve in tack 1) using Gardner's equation. The black curve in track 2 is the measured density log. In this case the simulated curve and the measured curve are very close. However, the simulated curve is higher than the measured curve at 2178.5 ms (TWT). This may be because of the strong spike on the P-wave curve at the same TWT, this demonstrates that the accuracy of simulated logs depends on the accuracy of the input log(s).

b) Relationship(s) Between P-wave and S-wave Velocities

Castagna's Relationship: Castagna et al. (1985) derived an empirical relationship between P-wave and S-wave velocity, which can be written as:

$$V_P = 1.16V_S + 1.36 \quad (3.10)$$

(where the velocity is in km/s)

It is the most common method of shear velocity prediction; this relationship is also known as the mud-rock equation or the "ARCO mud-rock line". It should be noted that the parameters (regression coefficients) of the linear relationship between V_P and V_S were derived from worldwide data. Thus, if regional or local shear-wave velocity is available, a "local" mud-rock relationship can and should be derived to constrain the relationship to local conditions (see section 3.1.4 for details). And, this equation is **only valid** for the "wet case" that is for brine-filled formations, thus it is equally important to factor in the presence of other pore-filling fluids (oil and or gas) in the reservoir intervals if any (see section 3.1.5 for further discussion).

Krief's Relationship: Krief et al. (1990) suggested the following linear relationship between the squares of P-wave and S-wave velocity:

$$V_P^2 = aV_S^2 + b \quad (3.11)$$

"It is important to note that the regression coefficients "*a"* and "*b"* are different for distinct lithological zones" (Royle and Sandor, nd); those determined by Krief et al. (with the velocity measured in km/s) are as follows:

Table 2: Kreif's constants, adapted from Hampson-Russell (2004)

Lithology	a	b
Sandstone (Wet)	2.213	3.857
Sandstone (Gas)	2.282	0.902
Sandstone (Shaly)	2.033	4.894
Limestone	2.872	2.755

Again, these regression coefficients are "global," for more accurate predictions there is need to factor in the local conditions by performing regression analysis on the available well data to generate "local" coefficients (see section 3.1.4). Where the pore-filling fluids are different from those in the table, fluid replacement modeling can be done to further constrain the model (see section 3.1.5).

NB: In Hampson-Russell Fluid Replacement module, the Krief relationship is re-arranged into: $V_S = \sqrt{\frac{1}{a}V_P^2 - \frac{b}{a}}$ so that the corresponding constants are $\left(\frac{1}{a}\right)$ and $\left(-\frac{b}{a}\right)$, the corresponding values of these constants are as follows:

Table 3: Modified Kreif's constants, adapted from Hampson-Russell (2004)

Lithology	1/a	-b/a
Sandstone (Wet)	0.452	-1.743
Sandstone (Gas)	0.438	-0.395
Sandstone (Shaly)	0.492	-2.407
Limestone	0.348	0.959

Results and discussion(s):

The S-wave velocity was not measured in all the three wells that were used in this research; the S-wave curves that were supplied with this data set were computed by Rock Solid Images (RSI) using their commercial petrophysical modeling software (Geophysical well Log Analyis^{TM}). The RSI curves were used as the benchmark in this part of the research, they are thus referred to as the 'original or real' S-wave curve.

Castagna's and Krief's relationships were used to generate S-wave curves from P-wave curves of *well 3* (Fig. 3.20). In the hydrocarbon bearing zones, Krief's relationship gives a curve that is closer to the real S-wave curve than Castagna's relationship. This is because Castagna's relationship is only valid for brine-filled sands. In hydrocarbon filled formation(s) which are seismically slower than brine saturated sands, this relationship overestimates the S-wave velocity. In section 3.1.5, we will discuss how to factor in the pore-fluid effect on 'Castagna-derived' S-wave logs.

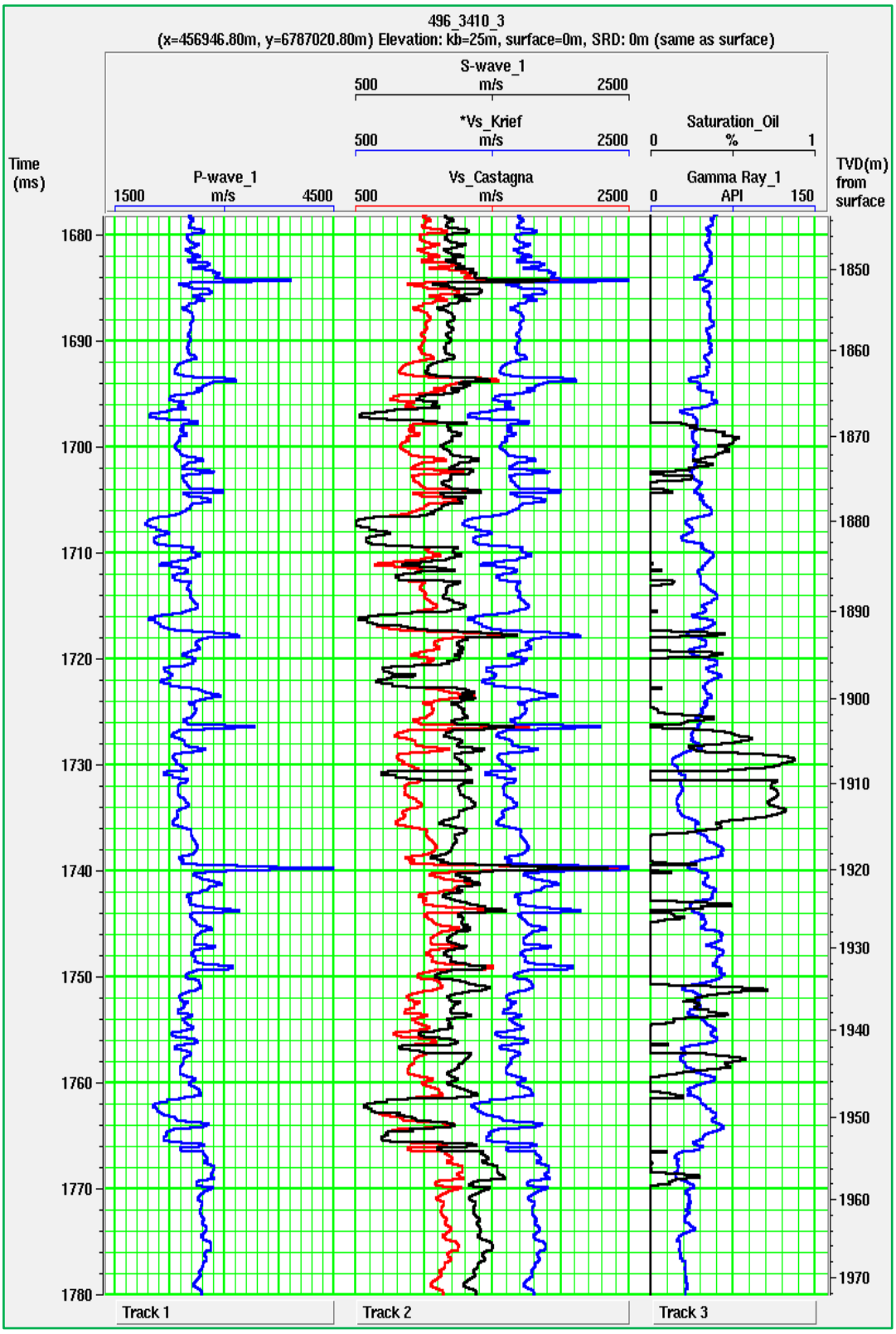

Figure 3.20: estimation of the S-wave velocity from the P-wave velocity of well 3 using Castagna's and Krief's relationship. In track 1 is the P-wave log, in track 2 the blue curve is from Castagna's relationship while the red curve is from Krief's relationship. The black curve in track 2 is the 'real' S-wave curve. Castagna's relationship overestimated the S-wave velocity in this hydrocarbon bearing interval because this relationship assumes a brine-filled formation. In track 3 is the oil saturation (black curve) and Gamma Ray log (blue).

c) Relationship Between P-wave Velocity and Resistivity

In many older fields, the only logs that are available are resistivity logs and it has been observed that, in wet clastic rocks, the resistivity log and the P-wave sonic tend to track each other. A number of empirical relationships have therefore been derived to allow the geophysicist to derive a p-wave sonic from a resistivity log (Hampson-Russell, 2004). The oldest and most widely used relationship is the one of Faust (1951); it reads:

$$V_p = a(Rd)^c \quad (3.12)$$

where: V_p = P-wave velocity

R = Resistivity value

d = Depth

a, c = constants

[In e-log module of Hampson-Russell, a = 1948, c = 1/6; these are the values derived by Faust. But in practice "a" needs not to be kept constant; it can be described either as a simple function of depth or as a zoned constant.]

There are a number of other empirical models that have been published and are available in the AVO Modeling, Pro4D Modeling, ProMC Modeling and Elog modules of the Hamspson-Russell software. They can be used to generate supplementary curves/logs that may be needed for specialized reservoir studies e.g. AVO modelling.

3.1.4 Rock physics control on log synthesis: Calibration to local conditions

The empirical relationships (Gardner, ARCO and Krief) in their "global" form tend to overestimate and sometimes to underestimate the missing logs/curves depending on the accuracy of the input logs. Figures 3.17, 3.18 and 3.19 give a comparison of the actual to density logs estimated from Gardner's equation to exemplify this phenomenon. The way around this is to develop relationships that are constrained to local conditions by means of petrophysical modeling. "Local conditions" is in this context referring to the lithology (including facies-to-facies and intrafacies variations) and pore fluid constituents of the rock formation being studied. This is possible if at least one or a few wells in the study area have any two complementary parameters that can be cross plotted to generate regression constants that are specific to that area. Whenever 'default' values in the modeling softwares are replaced by locally constrained constants, the empirical models should in principle better approximate the missing curves/logs. To get the best results, there should be sufficient well control data i.e. the *training data* should span a substantial portion of the areal (through multi-well modeling) and depth extent of the reservoir formation being studied. The procedures involved are hereby outlined, with examples.

1. Lindseth's relationship (equation 3.9) could for instance be re-written in this form:

$$\Delta t = c - d\rho \quad (3.13)$$

where: $\Delta t = 1/V_P$

$c = 1/b$

$d = a/b$

Using equation 3.13 it is possible to derive regression coefficients from a cross-plot of density, ρ against transit-time, Δt. The regression coefficients so obtained should principally better estimate the density.

2. Likewise, the values of the constants ("a" and "b") in Gardner's relationship (equation, 3.8) were empirically derived from a wide range of sedimentary rocks. It is possible to constrain this model to local conditions by transforming the 'global' equation into the following form:

$$\mathrm{Log}(\rho) = \log(a) + b\log(V_P) \quad (3.14)$$

It then is possible to determine "local" values of '*a*' and '*b*' by using ("least squares") regression line analysis. The local values are then used to construct a locally calibrated Gardner equation.

Results and discussion(s):

The procedure of localizing Gardner's equation is exemplified and further discussed in figures 3.21 and 3.22.

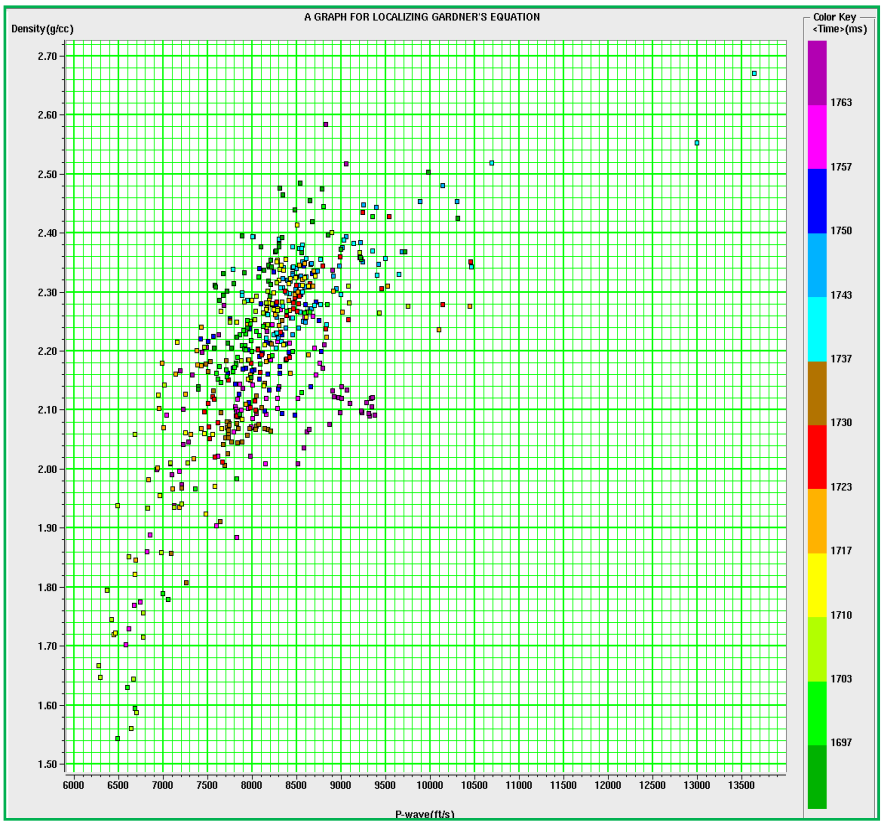

Figure 3.21: The first step in 'localizing' Gardner's relation is to cross plot the density against the P-wave velocity. The colour bar shows Two Way Travel time in milliseconds. The data is for well 3.

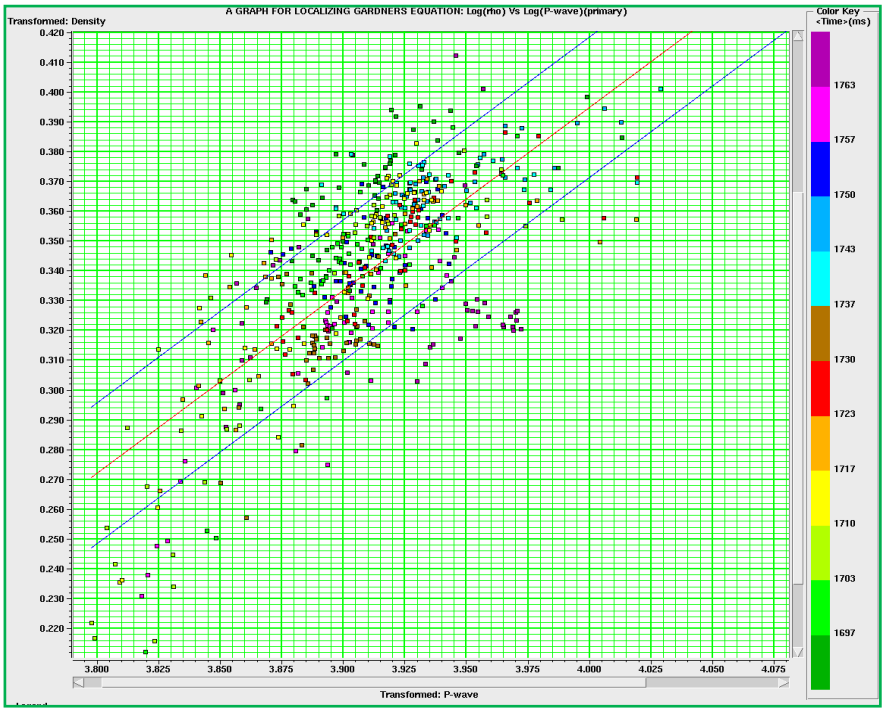

Figure 3.22: In order to derive local constants 'a' and 'b', the data and scales are logarithmised to produce a cross plot corresponding to equation 3.14. The local constants are used to formulate a local Gardner relationship which is then used to formulate a more accurate density log (see figure 3.23).

Figure 3.23 below shows a density log that was modelled using the global form of Gardner's relation (red curve) and a new curve which was synthesized using a localized Gardner equation (black curve). As expected, the 'localized' curve is a better approximate of the measured density (blue curve) than the 'global' curve.

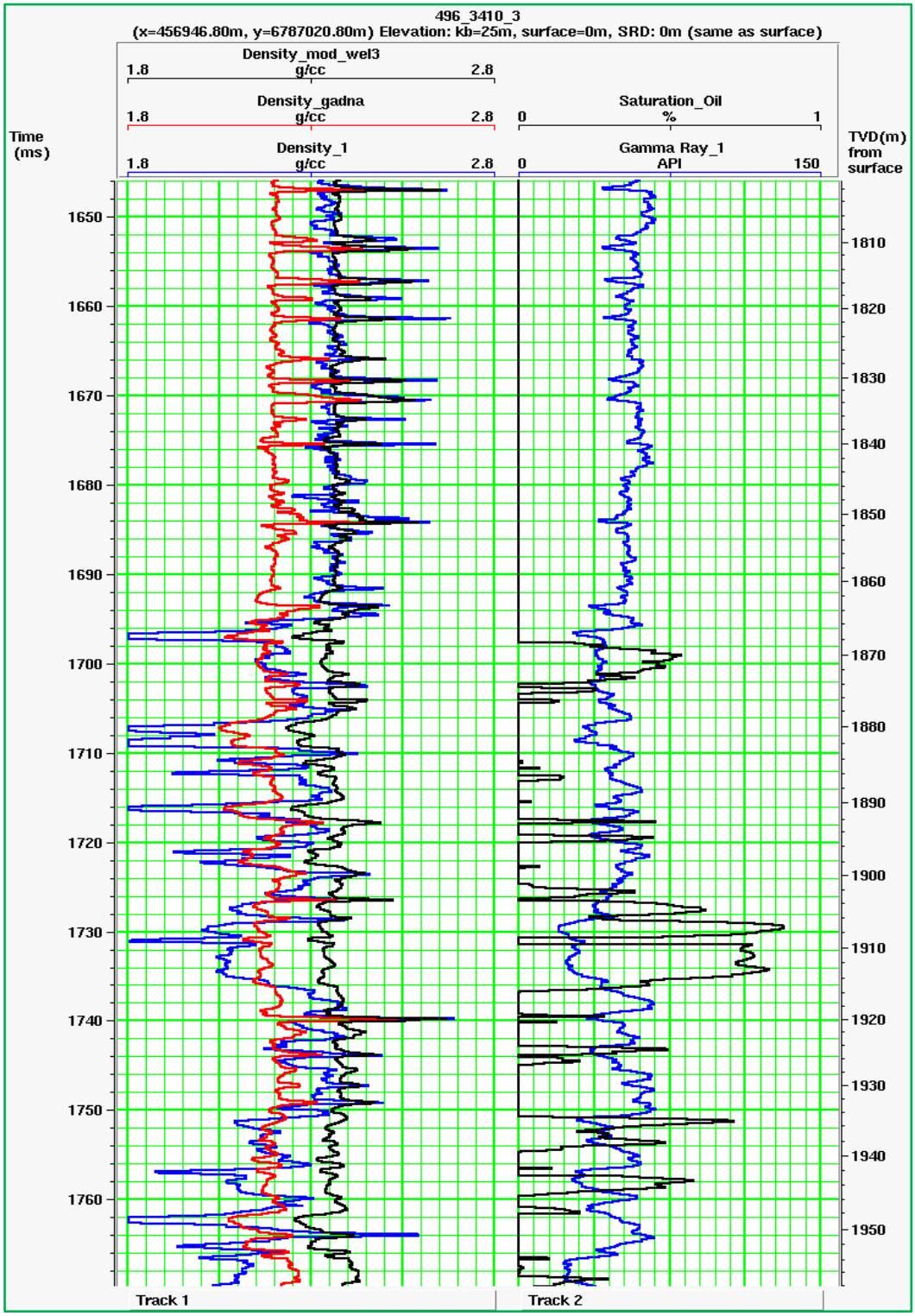

Fig. 3.23: The blue, red and black curves in track 1 are the measured (real), 'global' and 'local' density curves respectively. The black and blue curves in track 2 are, respectively, the oil saturation and Gamma ray logs. All the data is for well 3. The result indicate that 'localising' global empirical relationship is important; it improves the accuracy of the simulated logs in especially the reservoir zone.

3. For all the wells used in this research, the s-wave velocity was not measured. The s-waves curves that were supplied with the data were synthetically generated from P-wave data. This imposed a serious limitation in calibrating s-wave velocity prediction models to local conditions, hence heavily relying entirely on global relations. But the fact remains: "the global relationships (ARCO and Krief) tend to overestimate the shear-wave velocity whereas the local relationships (SP constrained and local mudrock) more accurately estimate the shear-wave velocities (Royle and Bezdan, nd). Because local or regional shear-wave information was not available, the global relationships were used in conjunction with Biot-Gassmann fluid replacement modeling to improve the shear-wave values in the reservoir interval (see section 3.1.5).

3.1.5 What if the pore fluids change? The Gassmann recipe

When Castagna's relation (section 3.1.3) is used to estimate the S-wave velocity from a P-wave log, the log so generated is based on the assumption that the pore-filling fluid is brine along the entire length of the bore hole. In case of a hydrocarbon bearing reservoir zone, the S-wave velocity will be overestimated since hydrocarbons saturated rocks are seismically much slower than brine saturated rocks. This is an example of a scenario where the conditions predicted by the mathematical model are different from the *in situ* conditions. Other reasons for discrepancies between the predicted and the *in situ* fluid saturations are mud-filtrate invasion and production, to these we will return a little later. Irrespective of the reason for pore fluid changes, fluid replacement modeling can be used to correct or at least account for any differences between the predicted and the *in situ* conditions. The fluid substitution algorithm that was used in this research was first published by Gassmann in 1951. The theoretical background of this algorithm is summarised below.

The Gassmann fluid replacement numerical model (as described by Avseth et al, 2005) begins with an initial set of velocities ($V_P^{(1)}$ and $V_S^{(1)}$) and densities ($\rho^{(1)}$) corresponding to a rock with an initial set of fluids, which we call "fluid 1." These velocities often come from well logs, but might also be the result of an inversion or theoretical model; in this study $V_P^{(1)}$ represents the measured (and subsequently conditioned) P-wave log while $V_S^{(1)}$ represents the "Castanga-derived" S-wave velocity. To replace one set of fluid(s) with another, fluid substitution is then performed as follows:

Step 1: Extract the dynamic bulk and shear moduli from $V_P^{(1)}, V_S^{(1)}$ and $\rho^{(1)}$:

$$K_{Sat}^{(1)} = \rho\left(\left(V_P^{(1)}\right)^2 - \frac{4}{3}\left(V_S^{(1)}\right)^2 \right) \tag{3.15}$$

$$\mu_{Sat}^{(1)} = \rho\left(V_P^{(1)}\right)^2 \tag{3.16}$$

Step 2: Apply Gassmann's relation (equation 3.17), to transform the bulk modulus:

$$\frac{K_{Sat}^{(2)}}{K_{Mineral} - K_{Sat}^{(2)}} - \frac{K_{fluid}^{(2)}}{\phi\left(K_{Mineral} - K_{fluid}^{(2)}\right)} = \frac{K_{Sat}^{(1)}}{K_{Mineral} - K_{Sat}^{(1)}} - \frac{K_{fluid}^{(1)}}{\phi\left(K_{Mineral} - K_{fluid}^{(1)}\right)} \tag{3.17}$$

Where $K_{Sat}^{(1)}$ and $K_{Sat}^{(2)}$ are the rock bulk moduli saturated with fluid 1 and fluid 2, while $K_{fluid}^{(1)}$ and $K_{fluid}^{(2)}$ are the bulk moduli of the fluids themselves.

Step 3: Leave the shear modulus unchanged:

$$\mu_{Sat}^{(2)} = \mu_{Sat}^{(1)} \tag{3.18}$$

Step 4: Correct the bulk density for the fluid change:

$$\rho^{(2)} = \rho^{(1)} + \phi\left(\rho_{fluid}^{(2)} - \rho_{fluid}^{(1)}\right) \tag{3.19}$$

Step 5: Re-compute the velocities using:

$$V_P^{(2)} = \sqrt{\left(K_{Sat}^{(2)} + \frac{4}{3}\mu_{Sat}^{(2)}\right) \Big/ \rho^{(2)}} \tag{3.20}$$

$$V_S^{(2)} = \sqrt{\mu_{Sat}^{(2)} / \rho^{(2)}} \tag{3.21}$$

Note: superscript (1) refers to "fluid 1" while superscript (2) refers to "fluid 2"

Results and discussion(s):

Figure 3.24 shows results of estimating an S-wave velocity log from a measured P-wave velocity log by use of Castagna's equation outside the reservoir zones and combining it (Castagna's relation) with Gassmann relation in the reservoir zone. The 'real' curve (black curve in track 1) was modeled by Rock Solid Images and is only included in the results for benchmarking our results. The 'Castagna' curve (blue curve in track 1) was derived from the measured P-wave velocity using the global form of Castagna's equation. The 'Pore Fluid Corrected' (red curve in track 1) curve is the one that was computed by using Castagna's equation outside the reservoir zone and combining it (Castagna's relation) with Gassmann's

equation in the reservoir zone. Also shown in figure 3.24 is a density curve generated from a P-wave curve using a localized Gardner equation (blue curve in track 2), this is juxtaposed with one that was generated by a combination of Gardner and Gassmann theory (red curve in tack 2) to correct for pore fluid effect in the reservoir zone. The black curve in track 2 is the measured density log. The correction on the density curve is very small because the density of brine and oil are not so different.

One important observation can be made: combining local (or global) empirical relations with Gassmann's Fluid replacement modeling improves the accuracy of the estimated well logs.

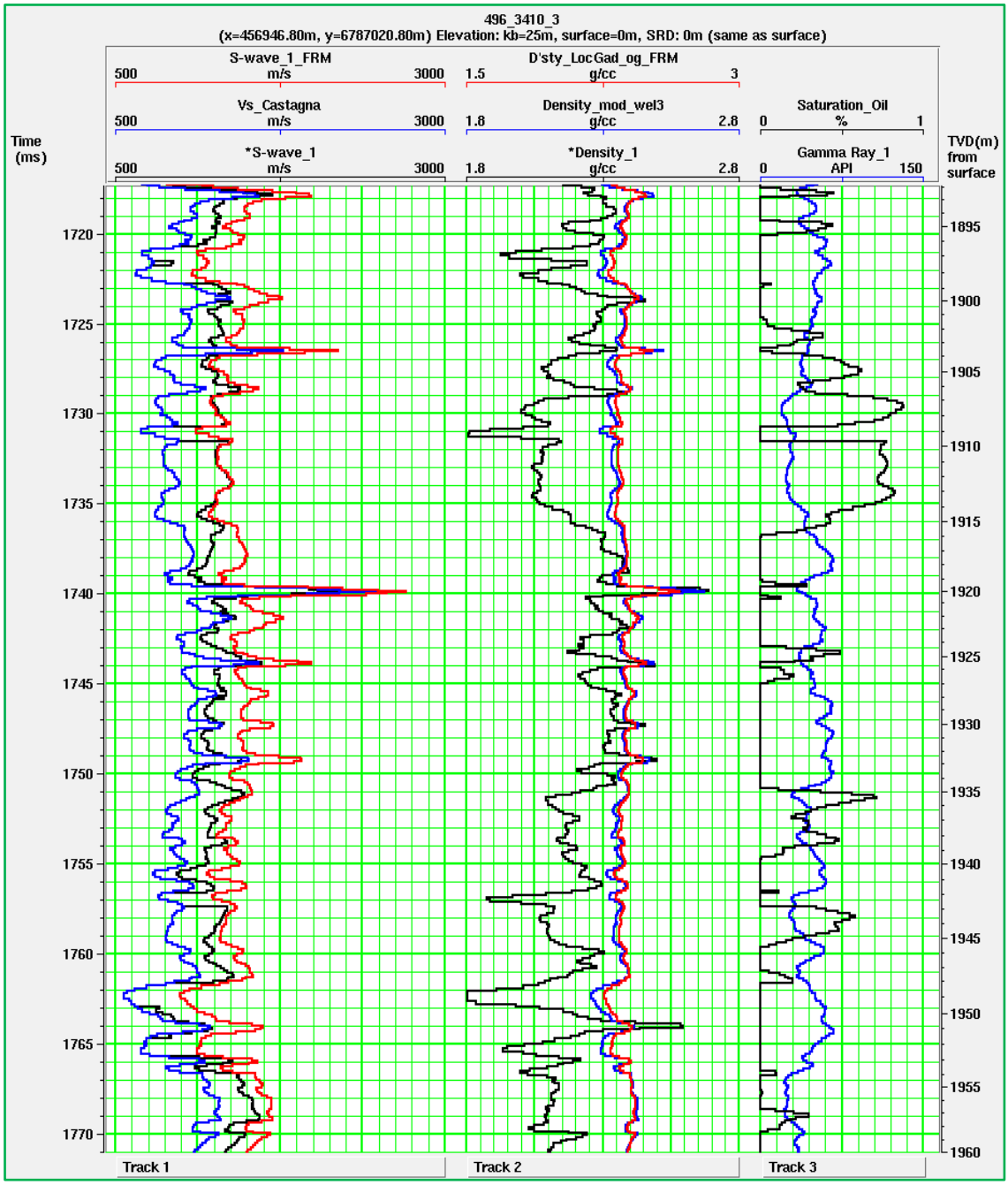

Fig. 3.24: The blue, red and black curves in track 1 are, respectively, the 'real', 'Castagna' and 'Pore Fluids Corrected' S-wave velocity curves. The blue, red and black curves in track 2 are, respectively, the 'real', 'Gardner' and 'Pore Fluids Corrected' density curves. The black and blue curves in track 3 are, respectively, the oil saturation and Gamma ray logs. All the data is for well 3.

3.1.6 Mixed saturation and mineralogies

What has been defined as a set of fluid(s) in the Gassmann recipe (section 3.1.5) can indeed be a whole mixture of different fluids. Unfortunately, Gassmann's equation was derived to describe the change in rock modulus from one pure-saturation to another. For example, it can be used to perfectly transform a Castagna[f] generated S-wave curve in to a fully-oil-saturated equivalent curve. Similarly what is defined as a rock matrix or flame in regards to Gassmann equation should be made up of a single mineral. Mathematical models have been developed that can seamlessly incorporate such intricate constraints (mixed lithologies and fluid saturations) into Gassmann's fluid substitution recipe. For simplicity, the mathematical details of (harmonic and arithmetic) averaging of mineralogies and saturations are hereby left out (but they are clearly laid down by among others: Avseth et al (2005), Walls et al (2004) and Tad et al 2003).

In the Fluid Replacement Modeling module of Hampson-Russell software all these algorithms are available, for instance it is possible to generate an S-wave curve from a P-wave and then perturb its reservoir section part to incorporate the presence of multiple fluids.

3.1.7 Fluid substitution correction for mud-filtrate invasion

In general, reservoir rocks around a well bore are at least invaded by mud filtrate (Roy et al, 1996). The severity of this condition varies greatly depending on the lithology, porosity, permeability, wettability of the rocks, pore pressure, drilling properties (mud weight, mud type, pressure and temperature), original fluid saturation and the elapse of time after drilling (Walls et. al., 2004 and Roy et al, 1996). The mud-filtrate invasion effect also depends on the type of in-situ fluids in the rock formation, for instance Roy et al (1996) observed that: replacement of hydrocarbons by mud filtrate has a more severe effect than the replacement of brine by mud filtrate in other Formations and in the water leg of a reservoir. Mud-filtrate invasion occurs during drilling with over-balanced mud weight conditions (i.e. high pressure drilling to balance pressure in over-pressured formations). "The positive pressure gradient between the wellbore and the Formation causes some of the mud liquids to penetrate into the permeable zones; displacing original fluids near the borehole wall" (Walls et. al., 2004).

The perturbation of the *in situ* fluid saturation(s) in the vicinity of the borehole wall (a region known as the invaded zone), has detrimental effects on well logs that have a shallow depth of investigation. The implications for reservoir geophysics are primarily related to the density log and the (monopole) sonic log because they sample rock properties well within the invaded zone (figure 3.25). If synthetic seismograms are made from the un-corrected sonic

[f] Castagna's model assumes a fully-brine-saturated rock.

and density logs, the results will not match the real seismic data. But how do you correct for the mud filtrate invasion effect?

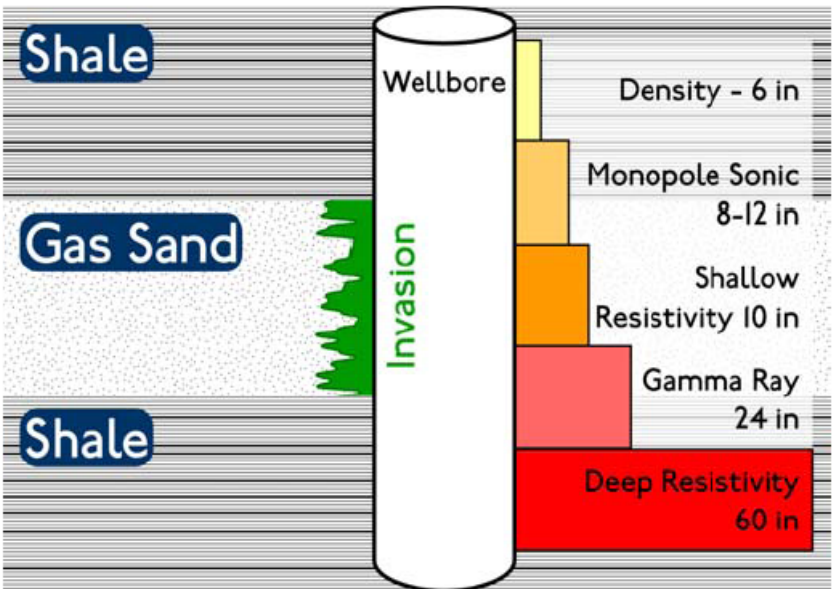

Fig. 3.25: Water-based mud invasion effect means that the measured logs will be seeing a rock 'wetter' than that seen by the surface seismic wave. This needs to be corrected or at least accounted for during well log analysis by means of fluid replacement modeling. Adapted from Walls et al., 2004.

It is possible to quantify and correct for the effect of mud-filtrate invasion by comparing the differences between the shallow, medium and deep resistivity logs. But according to Roy et al (1996), uncertainties in properties such as mud-filtrate and formation water resistivity at reservoir conditions make it difficult to obtain a complete invasion profile. Mud-effect correction using this technique is thence subject to some uncertainties. A more robust method to correct for this condition involves performing Biot-Gassmann fluid substitution on the measured log curves. In case of a multi-phase scenario; the respective saturations can be computed from the shallow and deep resistivity logs so that the saturation is incorporated into the fluid substitution algorithm.

Walls et al. (2004) showcased an example of correcting for mud-filtrate invasion effect using data for a well from Alaska. Their results are presented and discussed in figures 3.26 and 3.27.

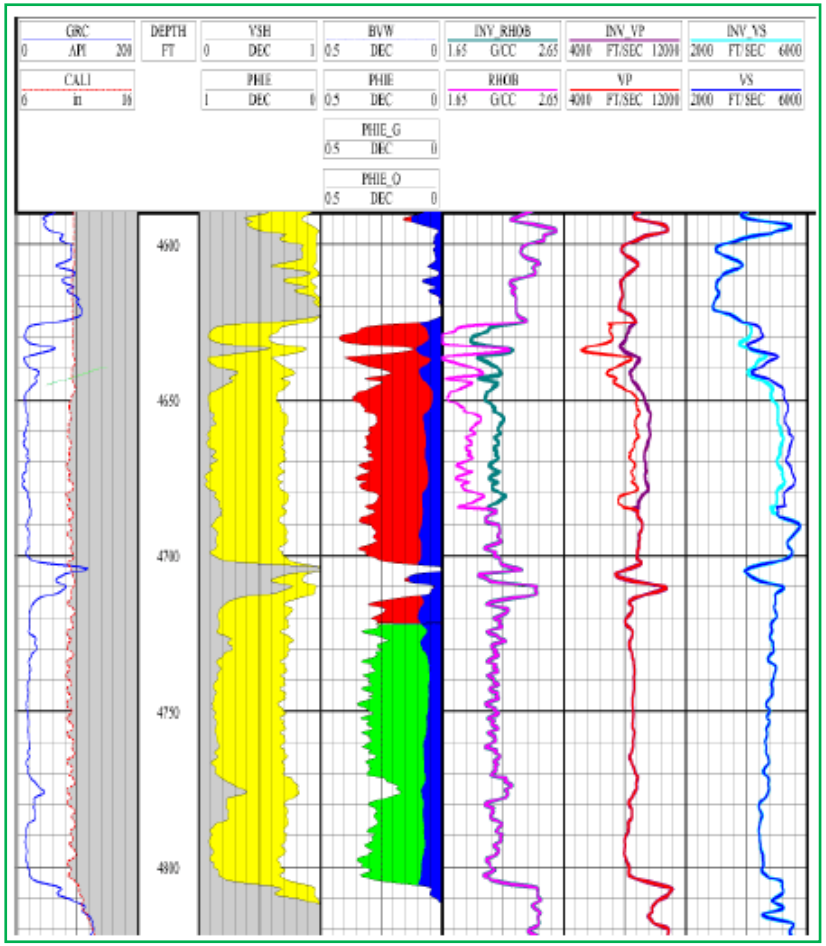

Fig. 3.26: As a result of water-base mud invasion, the logs used to make synthetic seismograms (sonic and density) may be seeing "wetter" rock than the seismic wave. Figure and caption, adapted from Walls et al. (2004).

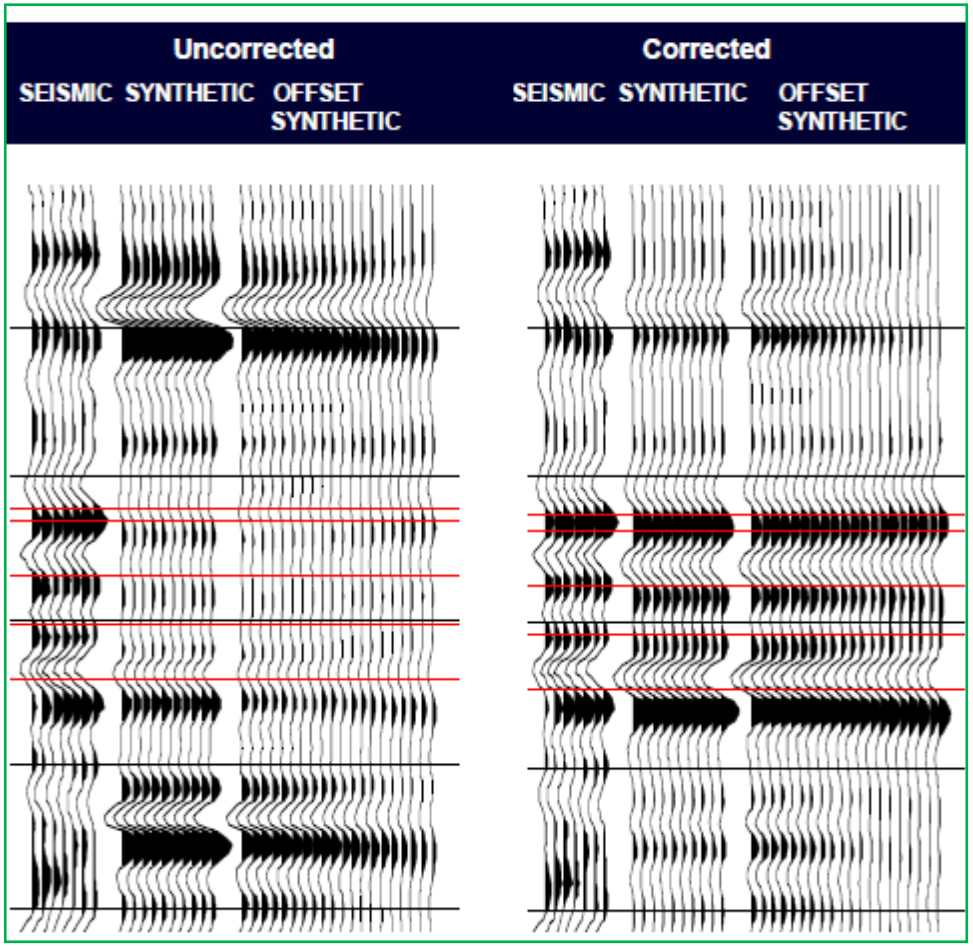

Figure 3.27: Original (left) and corrected (right) synthetic seismograms in a well with water-base mud invasion in a gas sand. First group of traces are stacked seismic near the wellbore. Second group is stacked synthetic traces. Third group is synthetic gather. Figure and caption, adapted from Walls et al. (2004).

3.1.8 Incorporating production history

In case there are multiple wells logs and seismic surveys that were recorded at different times over a producing field, (in the words of Walls et al, 2004) some wells may need to be moved forward in time (production history) and others may need to be moved backward in time, depending on when they were drilled in relation to when each seismic survey was shot. This will further improve the well to seismic tie by factoring in the saturation, pore pressure and possibly porosity changes which will have occurred during the intervening production time. These changes if left uncorrected may cause well to seismic miss-ties.

The correction involves the use of rock physics modeling to make the requisite "time shifts" by changing saturation, pore pressure, and even porosity in the key reservoir intervals. The resulting changes in Vp, Vs, and density can then be used to created synthetic seismograms that correspond to each seismic survey. Further, seismic differences can be computed to allow us to make quantitative predictions of changes in the reservoir. This kind of well log conditioning is akin to 4D seismic analysis but is quite different. This because wells logs may need correcting for production effects for as long as some wells were drilled prior to after a seismic survey, that is shot over a producing field.

"The works of the Lord are great; sought out of all them that have pleasure therein" - an inscription at the entrance of the new Cavendish Physics Laboratory in Cambridge (it is based on Psalm 111: 2)

4.0 Well-to-seismic tie: methods and procedures

Well-seismic tie is the best way to tie seismic back to the "ground truth" by comparison of the seismic image and well ("hard") data, but the ground truth always needs *fine-tuning* before the comparison can be done. In chapter 3, the methods of *fine-tuning* well data were presented. In this chapter the integration of 'fine-tuned' well data with a corresponding 3D seismic data set using advanced seismic-to-well calibration methods is considered. In the interest of brevity we shall omit any discussion of detailed processing of seismic data. This is not to deny it being important for a successful seismic-well tie but it is too big a topic to be satisfactorily reviewed and discussed in this research. Moreover, seismic data processing methods are relatively more developed and understood than well data treatment methods. The seismic data provided for this study were various vintages of 3D (4D to be precise) time migrated cubes over the study area. Thus, other than routine post-stack processing, no 'conventional' seismic processing was undertaken in this study, the assumption is that the data were well processed.

The single link existing between well data and seismic data is the wavelet; therefore, it should be carefully estimated (Nathalie and Pierre, 2000). The wavelet estimation processes and procedures are also presented. The accurately (or nearly so) determined wavelet is then used for forward seismic modelling.

We begin with a review of the major methods of joint calibration of seismic and well data. Later, a case study based on seismic forward modelling through synthetic seismogram generation is presented using real data from the study area. The most common methods that are available in geophysical literature are:

4.1 Velocity correlation method

The uniqueness of this method is that the well and seismic data is correlated in terms of velocity values (Linari, 2004) and not seismic amplitudes. The method works when there is at least one well with a check-shot survey in the project. Unlike conventional methods, this method does not use synthetic seismograms. According to Linari (2004), this method differs from and is advantageous over the use of synthetic seismograms in the following ways:

- Synthetics are a simulation of a seismic trace using many parameters, which must be tested in order to get the best approximation to real traces. Sometimes, it takes a considerably long time to test wavelet, phase, frequency, multiples, etc. for each well, and then to evaluate the best solution by mathematical or visual correlation with seismic data. Even in the presence of good responses, one given solution might be

adequate for a portion of the data, while another one best fits a different interval. Wells also fit the data differently.

- In some projects, particularly those in which many wells are available, the use of synthetics might lead to "individually" adjusting each well to a 3D seismic volume which acts as "the reference data" for that matter; this creates an environment where well data are adjusted to seismic data. In such cases, well data act as "soft data" and seismic data as "hard data," which sounds odd.

The methodology consists of three key steps:

1) recalculation of check-shot surveys,
2) generation of a pseudo-inversion (velocity) volume and conversion of the sonic (DT) log to velocity units, and
3) displaying the velocity log, the time-depth pairs from step 1, the pseudo-inversion (velocity) volume, and apply a minor visual adjustment of the 3D data to the well data by bulk-shifting as required.

Because this method was not further developed in this research, detailed procedures as presented by among others Linari (2004) and Box & Lowrey (2003) are hereby left out. Linari (2004) presented an interesting example where correlating in the velocity domain improved consistency of the correlation obtained with velocity layers instead of reflectors (see figures 4.1 and 4.2).

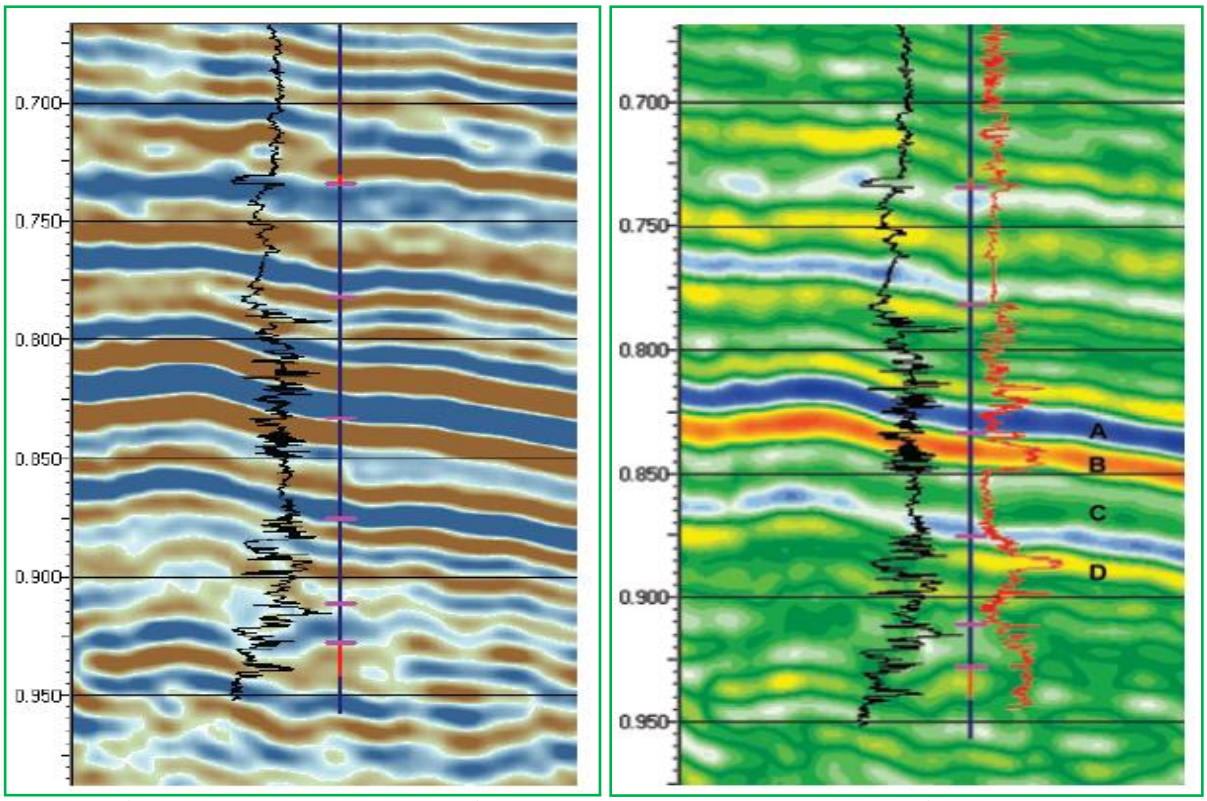

Figure 4.1: (left) Amplitude seismic line and GR log after check-shot recalculation. Pink markers indicate formation tops; red lines indicate perforated intervals. Figure and caption adapted from Linari et al (2004)
Figure 4.2: (right) Seismic velocity data and GR (black)-velocity (red) log after check-shot recalculation. Blue = low-velocity values; orange-yellow = high-velocity values; green = intermediate velocity values. Figure and caption adapted from Linari et al (2004)

Linari (2004) observed that this method has the following advantages: (1) high consistency of the correlation obtained with velocity layers instead of reflectors, and (2) very substantial savings of time. The method can be used as a complement to synthetic seismograms. In some cases it can be useful for special interpretation issues, like correlating in both sides of a complex fault or interpreting the geometry of a stratigraphic feature (Linari, 2004). The main challenge of this method is in ensuring a reliable inversion of seismic data to a velocity volume.

4.2 Vertical Seismic Profiling, VSP

Vertical seismic profile (VSP) data is generated by a surface source and recorded by geophones located at a sequence of prescribed depths spanning the entire length of the borehole. Sheriff and Geldart (1985) describe a number of variant forms of VSP surveying (details of which are outside the scope of this research) that differ in acquisition set up and geometry, but having quite related principles and primary goals.

The Stratigraphy at every depth point is usually known from geology or well logs so that the stratigraphic depth can be rigidly welded of on to the VSP image time. This dual-coordinate domain (depth and time) means that the calibration may be done in the time or depth domain because both stratigraphic depth (from geology or well logs) and seismic travel time are

known at each down-hole receiver station. In addition, the VSP and surface seismic data invariably match in character due to the usually common source and receiver type used in both surveys. Therefore, "VSP data is undoubtedly the best data for detailed event identification and wavelet determination (including phase); and can also be used to image the near-wellbore environment, and the image can be improved if a number of offsets are used for the source location" (Wayne, 2001). And because the detectors are close to the target formations, the VSP image is presumed to be more accurate than surface seismic data at the well location.

VSP and 3D data is often acquired by different contractors who according to Hardage (2009), often use:

- Different depth datums for the time origin.
- Different replacement velocities to move source stations to this depth datum.
- Different illuminating wavelets.

These are the main factors that create a mis-tie between the VSP image and a 3-D seismic image at the well location. Thus, the interpreter has to find the correct time shift between the VSP and 3D seismic image to ensure an optimal match between the two images; this is the fundamental step in VSP-to-seismic calibration. The reliability of this technique lies in "the fact that stratigraphy is rigidly welded on to the VSP image (figure 4.2), causing stratigraphic interfaces to move up and down in concert with the VSP image during the VSP-to-seismic image calibration process, which ensures that targeted thin-bed units are positioned in the correct time windows in the 3-D seismic volume when an optimal alignment is established between the VSP and 3-D images" (Hardage, 2009).

An example of a stratigraphic column rigidly welded on to a VSP image and subsequently inserted into a 3D seismic volume is presented in the figure 4.2 below.

Figure 4.3 presents the procedures involved in adjusting the VSP image to achieve optimal correlation with a corresponding 3D seismic image. In this example the VSP image was advanced by 18ms, accordingly the stratigraphic column should be advanced in unison with the VSP image.

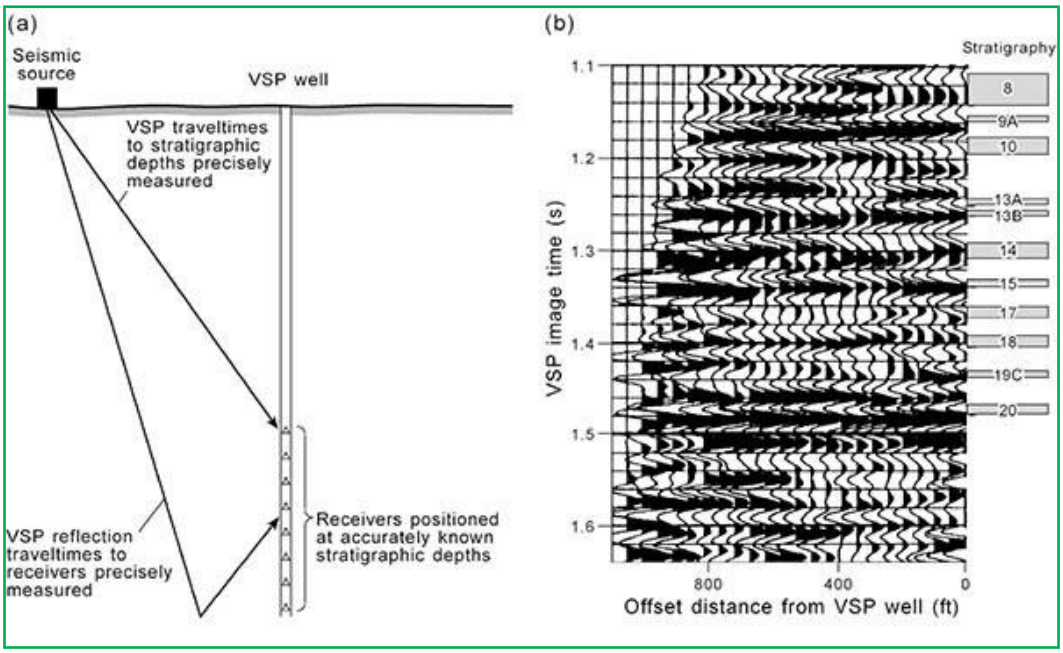

Figure 4.2 (a) because the receivers are placed at precisely known stratigraphic depths, the recorded travel times can be precisely paired and with the right stratigraphic depths. This duo coordinate domain means that any given stratigraphic unit can be precisely inserted into the VSP image. This is critical to geological interpretation of the results. (b). With the exception of unit 8, each reservoir labelled here is a thin-bed penetrated by the VSP well. When the VSP image is shifted up or down to better correlate with a surface recorded seismic image, the VSP-defined time window that spans each thin-bed unit should be considered as being welded to the VSP image, causing the stratigraphy to move up and down in concert with the VSP image as an optimal match is established between the VSP and seismic images. Figure and caption slightly modified from Hardage (2009).

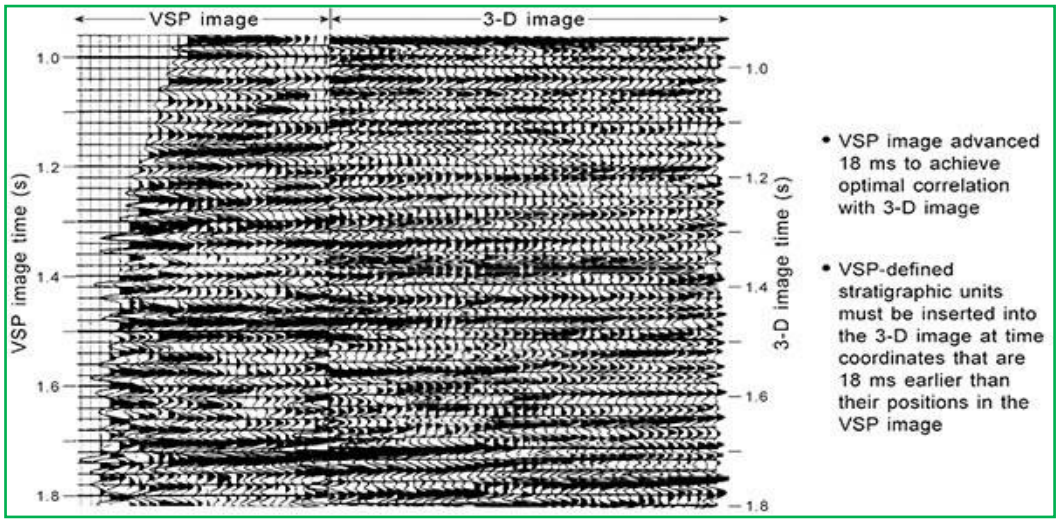

Figure 4.3: A VSP image juxtaposed with a 3D seismic image after applying a time shift of 18ms to the VSP image to cater for variation in seismic datum, adapted from Hardage (2009).

The VSP method was not further investigated in this research because no VSP data set was availed for this study area.

4.3 Seismic forward modelling: from sonic and density logs to the synthetic seismogram

The need for a perfect (or at least near so) synthetic seismogram that ties well with the recorded seismic data cannot be over emphasized, if we are to have much confidence in our interpretation. The synthetic seismogram is constructed from well logs (density and sonic to

be specific); to achieve a reasonably accurate synthetic seismogram the well logs should be well processed, edited and conditioned as earlier discussed (in section 3.1 of this research). It is equally important that the seismic data is as close as possible to a true representation of the real stratigraphy and rock properties; this can only be achieved by implementing the right processing flow (core seismic processing is outside the scope of this research). The link between the "ground truth" (well logs) and the recorded seismic data is the seismic wavelet. Therefore, wavelet extraction is very important in the seismic-to-well tie (as is discussed a little later). The idealized five-step work-flow in the actual seismic-to-well tie (as adapted from Roy, 1997) is as follows:

1. edit and calibrate the sonic and density logs;
2. review and assess the seismic data;
3. construct the well log synthetic sequences required;
4. run pilot analyses of the well tie;
5. estimate the wavelet, with diagnostic checks on its accuracy.

Step 1: the methods and procedures involved in conditioning and preparing (editing and calibration) of the logs were fully discussed in section 3.1. Regarding core seismic processing (**step 2**) is outside the scope of this research. The only kind of seismic processing that was done in this research involved data windowing to cut-out areas of no interest plus simple post-stack processing procedures (because the seismic data set used in this research composed of various vintages of stacked seismic data). Thus, we begin by describing the construction of synthetic seismogram (**step 3**) from a set of edited and calibrated sonic and density logs, and then the preliminary well tie (**step 4**) and wavelet extraction (**step 5**) will follow.

4.3.1 The convolution model: Constructing a synthetic seismogram

The easiest and commonest type of forward modeling is based on the convolution model, which assumes vertical ray paths and a horizontally layered earth. According to the convolution model, the seismic signal, *S*, is a convolution of the earth's reflectivity series or response, *R*, the seismic wavelet, *W*, and a compensation factor accounting for wavelet attenuation, i.e.:

$$S(t) = R(t)*W(t)*Q(t) \quad (4.1)$$

$$S(f) = R(f)*W(f)*Q(f) \quad (4.2)$$

Where *S(f)* and *R(f)* are the frequency-domain Fourier transforms of the time-domain responses *S(t)* and *R(t)* respectively. For completeness, the Fourier and inverse Fourier transforms for an arbitrary function, *g(t)* are defined (Sheriff and Geldart (1995)):

$$G(\omega) = \int_{-\infty}^{\infty} g(t) e^{-j\omega t} dt \quad (4.3)$$

= Fourier transform of *g(t)*,

Then:

$$g(t) = (1/2\pi) \int_{-\infty}^{\infty} G(\omega) e^{-j\omega t} d\omega \quad (4.4)$$

= inverse transform of G(ω).

Where ω and j carry their usual meanings (angular frequency and $\sqrt{(-1)}$ respectively).

In practice (e.g. in Hampson-Russell software) the compensation factor may be left out, in fact an additional term to account for noise may also be added to the convolution model above.

The reflectivity series is calculated from **acoustic/seismic impedance**, ***I***. The impedance, *I*, of an elastic medium is the ratio of the stress to the particle velocity (Aki and Richards, 1980) and is given by the product of sonic velocity, *V* and density, ρ (e.g. from the measured well log data) i.e.:

$$I = \rho V \quad (4.5)$$

In the simplest case of normal incidence reflection at an interface between two thick, horizontal, homogeneous, isotropic and elastic layers (figure 4.4 and 4.5); the normal incidence reflectivity for a wave travelling from medium 1 to medium 2, defined as the ratio of reflected wave amplitude to the incident wave amplitude, is:

$$R_{12} = \frac{I_2 - I_1}{I_2 + I_1} = \frac{\rho_2 V_2 - \rho_1 V_1}{\rho_2 V_2 + \rho_1 V_1} \quad (4.6)$$

$$\approx \frac{1}{2} \ln(I_2/I_1) \text{ for the special case where } |R| < 0.5 \text{ (Castagna, 1993)}$$

Subscript 1 and 2 refer to layer 1 and layer 2, respectively.

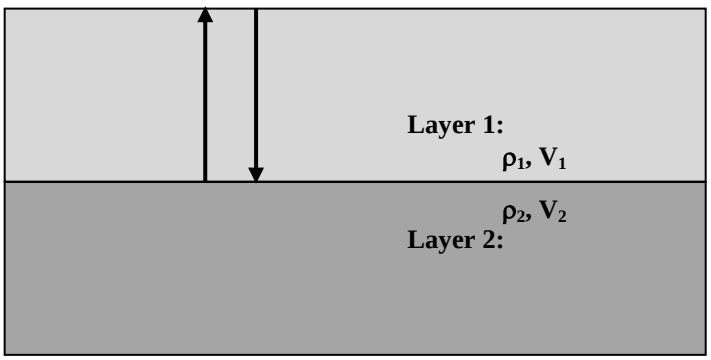

Fig. 4.4: A simple two-layer thick, horizontal, homogeneous, isotropic and elastic earth model; showing reflection at the interface due to contrast in acoustic impedance

Assumption(s): the model in figure 4.4 above is nothing but a simplistic convolution model to demonstrate what happens, in a rather complicated real earth. Horizontal layering means no mode conversion; isotropy and homogeneity mean no vertical or horizontal property variation all of which are not true in the real earth, but are necessary for mathematical treatment of the problem. It is for instance no match for the overly geologically complicated overburden in the Gullfaks field, which is being studied. In this case (two layered model) the transmitted energy has also been ignored. All these can and are sometimes considered in commercial seismic modeling software. The Reflectivity at every interface is calculated to generate the so called reflectivity time series; this is convolved with the seismic wavelet to generate the synthetic seismogram. Graphic representation of the convolution model is shown in figure 4.5.

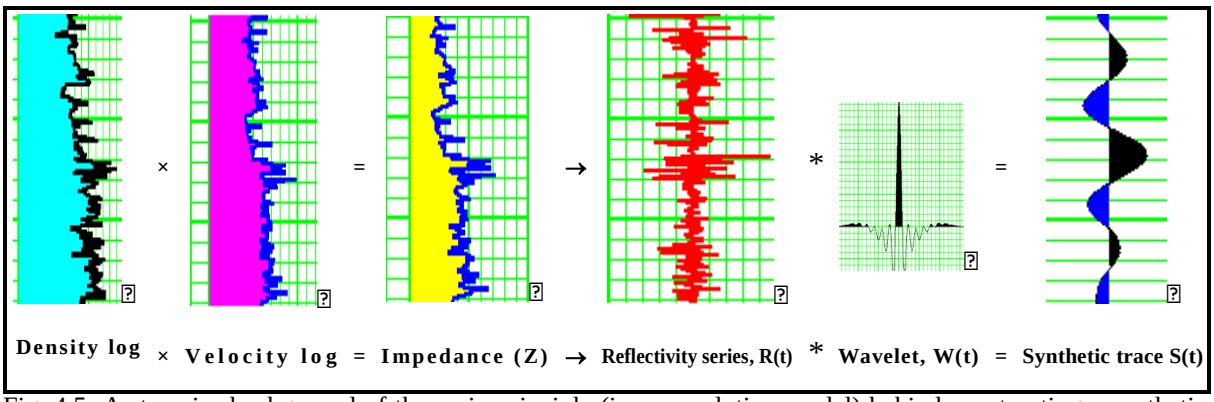

Fig. 4.5: A stepwise background of the main principle (i.e. convolution model) behind constructing a synthetic seismic trace from a density and sonic (velocity) log.

4.3.2 The preliminary well-seismic-tie

The first step in making a perfect well-tie is to run pilot analyses to establish the parameters for estimating the wavelet, key among which is a scan of time gates and traces around the well for the best match location (Roy (1997) and Roy & Tianyue (1998)). Scanning is done to establish the best-fit location which may be slightly away from the well location and within a certain time window. At this point, we need an initial wavelet to generate synthetic data to be compared with actual seismic data so that we can come up with the actual seismic trace in the vicinity of the well and the time range(s) to use in the final well tie. "In order to get the correct phase of the wavelet, we would prefer to use the well logs. Because well log correlation is not yet done, mis-tie between log and seismic data would make that extracted wavelet unacceptable" (Hampson-Russell (2011)). Using the usually noise-free, default 'ricker' wavelet is not a good idea. This presents a challenging riddle in that to extract a wavelet through logs, you must have an optimum correlation, and yet to correlate properly, you must know the wavelet. Hampson-Russell (2011) proposes the following "practical" solution:

a) Determine the approximate phase of the wavelet or assume some constant phase
b) Extract the wavelet statistically from the seismic
c) Correlate the logs to the seismic data
d) Run a Seismic-Well scanning algorithm to establish the best match location
e) Extract a new wavelet using the correlated well logs
f) Repeat the log correlation if required

The topic of wavelet extraction is further discussed in section 4.3.3.

The initial "guess":

Statistically extract a wavelet from a minicube around the location of the well. We can set the phase to zero so that the extracted wavelet is zero-phase and has the same amplitude spectrum as the seismic data. Using the extracted wavelet we build synthetic data from the well logs using the convolution theorem described in section 4.3.1. The synthetic and seismic data are then used to analyse the correlation between a synthetic trace computed from the impedance (or reflectivity series to be specific) and the composite trace (a "sum" of traces enclosed in a minicube around the location of the well). Figure 4.6 shows amplitude and frequency spectra of the statistically extracted wavelet. Figure 4.7 shows the (blue) synthetic traces juxtaposed with (red) composite traces from a minicube around the *well 11*.

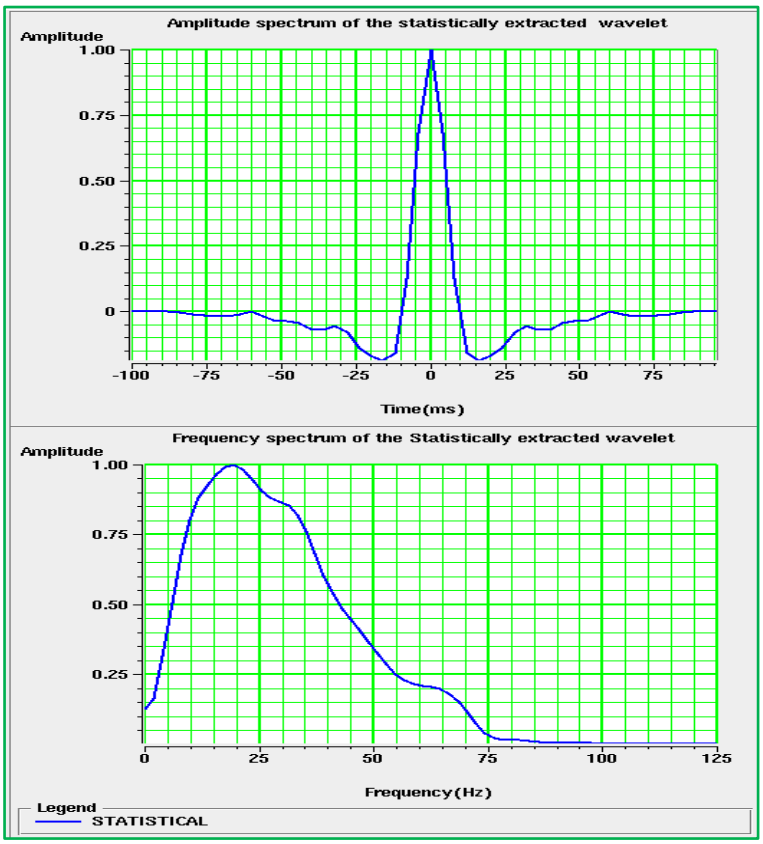

Figure 4.6: the amplitude and frequency spectra of the statistically extracted wavelet. This wavelet was then used to construct synthetic data to be used in the initial well log correlation. The data used is for well 11.

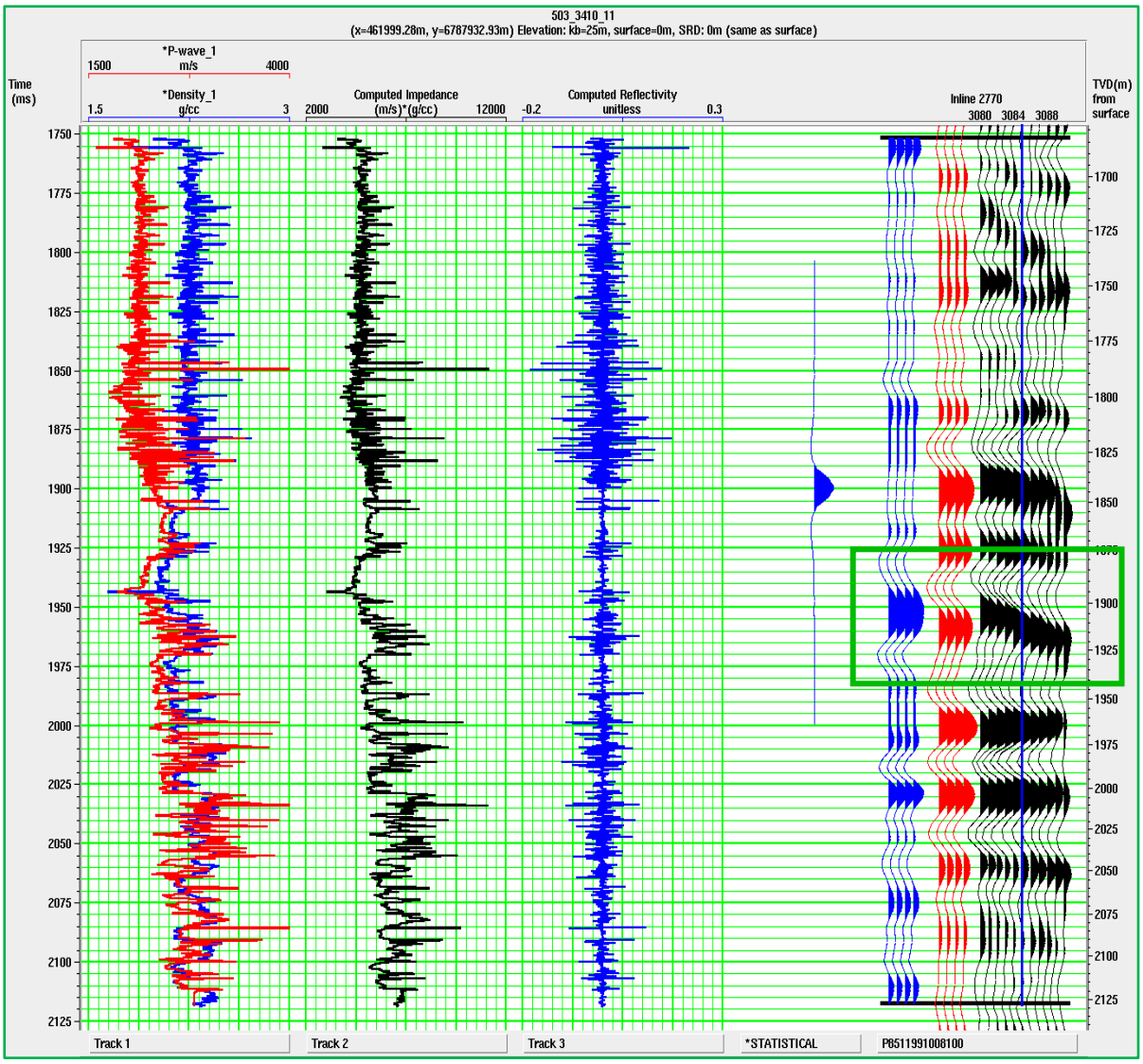

Figure 4.7: the (blue) synthetic traces were computed using by convolution of the statistical wavelet with the computed reflectivity series. The synthetic traces are juxtaposed with (red) composite traces from a minicube around the well 11. The blue line in the real seismic (black traces) is the well location and path. The green rectangle encloses a section where the mis-match between the synthetic and the real seismic is very clear.

Correlating well logs with seismic data: the bulk time shift

Clearly, there is a time shift between the (blue) synthetic and the (red) composite (real seismic) trace; see the portion enclosed in a green rectangle in figure 4.7. Mathematically, "the time shift between the synthetic trace and the composite seismic trace can be computed from the maximum of the envelope of the crosscorrelation between synthetic trace and the surrounding seismic traces" (Nathalie and Pierre (2000)). In the e-log module of the Hampson-Russell software, the bulk time shift removal is initiated by linking two corresponding reflectors within the desired time gate of the synthetic and the composite trace; the synthetic is then aligned using the picked values. Figure 4.8 presents results of applying a bulk-time shift on *well 11* data; there is an improvement in the correlation coefficient from 0.119 to 0.248 as a result of applying a bulk time shift.

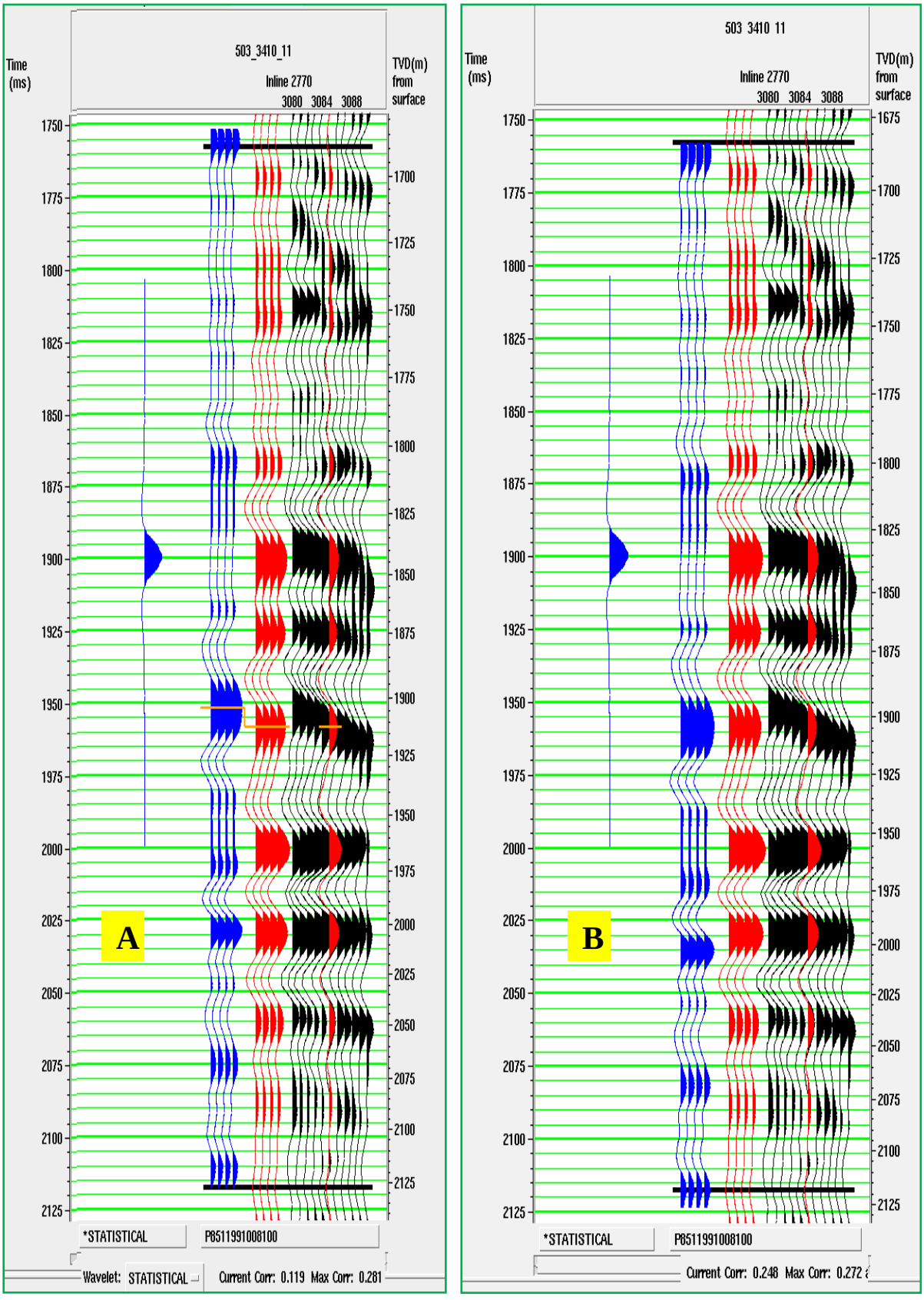

Figure 4.8: Before (A) applying a bulk time-shift the correlation coefficient was only 0.119; afterwards (B), the correlation coefficient rose to 0.248. . The data presented is for well 11.

To further improve the fit, a time-variant stretch is applied by picking a series of corresponding peaks on the synthetic and composite trace to create a down-hole velocity profile. This kind of "log correlation can be thought of as a type of check shot correction, where the depth-time pairs are provided manually by selecting points on the synthetic and tying them with corresponding points on the composite trace," Hampson-Russell (2011).

Figure 4.9 shows the picked points on the synthetic and real seimic data to build a down-hole "velocity profile' which acts as control data to readjust the well log so that it fits the seismic data. This kind of log correlation aligns the synthetic calculated from the well logs with one or more seismic traces near the well location. Figure 4.10 shows the process of readjusting the sonic data using the picked velocity points as control points. In this case, the data was fitted to a third degree polynomial using the picked points as the control points. Another synthetic data set was constructed using the check-shot corrected and correlated sonic log. As a result the correlation coefficient further improved from 0.248 to 0.401 (see figure 4.9).

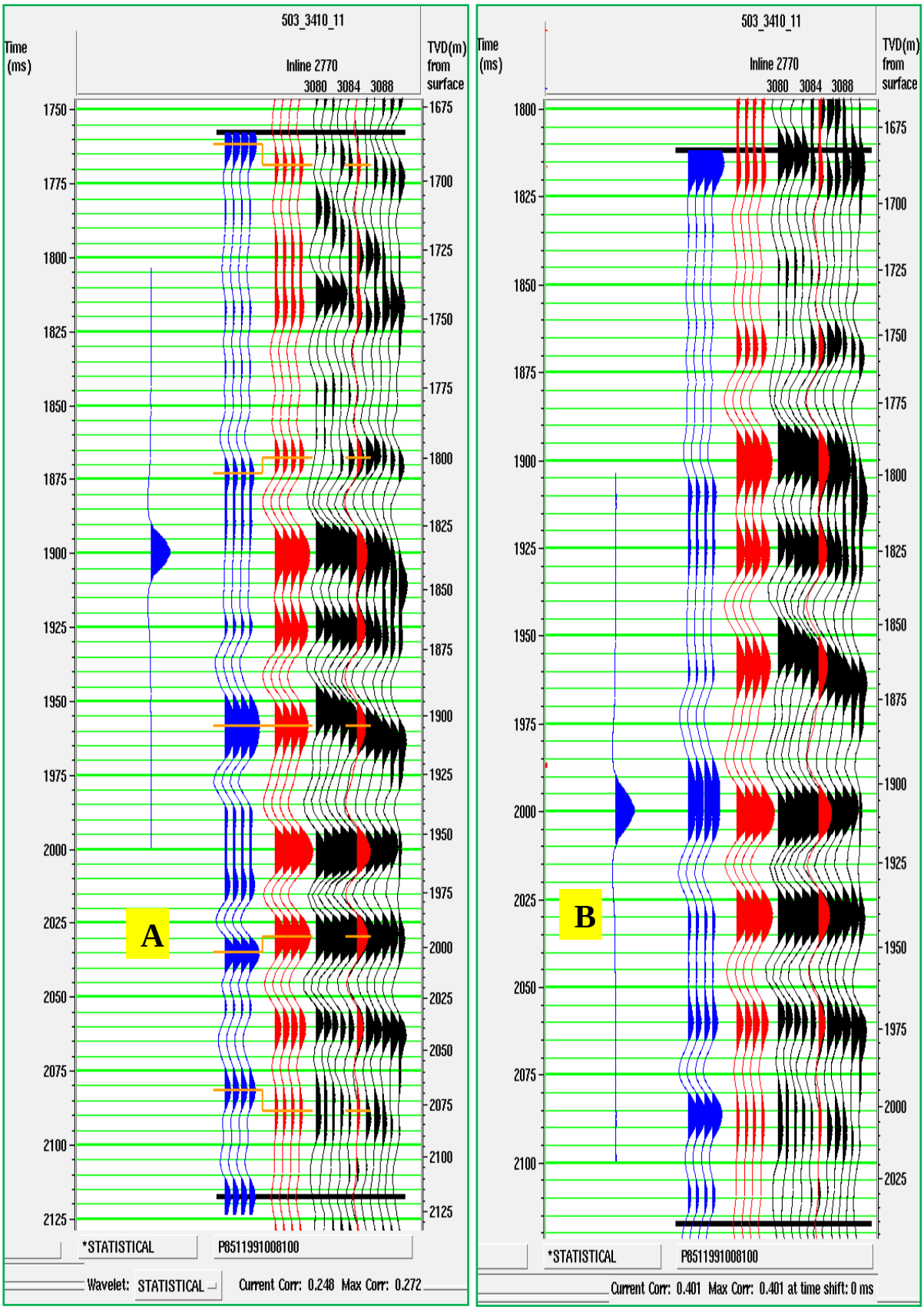

Figure 4.9: Before (A) applying a time variant shift the correlation coefficient was 0.248; afterwards (B), the correlation coefficient rose to 0.401. The data presented is for well 11.

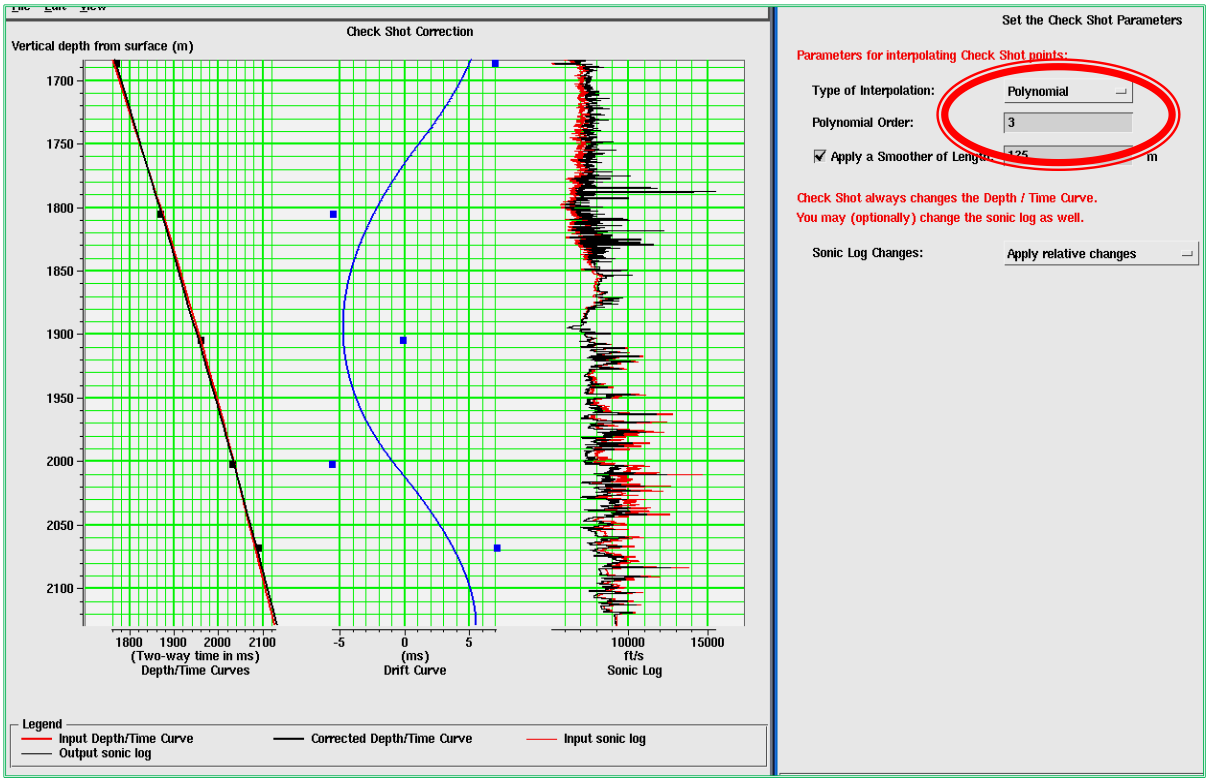

Figure 4.10: the series of points picked during the correlation process are used as control points to numerically fit the log data to an appropriate function, a third degree polynomial was most appropriate in this case (see the area encircled in red). Once the log has been 'check-shot' corrected using these series of points, correlation of the corresponding synthetic with the real data should significantly improve as discussed in figure 4.9. The data presented is for well 11.

Well-seismic scanning: finding the best match location

"The drill location of the well with respect to the seismic volume may not be optimal for extracting the wavelet," (Roy and Rob, 2003) because of various reasons. Roy and Rob (2003) presented a complete discussion on these reasons; for instance, "since velocity typically increases with depth, time migration commonly moves the best match location up-dip from the well". A Roy White seismic scanning algorithm exists which can searche for a new location within a specified vicinity of the posted well location to find the best trace location and time interval to be used in the calibration (wavelet extraction and well-seismic tying). The algorithm computes the predictability function which is defined as the proportion of the total energy in the seismic trace that can be predicted (PEP), from the well log reflectivity. This step is part of a wider algorithm that can be followed to extract a wavelet and check uncertainties associated with the wavelet (see section 4.3.3). A complete and detailed discussion of the well-seismic scanning has been the subject of many research papers in the recent past (e.g. Hampson, 2004; Roy and Rob, 2003; Roy (1997 and 1998)).

It should be noted that this seismic-well scanning scheme is run using a log which "has already been check-shot corrected (see section 3.1.1) and possibly correlated (like the one shown in figure 4.9). Consequently, this scheme starts with an assumed optimum correlation

at a lag of around 0 ms at the well location" (Hampson, 2004). Figures 4.11, 4.12 and 4.13 present results of the well-seismic scanning for the wells that were analysed.

Results and discussion(s):

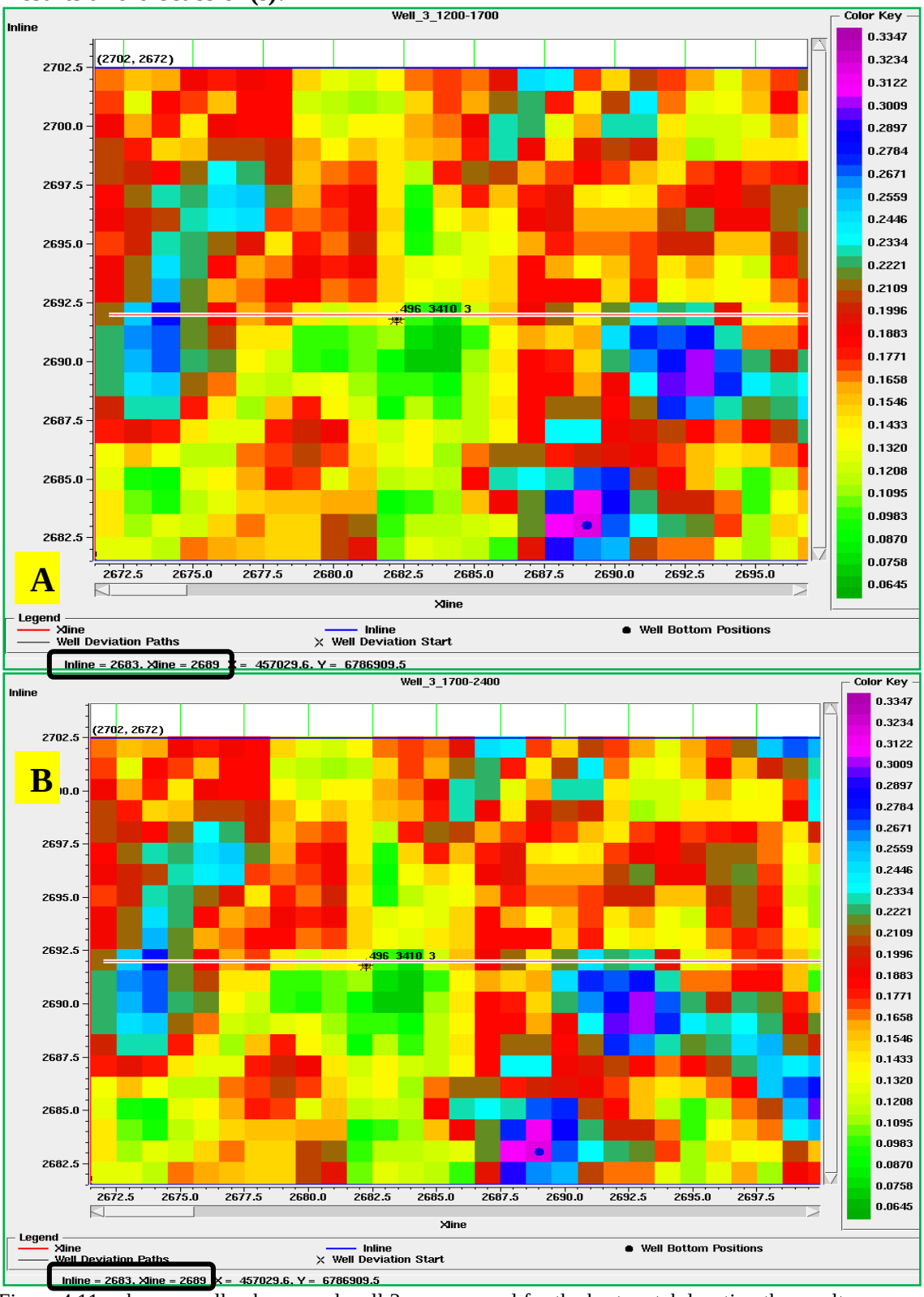

Figure 4.11: when a small cube around well 3 was scanned for the best match location the results were as shown above. In figure A we searched the time gate from 1200 to 1700 ms (TWT); this placed the best fit at in-line 2683 and cross-line 2689. When we repeated the search for the time gate between 1700-2400 (figure B), the results pointed to the same location. Notice that the maximum proportion of predicted energy (PEP) is the same in both cases.

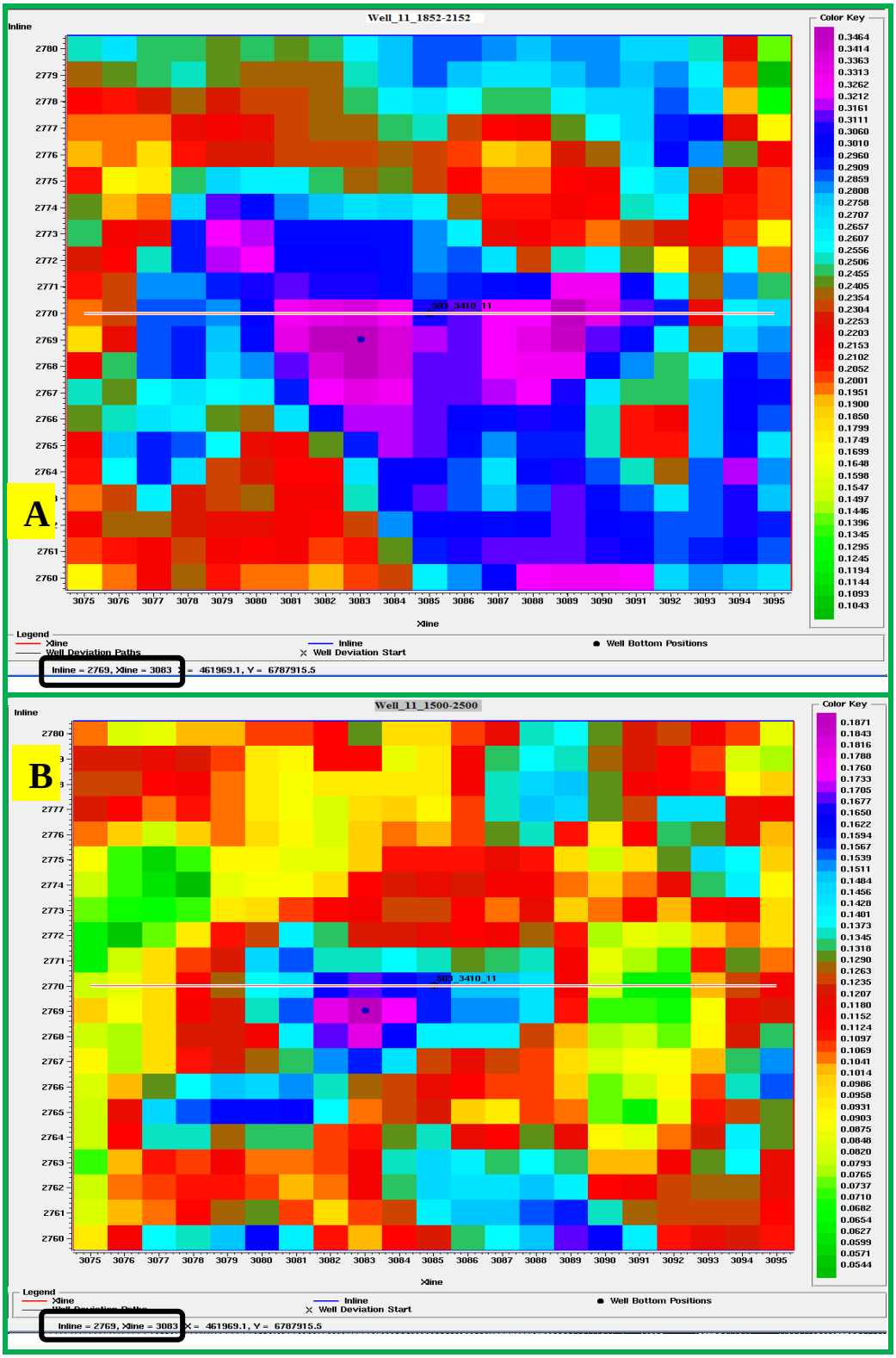

Figure 4.12: when a small cube around well 11 was scanned for the best match location the results were as shown above. In figure A we searched the time gate from 1852 to 2780 ms (TWT); this placed the best fit at in line 2769 and cross line 3083. When we repeated the search for the time gate between 1500 to 2500 ms (figure B), the results pointed to the same location. Notice that in this case the maximum proportion of predicted energy (PEP) is higher for the time gate: 1852-2152ms.

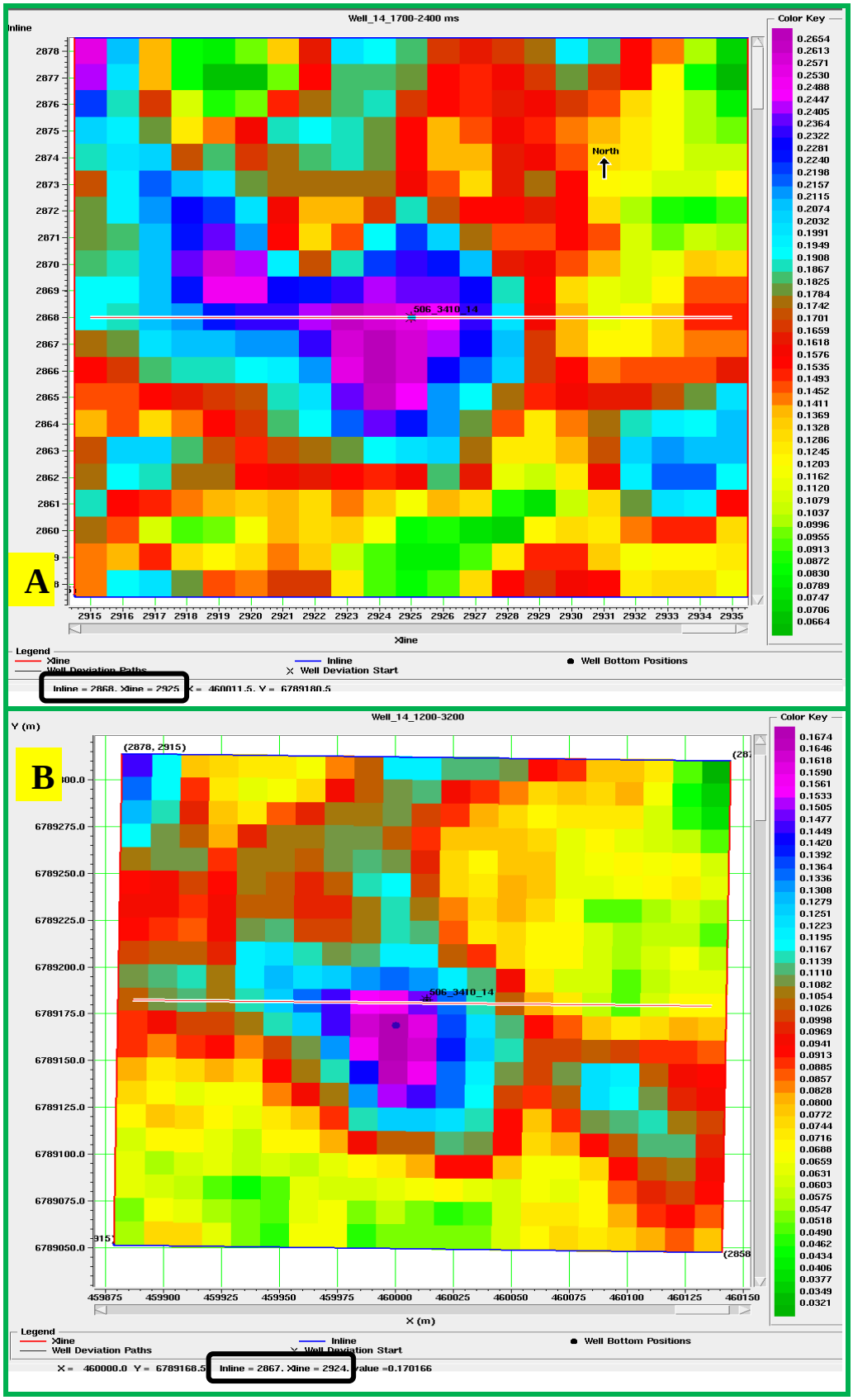

Figure 4.13: In A we searched the time gate from 1700 to 2400 ms (TWT); this placed the best fit at in line at the original well location. When we repeated the search for the time gate between 1200-3200 (figure B), the results pointed to inline 2867 and cross-line 2924. Notice that the maximum proportion of predicted energy (PEP) is higher in the first case. Thus, well 14 does not need to be "moved".

Once the best match location has been established and the well log(s) have been calibrated, a new wavelet can then be extracted from the calibrated well-logs and seismic data. Hampson-Russell (2011), describes three different algorithms which can be followed to implement the wavelet extraction, i.e.:

- the **full wavelet** option which uses the well log to determine the phase of the wavelet
- **constant phase** option which constrains the wavelet to a constant linear phase spectrum
- **Roy White** algorithm which uses a technique developed by Roy White to extract the wavelet amplitude and phase.

These algorithms are well described by Roy (1997); Roy & Tianyue (1998) and Hampson (2007). If the initial well tie is good, these algorithms produce similar results Hampson (2007). The Roy White algorithm is particularly interesting because it produces diagnostics (see appendix 2) which allow the user to estimate the error in the wavelet extraction.

Results and discussion(s):

- In figure 4.14, we have compared wavelets extracted by each of these algorithms from *well 11* logs. The extracted wavelet is then used to generate new synthetic data; after a little bulk-time shift the correlation between the synthetic and the real seismic will in principle improve tremendously.
- In figure 4.15, we have compared results of generating synthetic data using a wavelet generated by the Full wavelet option, Constant phase option and Roy White algorithms. Comparing the results in figure 4.15 with the results in figure 4.9 (from the statistically generated wavelet), we find that the correlation between the synthetic and real data significantly improves (from 0.401 to at least 0.543), irrespective of the wavelet extraction algorithm used.

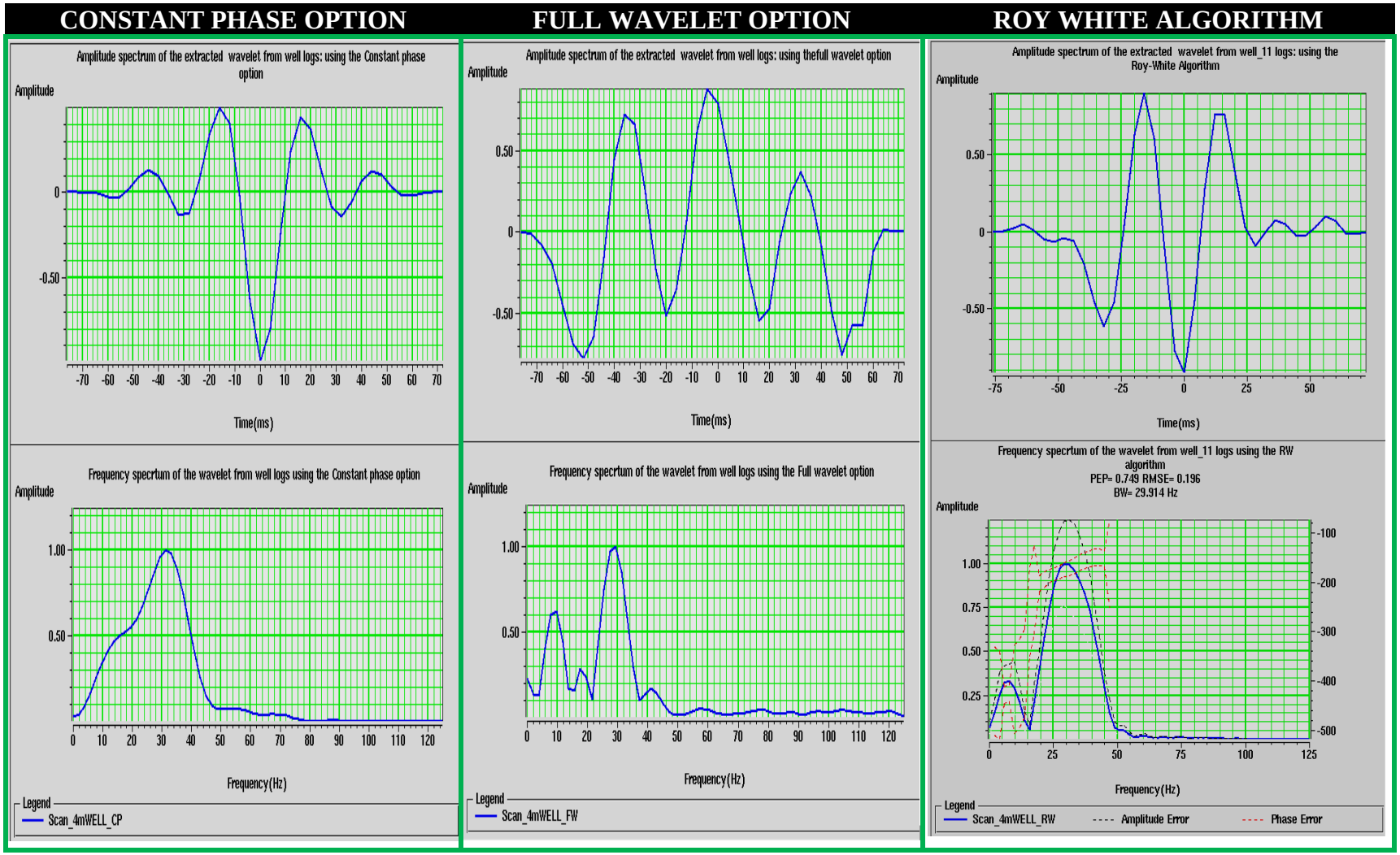

Figure 4.14: the three wavelets were extracted from well 11 logs. It can be seen that the 'Constant phase' and 'Roy White' wavelets are comparable. The 'Full wavelet' option gave a rather complex wavelet. It should be noted that the Roy White algorithm displays some diagnostic characteristic including the Proportion of the Energy of the (real) composite trace Predicted by the synthetic trace (PEP); these can be used to quality check the estimated wavelet.

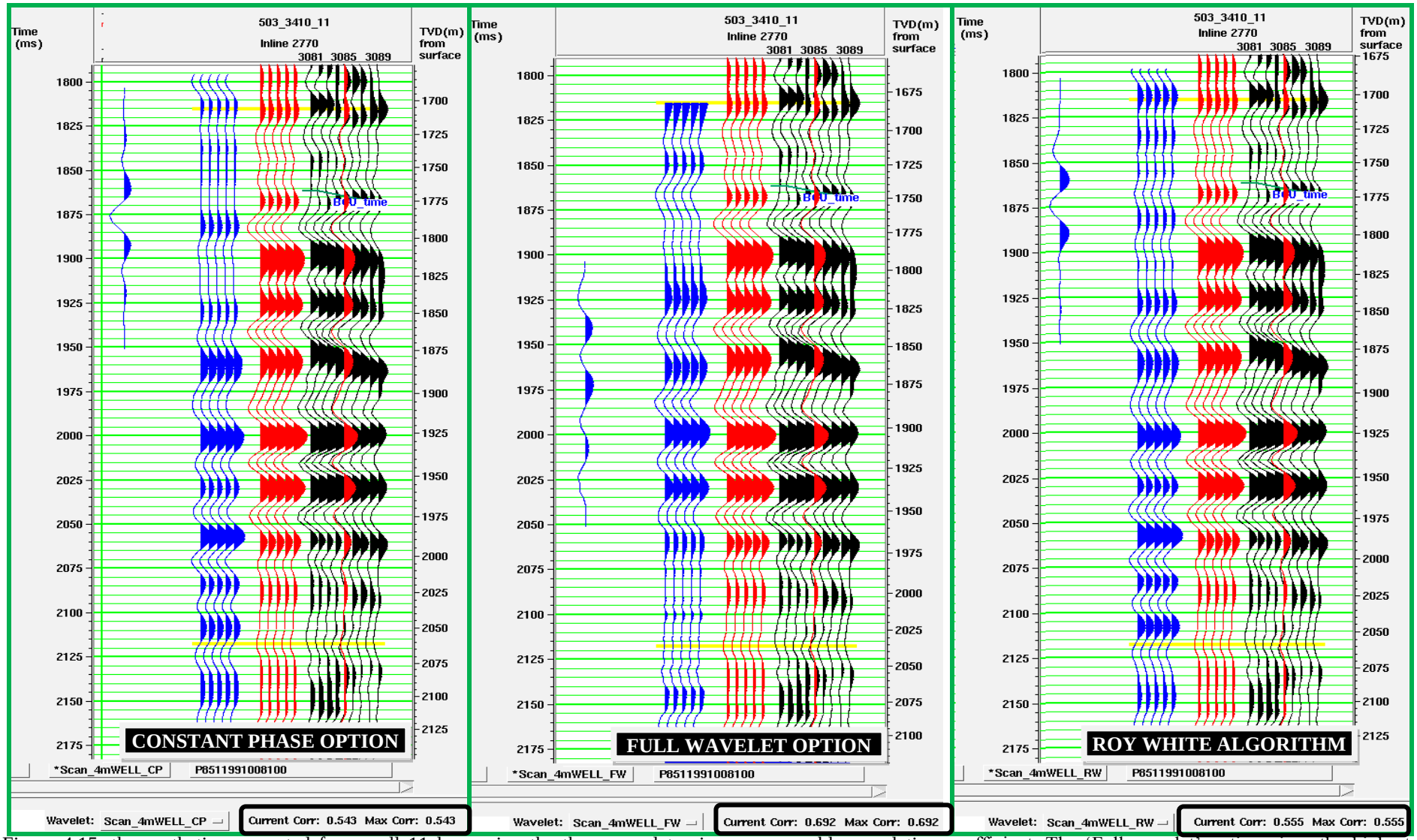

Figure 4.15: the synthetics generated from well 11 logs using the three wavelets give a comparable correlation coefficient. The 'Full wavelet' option gives the highest correlation coefficient (0.692). Comparing these with the results in figure 4.9, we find that the correlation between the synthetic and real data significantly improves (from 0.401 to at least 0.543), irrespective of the wavelet extraction algorithm used.

4.3.3 Wavelet extraction: a multi-well approach

Accurate determination of the wavelet is absolutely critical to the success of any seismic, processing, modeling and inversion project. "The inferred shape of the seismic wavelet may strongly influence the seismic processing, modeling and inversion results and therefore subsequent assessments of the reservoir quality" (Fugro, 2011). It therefore is necessary to investigate this issue in greater detail. This issue of wavelet extraction is a complex one, and is currently an area of active research (see for instance: Zhang et al., 2007; Nathalie and Pierre, 2000; Roy, 1997; and Roy & Tianyue, 1998) and is the subject of many academic theses (see for instance: Dey, 1999 and Schoepp, 1998). In the frequency domain, to extract a seismic wavelet takes the definition its amplitude and phase spectrum. Of these two, determining the phase spectrum is by far the more difficult and presents a major source of error in inversion (Hampson-Russell, 2011).

Wavelet extraction method(s): Hampson-Russell (2011) categorized the wavelet extraction methods into three:

- Purely deterministic: this is where the wavelet is measured directly using receivers and other means, such as marine signatures or VSP analysis. This method is not the subject of this research.
- Purely statistical: in this method the wavelet is determined from seismic data using statistical methods (for example the cepstrum domain processing method proposed by Zhang et al. (2007) and the Bayesian approach (see for instance: Gunning & Glinsky, 2005 and Buland & More, 2000)). In a nutshell, "this procedure uses only the autocorrelation from the seismic data. The phase is assumed known." (Hamspson, 2007). This method was briefly discussed in the previous subsection; its intricacies are hereby left out because it is not further developed in this research. The main limitation of this approach is that it tends to have difficulties in estimating the right phase spectrum reliably.
- Using both seismic and well logs: deductively, errors in the log measurements (and correlation) and seismic noise will affect the results of this method. Well log conditioning was addressed in section 3.1 of this research; seismic processing for noise suppression is outside the scope of this research. In principle this method is capable of providing the exact phase and amplitude spectrum of the wavelet. In practice one begins with a statistically "guessed" wavelet to calibrate the well logs and then the aligned logs can be used to extract a more accurate wavelet as discussed

in the previous section. In this research, a variant form of this method which we call "multi-well wavelet extraction" is described below.

For each of the methods above, one can use one of the following algorithms to implement the wavelet extraction process: Full Wavelet option, Constant Phase option or the Roy White algorithm. In section 4.3.2 details of each of these algorithms were discussed. In the proceeding analysis the Roy White algorithm was implemented so that we could use its advantageous diagnostics characteristics (see appendix 2) in evaluating the quality of the derived wavelet.

Multi-well wavelet extraction and analysis using the Roy White algorithm:

When there is more than one well, a single well-tie or individually fixing miss-ties at the various wells will not fix miss-ties at all other well locations. The solution is to perform "a multi-well analysis to extract one single wavelet" (Nathalie and Pierre, 2000) that is valid on the whole field/reservoir. The primary advantage of this approach is that it is possible to examine the quality of ties between synthetic and seismic at the selected wells for the extracted wavelet (see for instance Nathalie and Pierre, 2000 and Hampson, 2007). As earlier discussed, the wavelet extraction procedure begins by "guessing" a wavelet from seismic data; this wavelet is used to generate a synthetic from well logs. The well data and seismic data are aligned; a new wavelet is then computed from the chosen wells.

Using the Roy White algorithm is advantageous because it provides the framework (diagnostic characteristics) to quality check and compare the various results. The proposed algorithm based on the work of Nathalie and Pierre (2000), Roy and Rob (2003) and Hampson (2007) involves the following steps:

1) Statistically estimate the wavelet from seismic data. At this stage assume that the phase of the wavelet is known or that it is some known constant.
2) Build a synthetic using the "estimated" wavelet and; establish and apply the global time shift to all the logs; this could be followed by a time variant stretch.
3) Establish the optimum phase value of the wavelet, which is valid for all the wells. This can be done in a number of ways; the simplest is to "compute a set of synthetic traces where the phase varies from 0 to 360. The correlations between each (composite) seismic traces and the set of synthetic traces are computed and the best one – in terms of correlation coefficient – corresponding to the best phase is kept" (Nathalie and Pierre, 2000).
4) Well-seismic scanning: the optimal seismic trace to be used in further analysis may be slightly away from actual well location. To choose the optimal location of the well log

out of a minicube surrounding the well, we compute the time shift that should be applied to the log and the ratio of the amplitude of the real trace to the amplitude of the synthetic trace for each seismic trace in the minicube surrounding the well. The optimal location of the well is chosen from a mini location map around the well, colour-coded with the amplitude ratio value (or correlation coefficient) (Nathalie and Pierre 2000).

5) Then, extract optimal wavelets at each location and compare them. "The final wavelet can be an average of these optimal wavelets, or can be slightly modified through another step where the phase is re-adjusted" (Nathalie and Pierre, 2000). It is also important to run diagnostics on the accuracy of the final wavelet. Possibly repeat steps (3) to (5).

Results and discussion(s):

- Using the Roy White algorithm three wavelets were extracted from each of the three wells: 3, 11 and 14. Each of these wavelets was then subjected to multiwell analysis to investigate how it performs at other well locations. It was noted that all wavelets extracted from a single well produce poor correlation between the synthetic and the real data at the other well locations (figures 4.16, 4.17 and 4.18). For the case of well 11, the wavelet extracted produced poor correlation at all the well locations. If there is only one well not much can be done to improve the correlation (luckily there is more than one well in this study).
- When more than one well is available (like in this research); a wavelet can be extracted from all the wells by way of multiwell wavelet extraction. In this research we used the Roy White algorithm to extract a wavelet from:
    - All the wells: the resulting wavelet is shown in figure 4.19. When we performed multiwell analysis on the extracted wavelet (figure 4.20), the correlation at all the three wells was much better than when a wavelet from an individual well is used to correlate the well and seismic data. For some unknown reason, well 11 still had the least correlation using this wavelet. Sometimes, this may mean that the well is simply "bad", in which case a new wavelet can be re-extracted using the "good" wells only as explained in the next point.
    - Well 3 and 14: the wavelet that was extracted from the "good" wells is shown in figure 4.21. When we performed a new multiwell analysis on this wavelet,

the results were worse than those for the wavelet that was extracted from all the wells (figure 22). Well 11 might not be "bad" after all.

These results demonstrate that multiwell wavelet extraction can be used to obtain a wavelet that can be used throughout the seismic volume to produce reasonable correlation at every well; and that individually correlating every well is not the right thing.

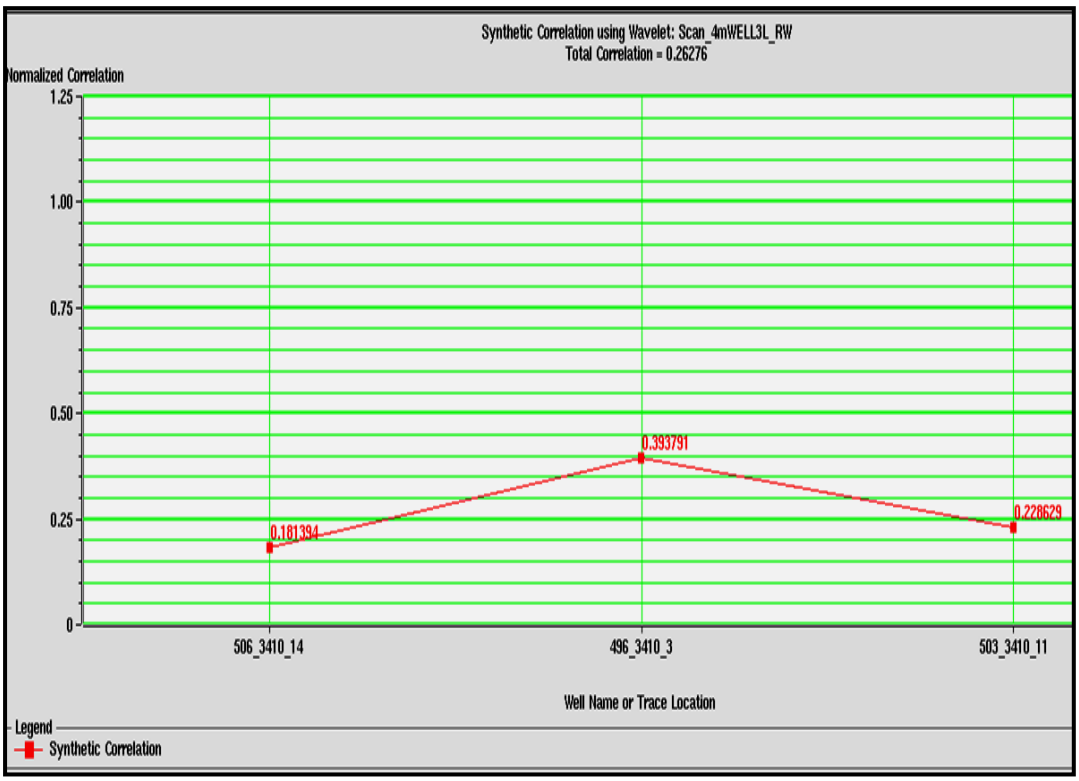

Fig. 4.16: Multiwell analysis of the wavelet extracted from well 3, as expected this wavelet performs fairly well at well 3 location. The correlation is not very good at all the other wells.

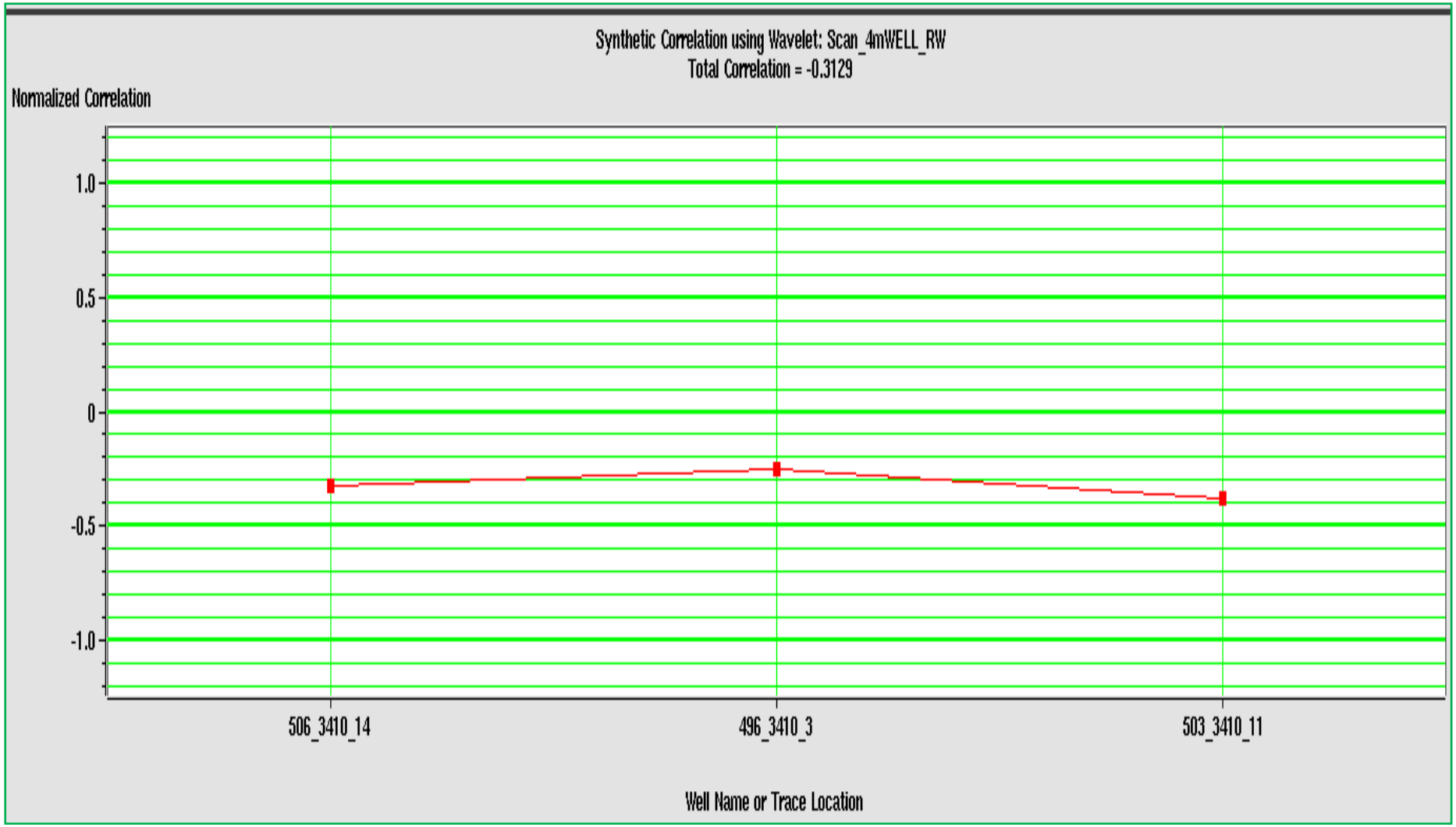

Fig. 4.17: Multiwell analysis of the wavelet extracted from well 11. For some reason this wavelet produces poor correlation at all the wells. Sometimes such is just a "bad" well, to this we will return in a while.

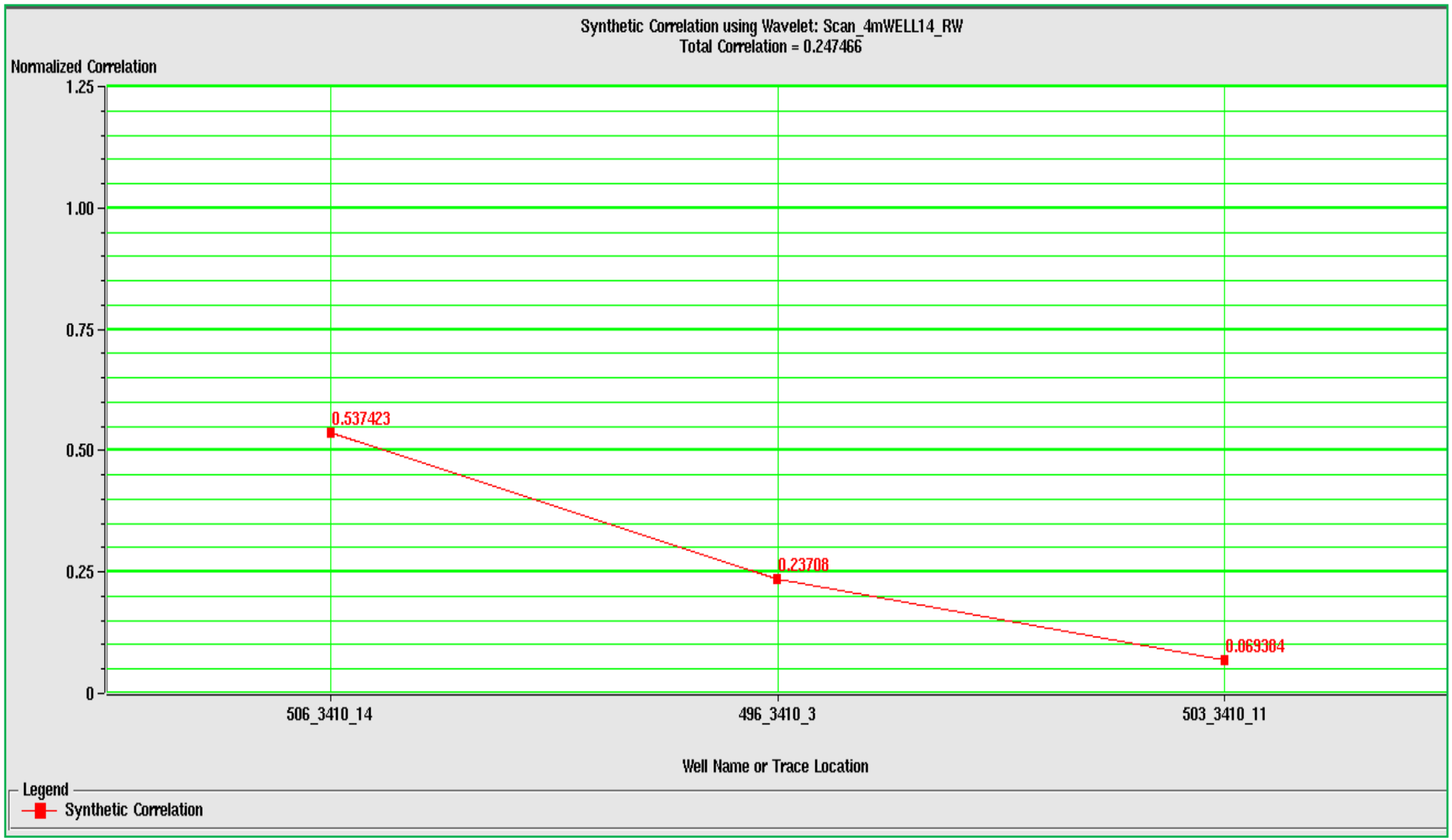

Fig. 4.18: Multiwell analysis of the wavelet extracted from well 14, as expected this wavelet performs fairly well at well 14 location. The correlation is poor at all the other wells. This demonstrates that when there is more than a well, multiwell wavelet correlation is often necessary.

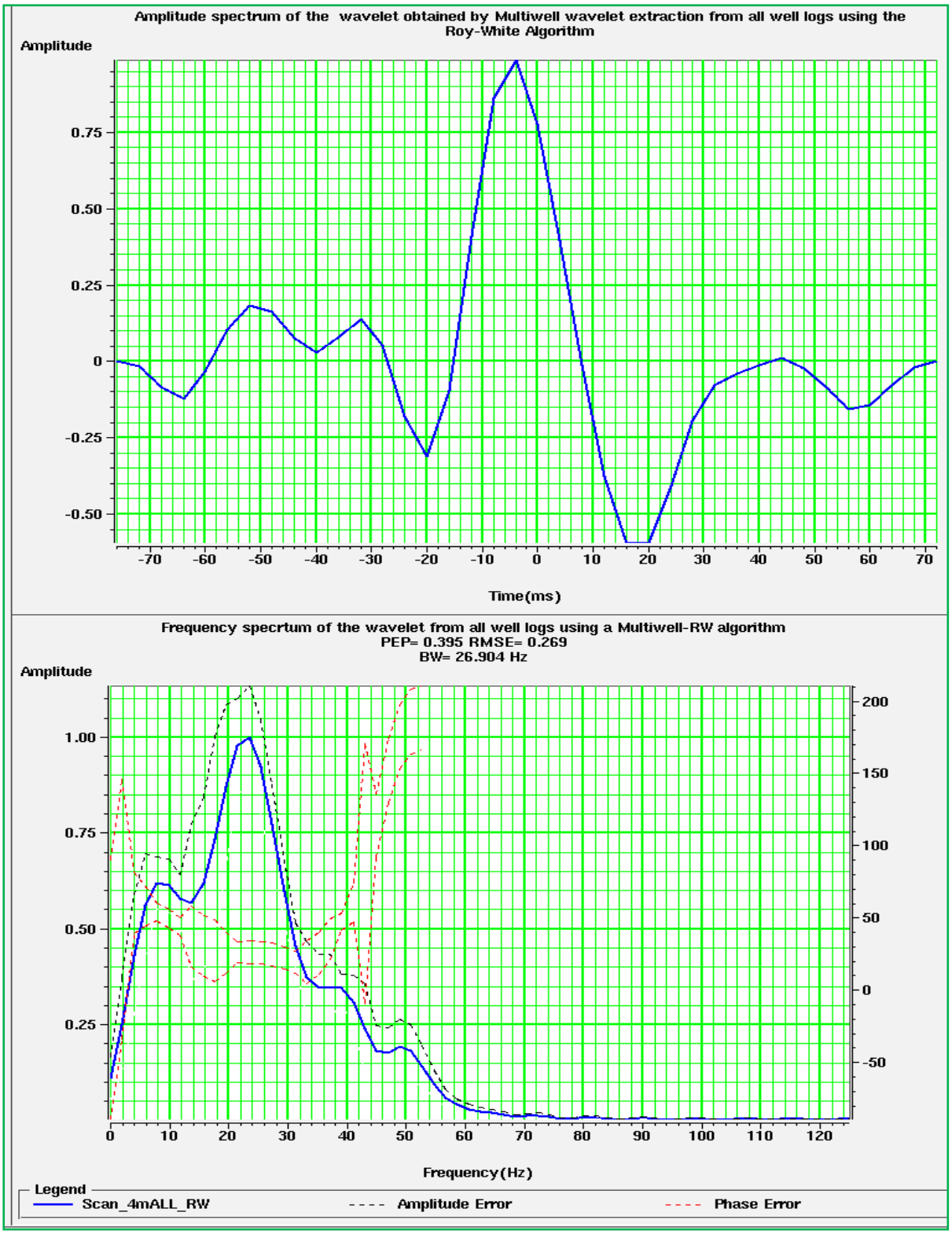

Fig. 4.19: amplitude and frequency spectrum of the wavelet extracted from all the wells by Multi-well wavelet extraction using the Roy White algorithm

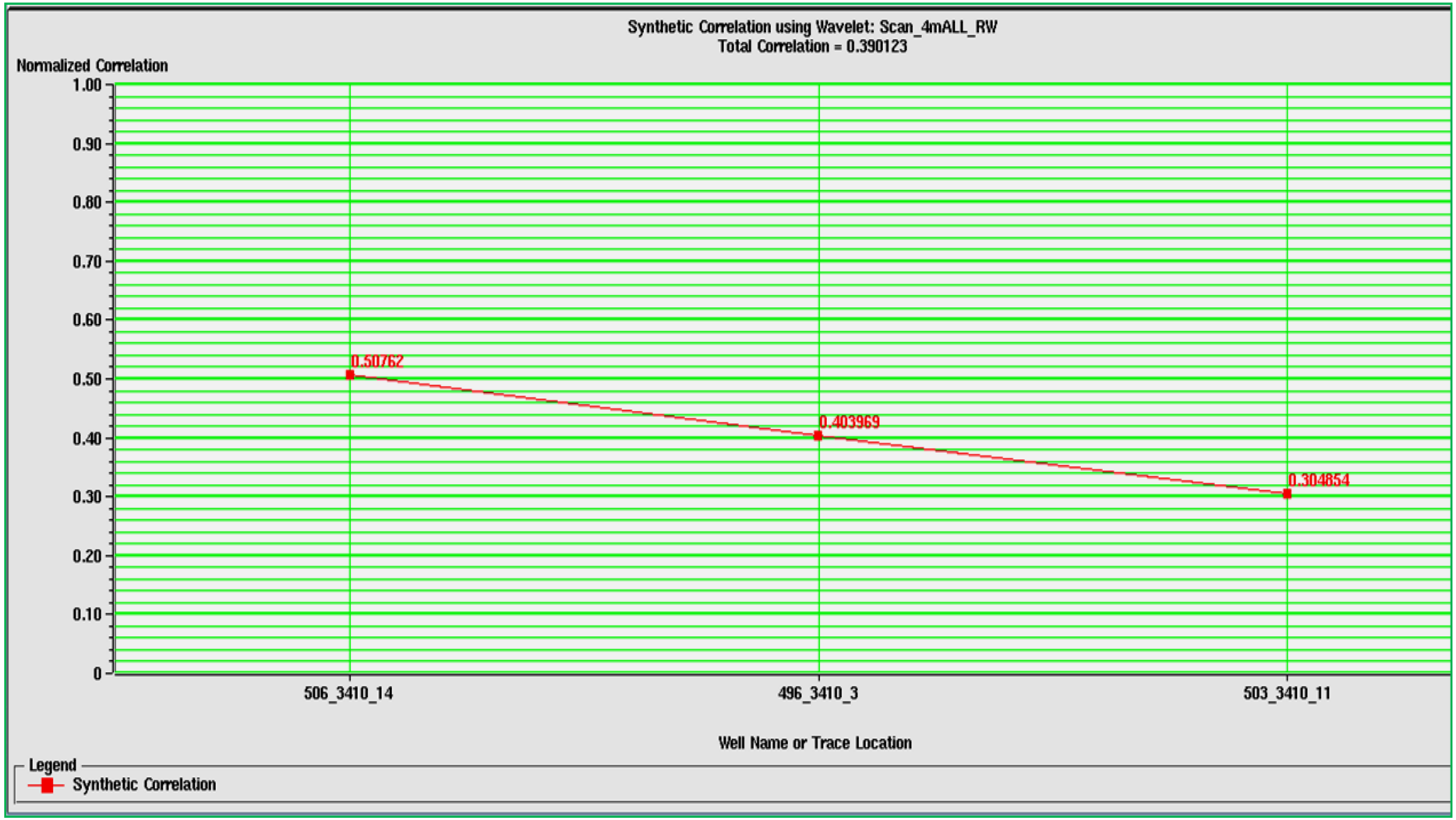

Fig. 4.20: Multiwell analysis of the wavelet extracted from all the wells. Although the correlation is in general not very good, it can be seen that this wavelet performs fairly well at each well location. Well 11 has the least correlation yet as earlier discussed it may be "bad". Such a well can be flagged and removed from new extraction and analysis processes.

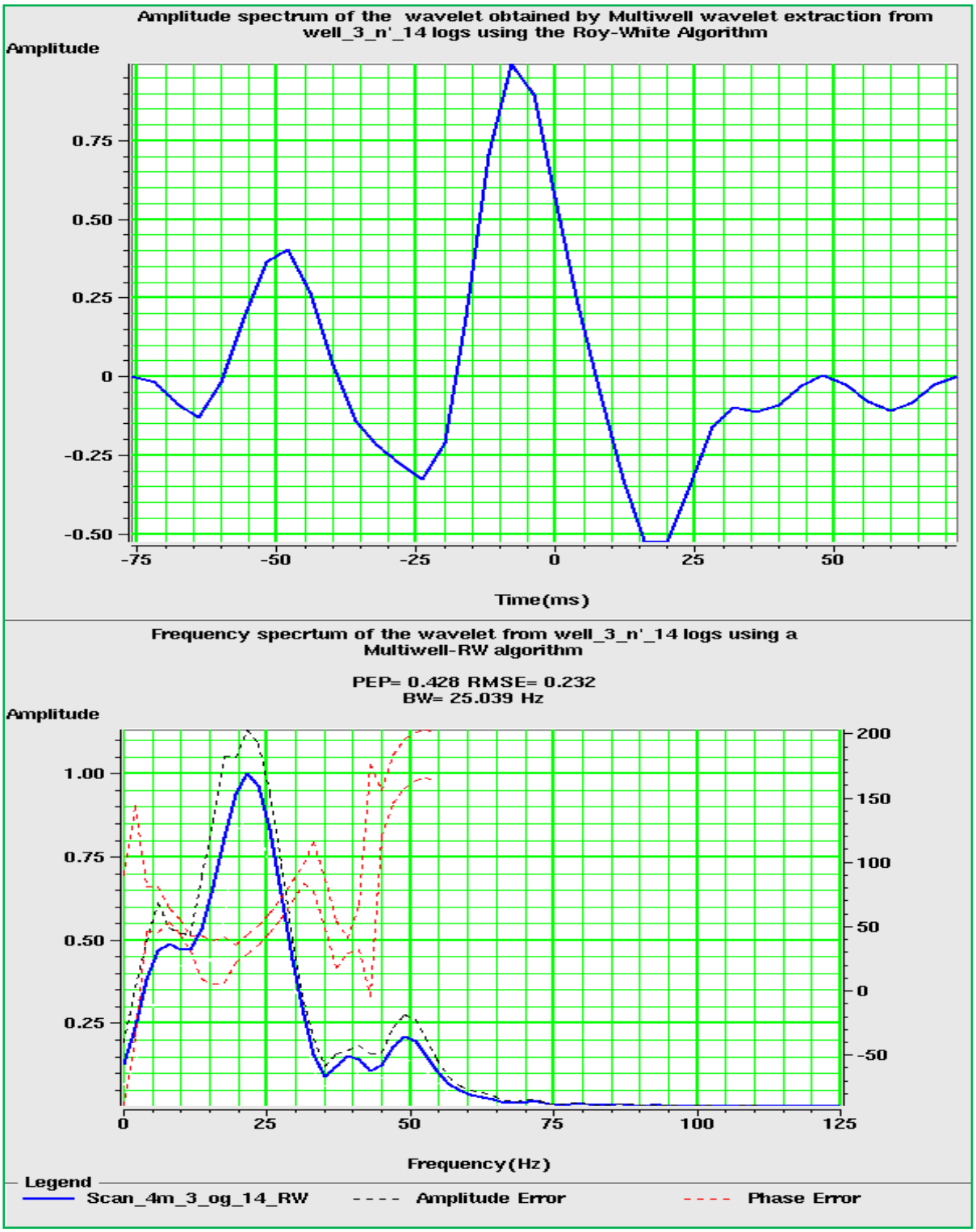

Fig. 4.21: the amplitude and frequency spectrum of the wavelet extracted from the "good" wells i.e. 3 and 14. Some times when a problematic well is removed from the extraction and analysis, the results can improve tremendously.

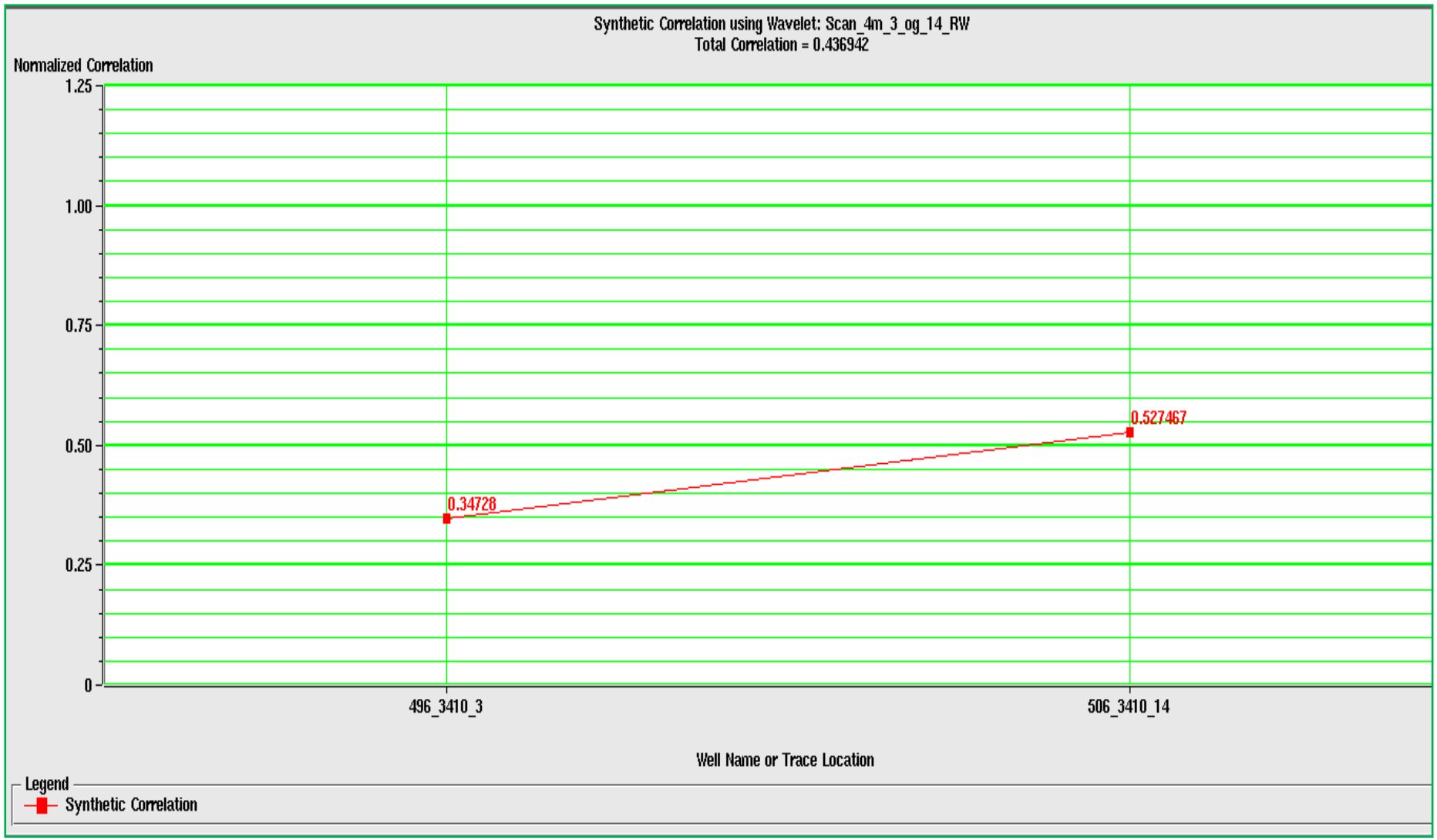

Fig. 4.22: Multiwell analysis of the wavelet extracted from well 3 and 14. As a result of eliminating well 11 from the extraction process, the correlation at well 14 has slightly improved. But then the correlation at well three has dropped by nearly 20%. Thus including well 11 may not be bad in this case.

"Do not believe in anything merely on the authority of your teachers and elders. But after observation and analysis, when you find that anything agrees with reason and is conducive to the good and benefit of one and all, then accept it and live up to it." - Gautama Buddha, the teacher

5.0 Summary, conclusion and other remarks

5.1 Summary of the main findings

This study has investigated two main issues: (1) editing, petrophysical modeling and analysis, and conditioning of well data in preparation for (2) joint calibration of seismic and well data to better define and characterize reservoirs.

The main findings are thus grouped into two categories:

- On editing, petrophysical modeling and analysis, and conditioning of well data; the following have been established:
    - Using locally calibrated versions of global empirical petrophysical relations improves the accuracy of the modeled well logs. For instance, when Gardner's equation is 'localized', the density log so generated from a given p-wave will better approximate the measured density log. This is very important because when some logs are damaged or completely missing, the only fall back is robust petrophyscial modeling.
    - Although the blocking technique is faster and more economical than the running window method in re-sampling and upscaling well data, the running window method produces a more accurate representation of the shape and trend of the original logs. The blocking techniques can introduce artificial blocks which can turn out to be deceptive in further analyses.
    - The Backus (running window) averaging method is a robust upscaling method. Surprisingly, it has not been fully embraced by some petrophysicists because of being time consuming.
- On joint calibration of seismic and well data; the following have been established:
    - Scanning the area in the vicinity of the well location to find the best match location greatly improves the correlation between well and seismic data. The true well location is sometimes not the best for correlation because seismic data migration can shift the position of best match up-dip.
    - Wavelet extraction is paramount in conducting a perfect seismic to well calibration. It is not enough to statistically 'guess' a wavelet, correlate the well logs and re-extract another wavelet from well logs; there is need to examine the quality and associated uncertainty of the extracted wavelet. This is when the Roy White algorithm comes in handy because it produces the very much needed diagnostics for quality control and uncertainty analysis.

- When there is more than one well in the study area, multi-well wavelet extraction followed by multi-well analysis can produce one wavelet that can be used at all well locations. This produces a forward seismic model that is uniform (in term of wavelet) throughout the calibration processes, the overall correlation between the well and seismic data should then improve tremendously. And it is helpful to follow the Roy White algorithm because it produces important diagnostics which can be used in selecting the 'best' wavelet.

5.2 Main contributions

The following can be singled out as the key contributions of this research:

Locally calibrated petrophysical models have been developed for the reservoir zones of the study area. These could be used for future prediction of missing or damaged well logs.

On the issue of joint calibration of seismic and well data, we have devised a work flow which emphasizes the need for multi-well wavelet extraction proceeded by multi-well analysis to extract one single wavelet. The scheme is easier to follow in conjunction with the Roy White algorithm.

5.3 Limitations of the study and suggestions for future research

This study assumed that the seismic data set used set was a perfectly processed one, this may not be true. And yet the quality of seismic data is one of the key ingredients to a perfect seismic-well tie; there are known case studies where reprocessing has substantially improved the correlation between seismic and well data. Roy et al. (1996) presented one such interesting example. This study being unexceptional, some of the results presented herein may in fact be biased by the fact that only well data were rigorous conditioned, in the safe knowledge of the fact that seismic data processing is much more understood that it deserves less attention. This issue is thus a potential candidate for future scrutiny.

How the methods examined and/or developed in this study do improve or degrade the quality of subsequent reservoir studies (AVO models, seismic attribute analysis), has in the interest of brevity and time been left out. This too is potential candidate for future work.

5.4 Challenges encountered

Some crucial data were not available to test some of the methods examined/developed in this study. For instance absence of VSP data hindered the examination of its well documented superiority over and above all other well data in the context of seismic-well calibration.

Some of the methods that were reviewed from geophysical literature were not further examined because they are not incorporated in the Hampson-Russell software that was used

in this research, for instance, we could not find the Backus averaging option in this software. The prospect of writing custom made programs (in for instance Matlab), was considered and later abandoned due to time constraints.

5.5 Conclusion

It has been demonstrated that with well processed seismic and well data, it is possible to achieve a high correlation between well data and seismic data; even when the two are measured at quite different scales. Many of the factors that conspire to degrade the achievable correlation between the two data sets can be removed or at least accounted for by intelligent processing procedures. The small differences that this can make on subsequent reservoir models can make much bigger differences on our understanding of a given reservoir.

Appendix 1: The Roy White diagnostic parameters

To help a reader who may want a quick reference of the mathematical meaning and interpretation of the Roy White Diagnostics parameters, an excerpt from a paper by Hampson (2004) is given below to act as a "quick guide". The excerpt summarises the main points in a paper by White and Simm (2003).

ROY WHITE

WAVELET EXTRACTION

WELL-SEISMIC SCANNING

The Roy White Wavelet estimation algorithms are a procedure for optimally estimating the seismic wavelet by calibrating and correlating well log data and seismic data. Ideally, there are two steps in this process:

(1) Determine the best trace location at which to extract the wavelet using the well.

(2) Given that tie location, determine the optimal wavelet.

1. **Well-Seismic Scanning**

This procedure assumes that the drill location of the well with respect to the seismic volume may not be optimal for extracting the wavelet. The reasons for this are well described in White and Simm (2003). Effectively this algorithm searches for a new location within a specified vicinity of the posted well location.

From the well, we calculate R(t), the reflectivity obtained from the sonic and density logs. Then, for each frequency, f, we define the spectral coherence function as the normalized magnitude-squared cross-spectrum between the reflectivity, R, and the seismic trace, S, i.e.:

$$\gamma^2(f) = \frac{|\Phi_{RS}(f)|^2}{\Phi_{RR}(f)\Phi_{SS}(f)} \qquad (A.1)$$

Proper estimation of the spectral coherence function requires alignment of R and S and averaging of the auto- and cross-spectra over frequencies within a selected analysis bandwidth, b. The spectral coherence measures the proportion of energy in the seismic trace that can be predicted from the well-log reflectivity in the bandwidth b centered at frequency f. We can by analogy define the proportion PEP of the total energy in the seismic trace that can be predicted from the well log reflectivity over the whole seismic bandwidth. We can call PEP the predictability for short. PEP can be measured directly from the seismic trace and the optimally matched (filtered) well-log reflectivity.

PEP = 1 – (energy in the residuals/trace energy). (A.2)

Where the residuals are the difference between the seismic trace and its matched or filtered reflectivity and the energy of a segment of a time series is its sum of squares.

The predictability PEP is a single scalar which measures the goodness-of-fit between the reflectivity calculated using the calibrated well and the seismic trace at the well location. To search for a better fit, three parameters are now introduced:

Lag = time shift in ms by which the reflectivity, R, is shifted before calculating the predictability

XSHIFT = shift along the x-direction from the borehole by which the match location is moved.

YSHIFT = shift along the y-direction from the borehole by which the match location is moved.

Effectively, PEP is a function of all three parameters:

PEP = PEP(Lag, XSHIFT, YSHIFT) (A.3)

Theoretically, we are looking for the three values which maximize PEP. Practically, the optimization is done in two stages. For any given value of **XSHIFT** and **YSHIFT**, the program calculates the optimum time shift, **bestLag**. This operation is performed for a selected range of values for **XSHIFT** and **YSHIFT**. The result is a map of values as a function of deviations from the original well location:

$PEP = PEP_{bestLag} = (XSHIFT, YSHIFT)$ (A.4)

Note that for each pair of values (**XSHIFT**, **YSHIFT**) PEP has already been optimized with respect to **Lag**. By examining this map, the user selects the optimum location visually for the subsequent wavelet extraction.

Appendix 2: List of figures

References

Aki, K., and Richards, P. G. (1980), Quantitative seismology, Theory and methods: W.H. Freeman & Co.

Avseth P., Mukerji T., and Mavko G. (2005), Quantitative seismic interpretation: applying rock physics to reduce interpretation risk. Cambridge University Press, Edinburgh, UK

Bayuk I., Ammerman M. and Chesnokov E. 2008: Upscaling of elastic properties of anisotropic sedimentary rocks. *Geophysical Journal International* 172, 842–860.

Box R. and Lowrey P. (2003): Reconciling sonic logs with check-shot surveys: stretching synthetic seismograms *In* the Leading edge (June 2003), 510-517.

Brooks J. and Thusu B., (1977): Oil-source rock identification and characterization of the Jurassic sediments in the northern North Sea. Chem. Geol. 20 (1977), 283-94; Elsevier Scientific Publishing Company, Amsterdam [Originally, Publication No. 79 of the Continental Shelf Institute, Trondheim, Norway]

Buland, A. and More, H. (2003), Bayesian wavelet estimation from seismic and well data *in* Geophysics, Vol. 68, No. 6 (November-December 2003); P. 200 – 2009, 13 Figs.

Castagna J. P. (1993). AVO analysis – tutorial and review; *In* offset dependent reflectivity – theory and practice of AVO analysis. ed. J.P. Castagna and M. Backus. *Investigations in geophysics*, No.8, (Society of Exploration Geophysicists, Tulsa, Oklahoma, pp. 3-36.

Castagna J. P., Batzle M. L. and R. L. Eastwood (1985): Relationships between compressional-wave and shear-wave velocities in clastic silicate rocks *In* Geophysics, Vol. 50, no.4 (April 1985); p. 571-581, 25 figs., 2 tables, Society of Exploration Geophysicists (1985).

Chesnokov E., Bayuk I. O., and Ammerman M. (2010): Determination of shale stiffness tensor from standard logs *In* Geophysical Prospecting, 2010, 58, 1063–1082. European Association of Geoscientists & Engineers (2010)

Dey, K. A. (1999), An analysis of seismic wavelet extraction: a Master's thesis, Department of Geology and Geophysics, University of Calgary.

Earthworks (2003): Improving a Well Tie with Backus Upscaling retrieved 29.08.2011 from http://www.sorviodvnvm.co.uk/ppt/backusupscaling.pps

Eltvik P., (2011), Introduction to the Gullfaks field. Retrieved (30.06.2011) from http://www.ipt.ntnu.no/~kleppe/Gullfakslandsbyen/Gullfakslandsbyen2011/statoil/index.htm

Evans, D., Graham, C., Armour A. and Bathurst, P (eds), (2003), The Millennium Atlas: Petroleum Geology of the Central and Northern North Sea: Published by The Geological Society of London.

Faust, L. Y. (1951), A velocity function including lithological variation in Geophysics, Vol. 18, p.271-288

Fossen, H. (1992), The role of extensional tectonics in the Caledonides of south Norway, *in* Journal of Structural Geology, Vol. 14, No.s 8/9, pp. 1033-1046, 1992. Pergamon Press Ltd

Fossen H., Rouby D., and Peter R. C (1996), Extension, Displacement, and Block Rotation in the Larger Gullfaks Area, Northern North Sea: Determined from Map View Restoration1, in AAPG Bulletin, V. 80, No. 6 (June 1996), P. 875–890.

Fossen, H., and Rørnes, A (1996), Properties of fault populations in the Gullfaks Field, northern North Sea. *In* Journal of Structural Geology, Vol. 18, No.s 2/3, pp. 179-190, 1996, Elsevier Science Ltd

Fossen, H. & Hesthammer, J. (1998), Structural geology of the Gullfaks Field, northern North Sea. *In:* Coward, M. P., Daltaban, T. S. and Johnson, H. (eds) *Structural Geology in Reservoir Characterization.* Geological Society, London, Special Publications, 127, 231-261.

Fossen, H., and Hesthammer, J. (2000), possible absence of small faults in the Gullfaks Field, northern North Sea: implications for downscaling of faults in some porous Sandstone *In* Journal of Structural Geology 22 (2000) 851-863. Elsevier Science Ltd

Fossen, H., and Hesthammer, J (2001): Structural core analysis from the Gullfaks area, northern North Sea, in Marine and Petroleum Geology 18 (2001) 411-439. Elsevier Science Ltd

Fugro (2011), Wavelets: normal incidence and angle seismic wavelet estimation accessed on 10.09.2011 from www.fugro-jason.com/software/JGW/modules/wavelets.htm

Goff J. C. (1983), Hydrocarbon generation and migration from Jurassic source rocks in the E Shetland Basin and Viking Graben of the northern North Sea. J. geol. Soc. London, Vol. 140, 1983, pp. 445-474, 29 figs., 9 tables

Gunning, J. and Glinsky, E. M. (2005), Wavelet extractor: A Bayesian well-tie and wavelet extraction program *in* Computers and Geoscience 32 (2006) 681 – 695.

Hampson, D. (2004), Summary of the Roy White Wavelet Extraction and Well-Seismic Scanning techniques in Hampson-Russell software *In* the knowledge base of the Hampson-Russell software. Hampson-Russell Calgary Office (November 2008)

Hampson, D. (2007), Wavelet extraction *In* the knowledge base of the Hampson-Russell software. Hampson-Russell Calgary Office (November 2007)

Hampson-Russell (2004), AVO theory, retrieved on 26.08.2011 from ftp://ftp.hampson-russell.com/pub/manuals/avo_theory.pdf

Hampson-Russell (2011), Hampson-Russell software guides, assistant and release notes accessed from the Hampson-Russell software on 08.08.2011

Handerson Petrophysics (2011), Some Causes for Bad Sonic Logs and Some Editing Options. Retrieved 08.08.2011 from http://www.hendersonpetrophysics.com/sonic_w_frames.html

Hardage, B., (2009), Welding Geology to Seismic Images; retrieved 15.06.2011 from http://www.aapg.org/explorer/2009/08aug/gpc0809.cfm

Hesjedal, A. (nd), Introduction to the Gullfaks Field. Retrieved 12.06.2011 from http://www.ipt.ntnu.no/~tpg5200/intro/gullfaks_introduksjon.html

Jakobsen, M. (2011), unpublished rock physics lecture notes. Department of Earth Science, University of Bergen

Jarvis, K. (2006), Integrating Well and Seismic Data for Reservoir Characterisation: Risks and Merits. AESC2006, Melbourne, Australia: 18th AGC and the Australian Earth Sciences Convention 2006, Melbourne, 2-6 July 2006 of the Geological Society of Australia.

Krief, M., Garati, J., Stellingwerff, J. & Ventre, J. (1990), A petrophysical interpretation using the velocities of P- and S- waves (Full-wave sonic). The log analyst, 31: 355-369.

Larter, S. & Horstad, I. (1992) Migration of petroleum into Brent Group reservoirs: some observations from the Gullfaks field, Tampen Spur area North Sea. *In, From Morton, A. C., Haszeldlne, R. S., Giles, M. R. & Brown, S. (eds), 1992,* Geology of the Brent Group. Geological Special Publication No. 61, pp. 441-452.

Linari Victor, (2004), A practical approach to well-seismic data calibration. In The Leading Edge; (August, 2004); v. 23; no. 8; p. 774-775. Society of Exploration Geophysicists

Lindsay R. and Koughnet R. V. (2001); Sequential Backus Averaging: Upscaling well logs to seismic wavelengths *In* the Leading Edge (February 2001)

Nathalie L. and Pierre D (2000): Well to seismic calibration: a multi-well analysis to extract one single wavelet. Retrieved 15.06.2011 from (Seismic calibration) http://www.beicip.com/index.php/eng/news/publications/2000_2002

Norwegian Petroleum Directorate, NPD (2010), Fields and discoveries in the northern part of the North Sea. Retrieved 12.06.2011 from: http://www.npd.no/Global/Engelsk/3%20-%20Publications/Facts/Facts2010/Figures/Chapter%2011/Fig-11-4.pdf

Mavko, G., Murkerji, T., and Dvorkin, J. (2009), The Rock Physics Handbook: tools for seismic analysis of porous media. – 2nd ed. Cambridge University Press, Cambridge CB2 8RU, UK

Petterson, O., Storli, A., Ljosland, E. and Massie, I. (1990), The Gullfaks Field: Geology and Reservoir Development *In:* Buller, A. T., Berg, E., Hjelmeland, O., Kleppe, J., Torsæter, O. and Aasen, J. O. (eds) *North Sea Oil & Gas Reservoirs – II.* Graham & Trotman Limited, P67-90

Rivenæs, J. C. (2011), unpublished lecture notes in Applied Reservoir Modeling. Department of Earth Science, University of Bergen, January, 24th-28th 2011

Roy, E. W. and Tianyue H. (1998), How accurate can a well tie be? *In* The Leading Edge / Volume 17 / Issue 8 (August, 1998), pp 1065-1071. Society of Exploration Geophysicists

Roy, W (1997), The accuracy of well ties: Practical procedures and examples. SEG Expanded Abstracts 16, 816 (1997); downloaded from http://dx.doi.org/10.1190/1.1886137. Society of Exploration Geophysicists

Roy, W. and Rob, S. (2003), Tutorial: Good practice in well ties *In* first break volume 21, October 2003. European Association of Geoscientists and Engineers

Roy, W., Rob, S., and Shiyu X (1996), Well tie, fluid substitution and AVO modeling: a North Sea example *In* the Geophysical Prospecting, 1998, 46, pp 323-346. European Association of Geoscientists and Engineers

Royle A. and Sandor B. (nd), Shear wave estimation techniques: a comparison. Retrieved 11.08.2011 from www.divestco.com

Schoepp, A. (1998), Improving seismic resolution with nonstationary deconvolution: Master's thesis, Department of Geology and Geophysics, University of Calgary.

Selley, C. R (1998), Elements of petroleum geology, 2nd Edition, 470pp. Academic Press

Sheriff R. E. and Geldart L. P. (1995), Exploration Seismology, 2nd ed. Cambridge University Press, the Edinburgh Building BB2 2RU, UK

Statoil (2011), fact information about Gullfaks field retrieved on 30.06.2011 from http://www.statoil.com/en/ouroperations/explorationprod/ncs/gullfaks/pages/default.aspx

Tad M. S., Sondergeldz C. H., and Rai C. S. (2003), Gassmann fluid substitutions: A tutorial: Geophysics, vol. 68, no. 2 (March-April 2003); p. 430–440, 8 figs., 2 tables. Society of Exploration Geophysicists

Tiwary D. K., Bayuk I. O., Vikhorev A. A., and Chesnokov E. M. (2009) Comparison of seismic upscaling methods: From sonic to seismic *In* Geophysics,Vol. 74, No. 2 (March-April 2009); P.WA3–WA14, 14 Figs. Society of Exploration Geophysicists

Walls J., Dvorkin J. and Carr M. R. (2004) Rock Solid Images: Well Logs and Rock Physics in Seismic Reservoir Characterization Offshore Technology Conference, 3 May-6 May 2004, Houston, Texas. Retrieved 01.08.2011 from http://www.rocksolidimages.com/pdf/Walls-Dvorkin-Carr_04.pdf

Wayne D. Pennington, (2001), Reservoir Geophysics *In* Geophysics, *vol. 66, no. 1 (January - February 2001); p. 25–30*

Wayne D. Pennington, (2002), Calibration of Seismic Attributes for Reservoir Characterization, Final Technical Report for project number DE-AC26-98BC15135. Michigan Technological University

Zhang, B., Zhou, F. and Li (2007): Technique for interactive wavelet extraction and decomposition in cepstrum domain. Society of Exploration Geophysicists, SEG/San Antonio 2007 annual meeting